MEASURING THE THERMODYNAMICS OF RECEPTOR TYROSINE KINASE INTERACTIONS: A STUDY OF HOMODIMERS, HETERODIMERS, AND RECEPTOR-ADAPTER PROTEIN COMPLEXES

by
Nuala Del Piccolo

A dissertation submitted to The Johns Hopkins University in conformity with the requirements for the degree of Doctor of Philosophy.

Baltimore, Maryland

January 2017

ABSTRACT

Protein-protein interactions regulate many biological systems. Understanding these interactions can provide insight into the function of proteins and the design of biological signaling networks, and can inform the development of more effective therapeutics. Protein-protein interactions can be described by thermodynamics, that is, the strength of binding, as well as by the distance between binding partners. In this thesis, I quantify protein-protein interactions in the Receptor Tyrosine Kinase (RTK) family, using novel quantitative fluorescence microscopy methods. In Chapter Three and Chapter Four, I characterize the formation of RTK homodimers using existing techniques. Specifically, I examine a subfamily of RTKs, known as the Fibroblast Growth Factor Receptors (FGFRs), in the presence of (i) pathogenic point mutations and (ii) activating ligands. In Chapter Five, I consider the formation of RTK heterodimers. I develop a method of measuring the thermodynamics of RTK heterodimer formation and apply it to the FGFR family. I also examine the effects of pathogenic point mutations on FGFR heterodimers. In Chapter Six, I study the interaction of RTKs with adapter proteins, an event that directly links RTKs to intracellular signaling networks. I develop and implement a procedure to measure the thermodynamics of this binding reaction, using the RTK Epidermal Growth Factor Receptor (EGFR) and the adapter protein Growth factor receptor-bound protein 2 (Grb2) as a model system. Overall, the work in this thesis demonstrates the utility of fluorescence microscopy for the quantitative characterization of protein-protein interactions in the membrane and reports previously unknown properties of the protein-protein interactions that regulate the RTK activation process.

Thesis Committee: Margarita Herrera-Alonso, Kalina Hristova (Reader), Feilim Mac Gabhann (Reader), Sua Myong, Marc Ostermeier (Chair)

Alternates: James Spicer, Jeffrey Gray

ACKNOWLEDGMENTS

First, I would like to thank my advisor, Dr. Kalina Hristova, for the opportunity to perform research in her lab and for her guidance and support over the years. I learned so much about research during my years in the Hristova lab, and I know this experience will be useful as I move forward in my career.

I would also like to thank past and present members of the Hristova lab: Fozia Ahmed, Dr. Patrick Byrne, Jaynie Criscione, Dr. Lijuan He, Sarah Kim, Dr. Christopher King, Alexander Komin, Michael Paul, Dr. Jesse Placone, and Dr. Sarvenaz Sarabipour. These fellow Hristova lab members trained me in the lab, performed experiments that my work relies on, collaborated with me on new experiments, and engaged in many useful scientific discussions.

Next, I would like to thank my thesis committee, for their useful comments on this work. Special thanks goes to my readers, Dr. Feilim Mac Gabhann and Dr. Kalina Hristova.

During my doctoral studies, I dedicated a large chunk of time to developing my teaching skills. I would like to thank the Johns Hopkins University Teaching Academy for providing the forum for this. I would also like to thank the professors who have inspired me to become a better teacher, especially Dr. Eileen Haase and Dr. Orla Wilson.

Finally, and most importantly, I would like to thank my friends and family for their support throughout my academic career. An especially big thank you goes to my parents, Dario Del Piccolo and Suzanne Wheeler-Del Piccolo, for always encouraging me in my academic endeavors. Thanks also goes to my grandparents, for their support and inspiration over the years. I would not have made it to Johns Hopkins without the

especial encouragement of my grandfather, Richard Wheeler. Lastly, I would like to thank my siblings, Chiara, Giulio, and Ivano, and friends, especially Zeinab Bakhiet, for always putting a smile on my face.

DEDICATION

To my parents, Dario Del Piccolo and Suzanne Wheeler-Del Piccolo

TABLE OF CONTENTS

LIST OF TABLES

LIST OF FIGURES

CHAPTER ONE Introduction

Protein-Protein Interactions in the Plasma Membrane

Protein-protein interactions regulate many biological systems, and are the focus of this thesis. The current understanding of biological processes, including protein-protein interactions, is often qualitative. However, a quantitative understanding of biology, and protein-protein interactions, is expected to provide insight into the design of biological signaling networks and protein function, and to inform the development of more effective therapeutics (1-6). Here, we seek to quantify the thermodynamics of protein-protein interactions in the plasma membrane.

Membrane proteins are notoriously difficult to study. They have both hydrophobic and hydrophilic domains and are often glycosylated. These physiochemical properties render methods used to study the interactions of soluble proteins less effective for membrane proteins, if they can be used at all (7-9). Hence, knowledge of membrane proteins, quantitative or otherwise, lags behind that of soluble proteins. However, membrane proteins, which comprise approximately 30% of all proteins, play a key role in many cellular processes. They regulate communication across the membrane, initiate many signaling networks, and represent a major drug target (4,6-9). Recent research has focused on developing new methods for the study of membrane proteins, and in this thesis, I will both use and contribute to this growing toolbox.

Receptor Tyrosine Kinases (RTKs)

Receptor Tyrosine Kinases (RTKs) are the second largest class of membrane proteins. There are 58 different RTKs, which can be classified into 20 families based on sequence similarity. These cell surface receptors play critical roles in many biological

processes, including growth, development, communication, and movement, and are often implicated in developmental disorders and cancers (4,10-13). In this thesis, I study protein-protein interactions in the context of four different RTKs: FGFR1, FGFR2, FGFR3, and EGFR.

RTK Activation

A prototypical RTK consists of a ligand-binding extracellular (EC) domain, a single-pass transmembrane (TM) domain, and a tyrosine kinase intracellular (IC) domain (4,10-12,14-17). The competing models for RTK activation are shown in Figure 1-1.

Figure 1-1, Panel A is a cartoon representation of the canonical model describing RTK activation. In the absence of ligand, receptors exist as monomers, and ligand binding cross-links two receptors into a dimer complex. Dimer formation brings the IC domains into close proximity, allowing receptors to cross-phosphorylate each other. Phosphorylated receptors, in turn, initiate downstream signaling cascades such as the MAPK, STAT, PKC, and PI3K pathways, and these biochemical networks determine functional outcomes (4,10-12).

Figure 1-1, Panel B diagrams the emerging model of RTK activation. Recent work has shown that RTKs form dimers even in the absence of ligand (18,19), suggesting that the simple unliganded monomer versus liganded dimer framework may not fully describe the RTK activation process. The emerging model of RTK activation considers monomers, unliganded dimers, and liganded dimers. Unliganded dimers are believed to prime the receptors for complete activation and to exhibit partial activity. In particular, the activity of unliganded dimers has been implicated in the progression of developmental disorders and cancers (4,10,15,20,21). Ligand binding to unliganded

dimers is proposed to induce a conformational change that leads to full activation of the RTK (18,19). The function of active dimers in the canonical and emerging models is the same: the IC domains cross-phosphorylate each other, which in turn activates downstream signaling cascades.

Fibroblast Growth Factor Receptors

The Fibroblast Growth Factor Receptor (FGFR) family of RTKs regulates development of the skeletal system, and has also been implicated in many cancers (13,14,22-24). There are four receptors in this family—FGFR1, FGFR2, FGFR3, and FGFR4—and I study FGFR1, FGFR2, and FGFR3, the three receptors required for proper skeletal development (14). The FGFRs bind 18 ligands, known as fibroblast growth factor (fgfs). FGFR dimers have a 1:1 ratio of receptor to ligand and are believed to have a symmetric structure (14,25).

Receptors in the FGFR family have a characteristic architecture. The EC domain consists of three immunoglobin-like domains (DI, DII, and DIII), with an acid box between DI and DII, and a flexible linker between DII and DIII. In the absence of ligand, the EC domain inhibits dimer formation (26). Ligands bind to receptors via specific interactions with DII, the linker, and DIII (13,14,22), and dimerization occurs through inter-receptor contacts. The EC domain is followed by a TM domain, which has been shown to promote dimer formation (26,27). The FGFR IC domain is a tyrosine kinase that is thought to adopt an autoinhibitory conformation in the absence of ligand (13,22).

Epidermal Growth Factor Receptor

The Epidermal Growth Factor Receptor (EGFR) is a member of the ErbB family of RTKs. While other families of RTKs are often linked to specific tissue types, the

ErbBs have been shown to regulate the development of a wide variety of tissue types. EGFR was the first RTK directly linked to human cancers and thus has been studied more extensively than many other RTKs (4,10,11,15-17,28). There are at least 7 ligands that bind EGFR. Like the FGFRs, EGFR binds these ligands in a 1:1 ratio of receptors to ligands, but the EGFR dimer is notable for its asymmetric structure (5,10).

The EC domain of EGFR is composed of four domains: DI and DIII are leucine-rich domains, and DII and DIV are cysteine-rich domains. In the absence of ligand, the EC domain adopts a closed conformation, mediated by intra-receptor contacts between DII and DIV. Ligand binding to DI and DIII exposes the so-called dimerization interface of DII, which participates in inter-receptor contacts and the formation of dimers (4,10,11,15,16,28,29). The EC domain is followed by a TM domain, which is also expected to promote dimerization (30). The EGFR IC domain consists of a tyrosine kinase domain followed by a long tail. The EGFR IC domain is unique in that it forms an asymmetric dimer and that the phosphorylation sites linking receptor activity to downstream signaling cascades are found on the tail, instead of the kinase (5,10,12,29,31).

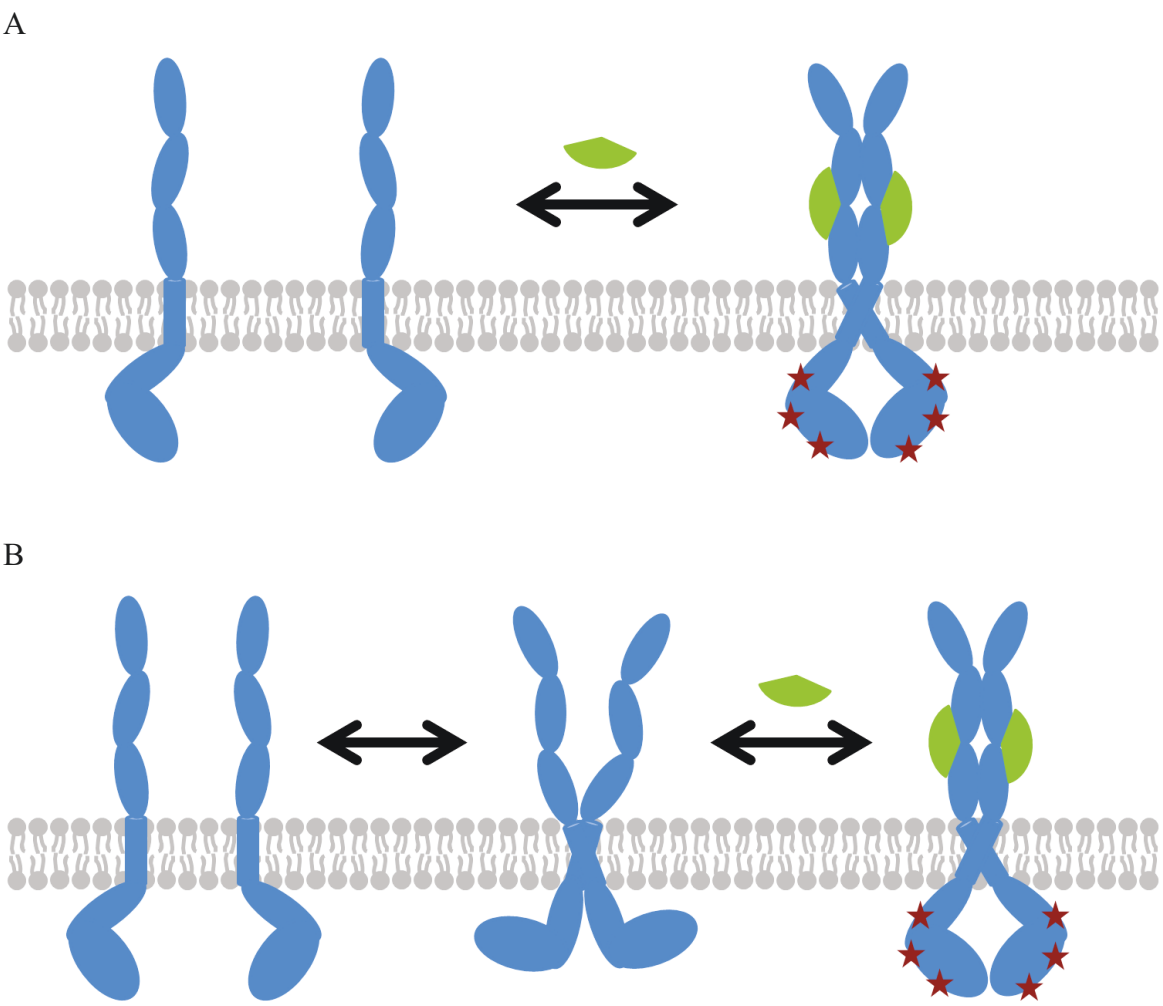

Figure 1-1. The canonical and emerging models of RTK activation.

(A) In the canonical model of RTK activation, receptors exist as monomers in the absence of ligand. Ligand addition cross-links the receptors into dimers. Dimer formation brings the kinase domains into close proximity, allowing for cross-phosphorylation and activation of receptors. (B) In the emerging model of RTK activation, receptors exist as both monomers and dimers in the absence of ligand. The properties and functions of the unliganded dimer remain open questions. Ligand binding is supposed to induce a conformational change in the dimer, perhaps increasing activation of the dimer.

CHAPTER TWO Experimental Techniques

The experiments described in Chapter Three, Chapter Four, Chapter Five, and Chapter Six rely on the same or very similar molecular biology, cell culture, and FRET microscopy protocols. The details of these experimental procedures are compiled in this chapter.

Molecular Biology

Traditional cloning techniques were employed in this work. That is, we use polymerase chain reaction to replicate DNA sequences, and restriction enzymes and ligations to assemble pieces of DNA. Following assembly, all plasmids were amplified using DH5α *E. coli* cells.

In Chapter Three, Chapter Four, and Chapter Five, we study the FGFR subfamily of RTKs. Since the lab has previously studied the FGFRs quite extensively, the wild-type FGFR1, FGFR2, and FGFR3 plasmids were generated by other lab members (18,26). These plasmids code for the EC and TM domains of the receptor, followed by a flexible $(GGS)_5$ linker and a fluorescent protein (eYFP or mCherry). In Chapter Three and Chapter Five, we study pathogenic point mutations in FGFR3. The mutations for Achondroplasia (32) and Crouzon Syndrome with acanothsis nigricans (33) were engineered into the wild-type FGFR3 plasmids by other lab members. The Thanatophoric Dysplasia Type I mutations were introduced using the Agilent Technologies QuikChange II mutagenesis kit, according to the manufacturer's instructions (34).

In Chapter Six, we study the interaction between EGFR and Grb2. The EGFR gene in the pSSX vector (35) was a kind gift from Daniel Leahy. We inserted the genes for a GGS linker and mTurquoise between the KpnI and NotI restriction sites of the

pSSX plasmid, in order to fluorescently label the C-terminus of the receptor. The empty pSSX vector and the Grb2 gene were kind gifts from Daniel Leahy and Jin Zhang, respectively. First, genes for the GGS linker and YFP were inserted into the empty pSSX vector, between the XbaI and NotI restriction sites. Next, we added a Kozak sequence and Grb2 between the BamHI and XbaI restriction sites, to generate a plasmid coding for Grb2 followed by a short flexible linker and a fluorescent protein.

Cell Culture

Chinese Hamster Ovary (CHO) cells were used for all cell studies in this thesis. These epithelial-like cells are commonly used to express recombinant proteins (36-38). Benefits of CHO cells include their high protein expression, the similarity of their post-translational protein modifications to those of humans, and their short doubling time. CHO cells are particularly well-suited to the experiments in this thesis. Namely, they have been shown to not express the FGFRs or EGFR, so the possibility that our recombinant RTKs interact with natively expressed receptors need not be considered.

CHO cells were maintained in an incubator at 37^{o}C with 5% carbon dioxide. Culture media consisted of Dulbecco's Modified Eagle's Medium supplemented with 1.8 g/L glucose, 1.5 g/L sodium bicarbonate, 10% fetal bovine serum, and 1 mM nonessential amino acids. Cells were passed every other day.

Transient transfections of CHO cells were performed using FugeneHD, at a ratio of 3 uL of transfection reagent per 1 ug of plasmid. Transfections proceeded for 24 hours prior to an experiment, which allowed for receptors to be synthesized, trafficked to the membrane, and glycosylated.

The experiments described in Chapter Three and Chapter Five were performed in the absence of ligand. In Chapter Four, we worked with five fgf ligands. fgf4, fgf8, fgf9, and fgf16 were all purchased from R&D Systems, and fgf18 was purchased from Peprotech. The EGF ligand used in Chapter Six was a kind gift from Daniel Leahy. All experiments in the presence of ligand were performed under saturating conditions.

Model Membrane Systems

The plasma membrane is hydrophobic barrier that separates the cell from its environment. It is a heterogeneous and dynamic system composed of lipids and proteins, with an asymmetrical composition between the two leaflets (8,39,40). Recent experiments have overturned the notion that the membrane is a smooth surface, instead showing that the plasma membrane of a resting cell is highly wrinkled and folded (41,42). Organization of membrane structure and local lipid and protein composition are regulated by the cytoskeleton; by lipid-lipid, lipid-protein, and protein-protein interactions; and perhaps by the formation of lipid rafts (8,39). These complexities preclude direct quantification of protein-protein interactions in native membranes (7-9,40).

In this thesis, we instead work with two model membrane systems (41,43). Both models are derived from live CHO cells, so they retain many of the properties of native membranes. Both models mimic the lipid and protein content of the membrane of the cells from which they are derived (44,45). Additionally, receptors are trafficked to the membrane by the native cellular machinery, so they undergo all relevant post-translational modifications, including glycosylation (37,38). However, these models simplify the plasma membrane system enough to enable quantitative measurements of

protein-protein interactions. Most importantly, the membrane is stretched out, eliminating the wrinkling and folding of live cells, which enables direct measurement of receptor concentrations and interactions in the membrane (46). Additional details about the two model systems—cell-derived vesicles and swollen cells—are given below.

Cell-derived Vesicles

Cell-derived vesicles are spheres of plasma membrane that can be used as a model membrane system (40,43,45,47,48). Vesicle production is typically induced using chemicals or osmotic pressure buffers (43,45,47-49). Here, we employ an osmotic pressure-based technique to derive vesicles from the plasma membrane of live CHO cells. We reported this method, known as the chloride salt vesiculation protocol, in 2012 (43). Briefly, cells are rinsed with a hypotonic rinse buffer and then incubated in a hypertonic buffer, which causes the cells to release large plasma membrane vesicles into solution. The biological mechanism through which cells generate and release these large vesicles remains unknown (40).

Vesicles derived from CHO cells using the chloride salt vesiculation technique are similar in size to live cells (they have an average diameter of 17.2 μm) (43) and have a lipid content that matches the cells from which they are derived (44). However, these vesicles lack both the cytoplasm and cytoskeleton (44). Vesicles are an equilibrium model membrane system, so the concentration of RTKs and other proteins and lipids is fixed. Figure 2-1, Panel A shows two fluorescent images of vesicles derived from CHO cells expressing FGFR3 labeled by a fluorescent protein.

Swollen Cells

Swollen cells are live cells that have been treated with a hypotonic buffer, causing them to expand. Specifically, the buffer consists of one part cell culture media to nine parts DI water and has a pH of 7.4. Swelling cells using this hypotonic buffer is a reversible process (41). The swelling process stretches out the membrane of the cell, so that it is no longer folded and wrinkled (41,46). A stretched membrane is important for accurate measurement of fluorophore concentrations and FRET efficiency using our quantitative FRET microscopy techniques (46). Swollen cells retain both the cytoplasm and cytoskeleton, and we expect the lipid and protein content to be identical to that of unswollen cells. Like vesicles, swollen cells are an equilibrium model membrane system, because the tension in the membrane of a swollen cell inhibits endocytosis (50). In Figure 2-1, Panel B, we show a fluorescent image of a swollen CHO cell expressing EGFR labeled with a fluorescent protein.

Quantitative Fluorescence Microscopy Methods

Förester Resonance Energy Transfer (FRET) is a molecular-level physical process that is often employed to report on protein-protein interactions (51,52). FRET relies on the special properties of fluorescent molecules, namely, their ability to undergo radiative decay. Radiative decay is a process in which relaxation of electrons from the excited state to the ground state is accompanied by photon emission. The excitation and emission wavelengths of a fluorescent molecule depend on the energy differences between the ground and excited electron states and vary from fluorophore to fluorophore. In FRET, the emission wavelength of one fluorophore (the "donor") matches the excitation wavelength of the second fluorophore (the "acceptor"), such that photons emitted from the donor molecule will excite the acceptor molecule, when the two are in

close proximity. The efficiency of this process is highly distance dependent and is described by the following:

$$E = \frac{1}{1+\left(\frac{d}{R_0}\right)^6} \quad (2\text{-}1)$$

where E is the FRET efficiency, d is the distance between the acceptor and donor, and R_0 is the Förster radius of the FRET pair. Figure 2-2, Panel A diagrams the excitation and emission wavelengths for yellow fluorescent protein (YFP) and the red fluorescent protein mCherry. Panel B shows FRET efficiency as a function of distance when YFP is the FRET donor and mCherry is the FRET acceptor. The YFP-mCherry FRET pair is used in Chapter Three, Chapter Four, and Chapter Five.

In this thesis, we use FRET, in conjunction with fluorescence microscopy, to report on protein-protein interactions in the RTK family. We use two novel fluorescence microscopy techniques, both of which ultimately measure three quantities: the donor concentration, the acceptor concentration, and the FRET efficiency.

Quantitative Imaging-FRET (QI-FRET)

Quantitative Imaging-FRET (QI-FRET) is a fluorescence microscopy technique developed in the Hristova lab to measure the thermodynamics of protein-protein interactions in plasma membranes (53-55). QI-FRET is performed using a Nikon Eclipse scanning confocal microscope and a 60x objective. The cross-section of vesicles or swollen cells is imaged in each of three channels, corresponding to the donor, the acceptor, and FRET efficiency. The microscope is calibrated using solutions of fluorescent protein, so that fluorescence intensity and fluorophore concentration can be directly correlated. This calibration is used to convert fluorescence intensity along the membrane in each channel to donor concentration, acceptor concentration, and FRET

efficiency. A representative cell-derived vesicle and its QI-FRET analysis are shown in Figure 2-3, Panel A.

Fully Quantified Spectral Imaging (FSI)

Fully Quantified Spectral Imaging (FSI) is another fluorescence microscopy technique developed in the Hristova lab and also reports on protein-protein interactions in plasma membranes (46). The FSI method utilizes the Aurora Spectral Technologies OptiMiS system (56), attached to a two-photon microscope (51). The OptiMiS system yields a full fluorescence spectra for every pixel in an image, and the two-photon microscope facilitates high spatial resolution and minimizes photobleaching of fluorophores (57). In the FSI method (46), the cross-section of a vesicle or swollen cell is imaged twice, following excitation of the donor and the acceptor, respectively. The microscope system is calibrated by imaging i) solutions of fluorescent protein and ii) vesicles or swollen cells transfected with only the donor or only the acceptor. This calibration establishes the relationship between fluorophore concentration and fluorescence intensity, and allows for pixel-level deconvolution of fluorescence spectra along the membrane into donor concentration, acceptor concentration, and FRET efficiency. A representative swollen cell and its FSI analysis is shown in Figure 2-3, Panel B.

A

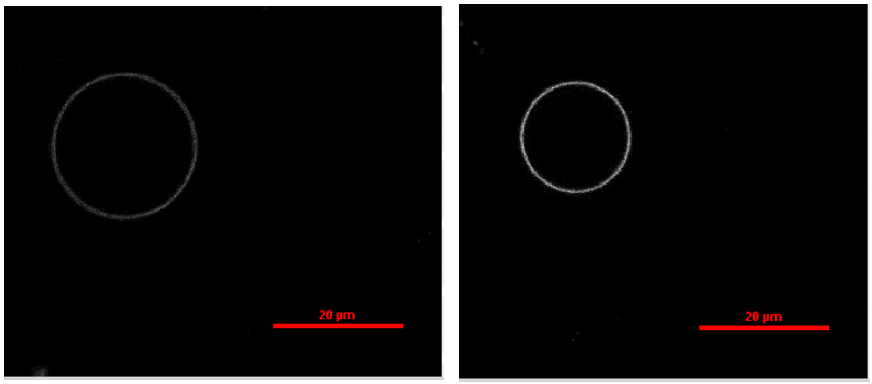

B

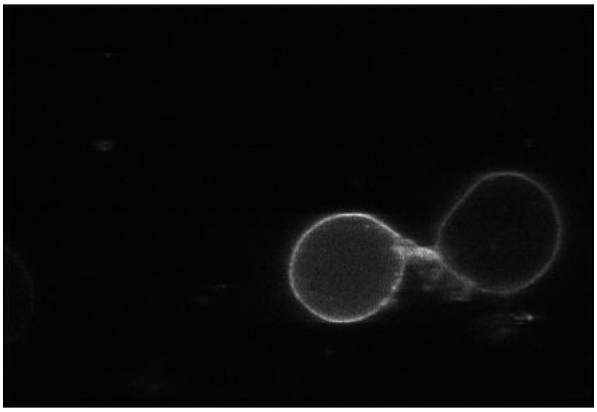

Figure 2-1. Live cell-derived model membrane systems.

Fluorescent images of (A) cell-derived vesicles and (B) swollen cells. Both model membranes are derived from CHO cells that have been transfected with RTKs labeled with fluorescent proteins.

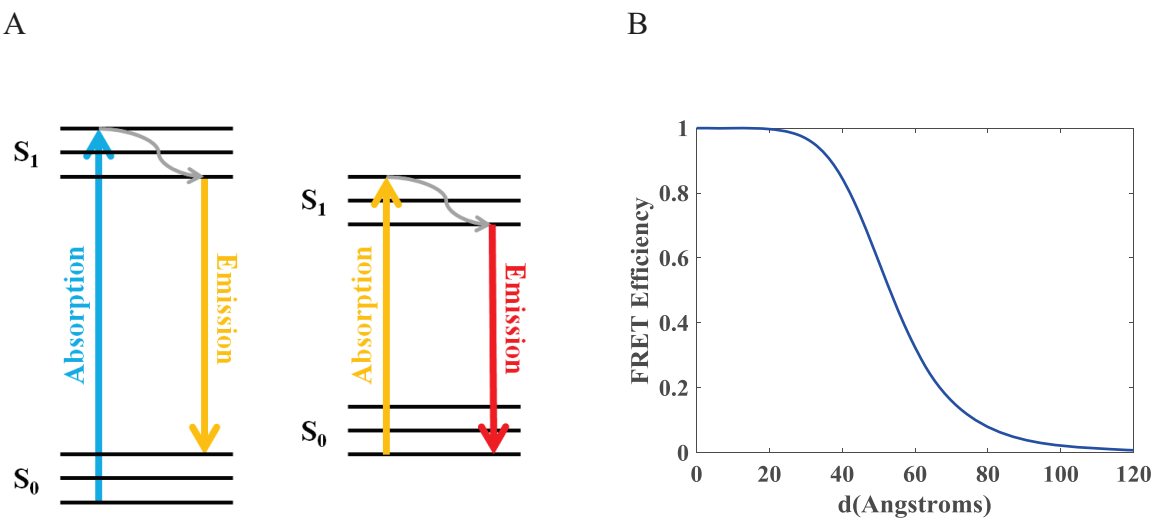

Figure 2-2. Diagrams describing Förster Resonance Energy Transfer (FRET) and the YFP-mCherry FRET pair.

(A) Jablonski diagrams showing the excitation and emission wavelengths for the donor YFP (left) and the acceptor mCherry (right). (B) FRET efficiency as a function of distance, for the YFP-mCherry FRET pair.

A

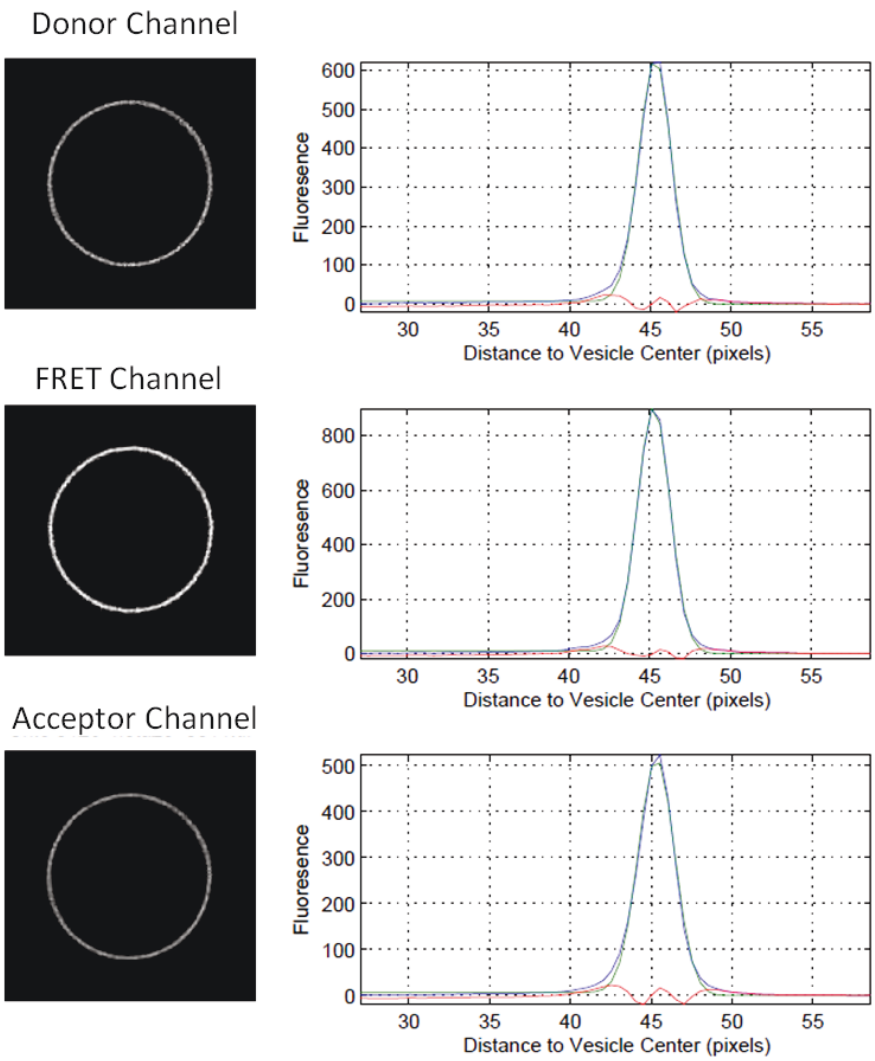
Donor Channel
Fluoresence
Distance to Vesicle Center (pixels)
FRET Channel
Fluoresence
Distance to Vesicle Center (pixels)
Acceptor Channel
Fluoresence
Distance to Vesicle Center (pixels)

B

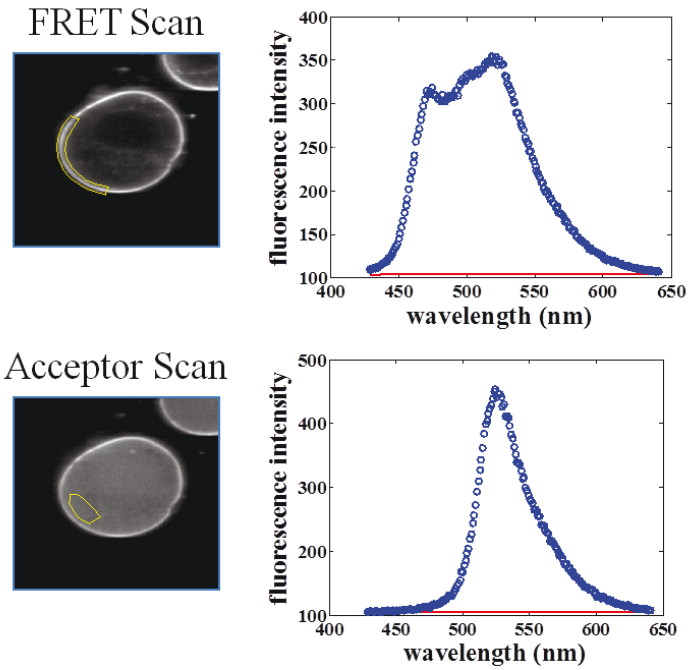

Figure 2-3. Quantitative FRET microscopy methods.

(A) A representative image of a cell-derived vesicle and its QI-FRET analysis. In the QI-FRET technique, the cross-section of each vesicle is imaged in three channels: donor, FRET, and acceptor. Then, the fluorescence intensity along the vesicle membrane is integrated (blue line) and fit to a Gaussian distribution (green line), while correcting for background fluorescence (red line). These intensities are used to calculate three quantities—donor concentration, acceptor concentration, and FRET efficiency—in each vesicle. This technique is used in Chapter Three, Chapter Four, and Chapter Five, to examine interactions between RTKs. (B) A representative image of a swollen cell and its FSI analysis. In the FSI method, an image of the cross-section of each cell is captured in two scans: FRET and acceptor. The fluorescence spectra (blue line) in the regions of interest are deconvoluted to determine the contributions from the donor, the acceptor, and FRET efficiency, while accounting for background fluorescence (red line). These

contributions are used to measure three quantities in each region of interest: the donor concentration, the acceptor concentration, and the FRET efficiency. This cell is from the experiments described in Chapter Six, where we examine the interaction between a RTK (on the membrane) and an adapter protein (in the cytoplasm).

CHAPTER THREE Effect of Thanatophoric Dysplasia Type I Mutations on FGFR3 Dimerization

This research was originally published in the Biophysical Journal. Nuala Del Piccolo, Jesse Placone, and Kalina Hristova. Effect of thanatophoric dysplasia type I mutations on FGFR3 dimerization. *Biophysical Journal*. 2015; **108**: 272-278.

The text reproduced here has been revised to match the style of this thesis.

Thanatophoric Dysplasia Type I

Thanatophoric dysplasia type I (TDI) is a lethal human skeletal growth disorder with a prevalence of 1 in 20,000 to 1 in 50,000 births. It is one of the most severe of the skeletal dysplasias and typically leads to neonatal death (58-60). Typical features of the TDI phenotype include shortened limbs with bowed femurs and cloverleaf skull deformities.

TDI is known to arise due to five different mutations, all involving the substitution of an amino acid with a cysteine in Fibroblast Growth Factor Receptor 3 (FGFR3): Arg248Cys, Ser249Cys, Gly370Cys, Ser371Cys and Tyr373Cys (61-63). Of these, Arg248Cys and Tyr373Cys account for 60 to 80% of all cases of TDI. These cysteine mutations have been shown to increase the phosphorylation and activation of the receptor in the absence of ligand (64,65), increase downstream extracellular signal-related kinase signaling (66), and increase BaF3 cell proliferation (67). The mutations compromise the downregulation of activated FGFR3 dimers in the plasma membrane (68) and increase retention of FGFR3 dimers in the endoplasmic reticulum (69). Furthermore, it has been shown that overactivation of FGFR3 leads to the inhibition of chondrocyte proliferation during development, which impedes bone growth (23,70).

FGFR3 is a receptor tyrosine kinase (RTK) which consists of an extracellular (EC) domain involved in ligand binding, a single-pass transmembrane (TM) domain, and an intracellular (IC) tyrosine kinase domain. Like all RTKs, FGFR3 functions via a lateral dimerization process that brings the kinase domains into close proximity so that they can phosphorylate and activate each other (62,71-73).

Mutations to cysteine residues in RTKs have been proposed to cause cross-linking of the receptors via disulfide bonds, thereby inducing constitutive dimerization and activation (64,74-76). However, the effect of the mutations on unliganded RTK dimer stability has never been characterized in quantitative terms. In this study, we characterize the effect of three TDI mutations, Arg248Cys, Ser249Cys, and Tyr373, on the stability and the structure of FGFR3 dimers. We accomplish this by using a Förster Resonance Energy Transfer (FRET)-based technique (26,54) that yields dimerization free energies of glycosylated RTKs and reports on structural differences between RTK dimers. Measurements are performed in plasma membrane vesicles derived from CHO cells with the use of a novel osmotic stress vesiculation method (43). We find that the three TDI mutations cause a modest stabilization of the FGFR3 dimer. We also observe modest structural perturbations in the FGFR3 dimer because of the mutations.

Homodimerization Model

The two-state thermodynamic model describing the equilibrium between RTK monomers and RTK dimers is given by the following reaction scheme:

$$M + M \overset{K}{\leftrightarrow} D \tag{3-1}$$

where M and D denote monomers and dimers, respectively. K is the homodimer association constant, which can be expressed as:

$$K = \frac{[D]}{[M]^2} \tag{3-2}$$

where the bracket notations indicate two-dimensional concentrations. This association constant can be used to calculate the Gibbs free energy of dimerization:

$$\Delta G = -RT ln\, K \tag{3-3}$$

where the standard state is defined as 1 square nanometer per receptor (54). Receptor concentration is constant in vesicles, so the law of mass conservation can be applied:

$$[M] + 2[D] = [T] \tag{3-4}$$

where T is the total number of receptors. Total dimer fraction can be written as

$$f_D = \frac{2[D]}{[T]} \tag{3-5}.$$

Together, the equilibrium equation and the mass conservation equation describe the process of RTK homodimer formation. This system of equations can be solved so that the homodimerization model can be described with a single equation:

$$f_D = \frac{1}{[T]}\left([T] - \frac{1}{4K}\left(\sqrt{1 + 8K[T]} - 1\right)\right) \tag{3-6}.$$

Interpretation of Homodimer FRET Data

Figure 3-1 is a cartoon representation of the monomer and dimer species present in homodimer FRET experiments. The measured FRET efficiency depends on both the proximity FRET efficiency, which arises due to the random close approach of donors and acceptors in the two-dimensional membrane, and the dimer-specific FRET efficiency, which occurs due to the formation of homodimers containing both a donor and an acceptor. We correct for the proximity FRET as discussed in (77) and are left with the dimer-specific FRET efficiency, E_D. Dimer-specific FRET in each vesicle can be written as:

$$E_D = f_D x_A \tilde{E} \tag{3-7}$$

where f_D is the dimeric fraction, x_A is the fraction of acceptors in a vesicle, and $\tilde{E}$ is the so-called Intrinsic FRET. Equation 3-7 assumes that the probabilities for the formation of donor-donor, donor-acceptor, acceptor-donor, and acceptor-acceptor dimers (see Figure 3-1) are the same. This is a reasonable assumption because we use monomeric fluorescent proteins that are not expected to affect the propensity for dimer formation.

The Intrinsic FRET is a structural parameter that depends on the separation and orientation of the donor and the acceptor in a dimer. The dependence of the Intrinsic FRET, or $\tilde{E}$, on the distance between the fluorescent proteins in the dimer is given by the following:

$$\tilde{E} = \frac{1}{1+\left(\frac{d}{R_0}\right)^6} \tag{3-8}$$

where d is the distance between the acceptor and the donor in the dimer, and R_0 is the Förster radius of the FRET pair (54). For eYFP and mCherry, R_0 is 53.1 Å, which we measured in previous work (46,54), under the assumption of free fluorophore rotation. The assumption of free rotation of the fluorescent proteins in these experiments is justified, because they are attached to the receptors via long flexible linkers (78). Since $\tilde{E}$ is generally unknown (because the structures of the wild-type and the mutants are unknown and may be different), the quantity considered when fitting the homodimer model to experimental FRET data is given by the following:

$$f_D\tilde{E} = \frac{E_D}{x_A} \tag{3-9}.$$

Predictions for dimeric fractions, generated by Equation 3-6, are fit to the experimental data, measured according to Equation 3-9, while varying the two unknown parameters, namely the dimerization constant, K, and the Intrinsic FRET, $\tilde{E}$. A least-

squares two parameter fitting procedure for K and $\tilde{E}$ is performed for each data set using MATLAB.

The best fit K and $\tilde{E}$ parameters are used to calculate additional characteristics of the homodimer. From the dimerization constant, we can use Equation 3-3 to calculate the dimer stability. The Intrinsic FRET allows us to calculate the distance between the fluorescent proteins in each homodimer, according to Equation 3-8.

Statistical Analysis

A χ^2 analysis is used to compare the wild-type data set with each of the TDI mutant data sets. In particular, we test the null hypothesis that the data sets being compared are not different. For each data set, the results are averaged within bins of $5x10^4$ receptors/nm^2. These bins are compared with each other in a pairwise fashion using the following equation:

$$\chi_i^2 = \left(\frac{avg_{wt,i} - avg_{mut,i}}{SE_i}\right)^2 \quad (3\text{-}10)$$

where i is the number of bins, and $avg_{wt,i}$ and $avg_{mut,i}$ are the average values in the wild-type and mutant bins, respectively. The standard error for each bin, SE_i, is defined as follows:

$$SE_i = \sqrt{\left(SE_{wt,i}\right)^2 + \left(SE_{mut,i}\right)^2} \quad (3\text{-}11)$$

where $SE_{wt,i}$ and $SE_{mut,i}$ are the standard errors in the wild-type and mutant bins, respectively. Finally, using these χ_i^2 values and df, the degrees of freedom, equal to the number of bins minus one, we calculate the reduced χ^2 value as follows:

$$\overline{\chi^2} = \frac{\sum_i \chi_i^2}{df} \quad (3\text{-}12).$$

We determine p-values using a χ^2 table (79). The cutoff for significance is $p < 0.05$.

Additional statistical analysis is used to compare the K and $\tilde{E}$ parameters determined for the wild-type with those determined for each of the mutants. We test the null hypothesis that the average values are not different from each other. We use GraphPad Prism to perform analysis of variance (ANOVA) and t-tests, and to calculate p-values.

Results

In the experiments reported in this study, we characterized the unliganded dimerization of wild-type FGFR3 and three TDI mutants in plasma membrane-derived vesicles. Experiments were performed with receptors in which the intracellular domains were substituted with fluorescent proteins (eYFP or mCherry) to allow for FRET detection.

The fluorescent proteins were attached to the TM domains via flexible $(GGS)_5$ linkers. The $(GGS)_5$ linker has been shown to be unstructured and behave like a random coil with an apparent radius of about 45 Å (78), when fused between two proteins. It has been further shown that models that assume free rotations of the fluorescent proteins attached to the two sides of the linker correctly predict the measured FRET efficiency (78). Based on these studies, it can be safely assumed that the fluorophores are rotating freely, and the distance between the fluorophores depends only on the points of attachment of the linkers to the protein, in this case the distance between the C-termini of the TM domains in the dimer.

To obtain vesicles containing FGFR3, we first co-transfected CHO cells with plasmids encoding for either the wild-type or the TDI mutants linked to eYFP and mCherry. Since the receptors are produced in CHO cells, they undergo all required post-

translational modifications, including full glycosylation. Following transfection, plasma membrane-derived vesicles were produced from the CHO cells using an osmotic stress method (43). Such vesicles do not have the actin cytoskeleton (45,47,48), which is known to play an important role in maintaining the lateral heterogeneity of biological membranes. Consistent with this, we invariably observe homogeneous distribution of fluorescence throughout the vesicle membrane (43,54).

The vesicles were transferred to chambered cover-glass slides for image acquisition. They were imaged using a Nikon Eclipse C1 laser scanning confocal microscope. Each vesicle was imaged using three separate scans: a donor scan, a FRET scan, and an acceptor scan, as described in previous publications (32,33,53,80,81). Following image acquisition, vesicles were processed using an in-house MATLAB script (54). For each scan of every image, this program identified the membrane of the vesicle and fit the fluorescence intensity across the membrane with a Gaussian function (see Figure 2-3). Solutions of purified fluorescent proteins were used to calibrate the donor and acceptor fluorescence intensities as described previously (53). The FRET efficiency, the donor concentration, and the acceptor concentration were determined in each vesicle using the QI-FRET method (54,55).

In Figure 3-2, we show the FRET efficiencies per vesicle plotted against the acceptor concentration in that vesicle; each data point corresponds to a single vesicle. Data for the wild-type, Arg248Cys, Ser249Cys, and Tyr373Cys constructs are shown as open blue diamonds, filled red squares, filled green triangles, and filled purple circles, respectively. Each data set contains ~500+ single vesicles and was collected in more than 10 independent experiments. The solid black line in Figure 3-2 indicates the expected

FRET efficiency due to the random approach of donors and acceptors (see (77) for details). This proximity FRET contribution occurs because the fluorophores are confined to the two-dimensional membrane and has been discussed in the literature (77,82,83). The data fall well above this line, which indicates that the FRET we observe is due to specific interactions between the receptors. Furthermore, FRET efficiencies measured for the mutants are higher than the efficiencies for the wild-type. Therefore, the TDI mutations have an effect on FGFR3 dimerization.

FRET due to FGFR3 dimerization was determined by correcting for proximity FRET (which depends only on the acceptor concentration (77)) from the measured FRET. Then, we calculated the product of the dimeric fraction in the vesicle, f_D, and the Intrinsic FRET, $\tilde{E}$, using Equation 3-9. To do so, we need the donor and the acceptor concentrations in each vesicle, shown in Figure 3-3. As discussed previously (54), these are two-dimensional concentrations in the membrane. The dimerization constant is a thermodynamic parameter which describes the propensity for dimerization in quantitative terms. The Intrinsic FRET, $\tilde{E}$, is a structural parameter which is very sensitive to changes in dimer structure, since FRET efficiency falls off with the sixth power of distance between fluorophores as seen in Equation 3-8. The product of these two parameters, $f_D\tilde{E}$, is plotted in Figure 3-4 as a function of the total receptor concentration, after averaging the data in bins of width $5x10^4$ receptors/nm^2.

Using χ^2 analysis (79), we performed a pairwise comparison of the binned wild-type data set with each of the mutant data sets. Reduced χ^2 values of 133.97, 55.33, and 28.91 were calculated for the Arg248Cys, Ser249Cys, and Tyr373Cys mutants,

respectively. The corresponding p-values were all <0.001 and the observed differences were highly statistically significant for all the mutants.

Since the experimental data in Figure 3-4 depend on both the dimerization constant, K, and the Intrinsic FRET, Ẽ, we used Equation 3-9 and performed a two parameter fit on each data set to determine the optimal K and Ẽ values for each construct. The results of the fit are shown in Table 3-1, along with their standard errors (67% confidence intervals). Next, the K and Ẽ values were used to calculate additional characteristics of the dimer; these results are also shown in Table 3-1. The dimerization Gibbs free energy (dimer stability, ΔG) was calculated using the dimerization constant and Equation 3-3. We also calculated the effect of the mutations on dimer stability ($\Delta\Delta G$), given by the difference in dimer stability between a given mutant and the wild-type. From the optimal Intrinsic FRET values, we calculated the distance between the fluorescent proteins in each of the different FGFR3 dimers using Equation 3-8.

The dimeric fractions are shown in Figure 3-5, along with the binding curves corresponding to the optimal K values. The data are shown as averages within bins of $5x10^4$ receptors/nm^2. A reduced χ^2 analysis demonstrated that the small differences between the wild-type and the mutants are statistically significant. The reduced χ^2 values are 36.03, 7.51, and 8.35, such that the p-values are all <0.001. Further statistical analysis, however, shows that the effects are very modest, with the p-values from t-tests being 0.001, 0.15 and 0.006 for the Arg248Cys, Ser249Cys, and Tyr373Cys mutants, respectively. By ANOVA, only the effect of the Arg248Cys mutation is highly statistically significant. Statistical analysis of the values of Ẽ yields p-values of <0.001, <0.001, and 0.03 for the Arg248Cys, Ser249Cys, and Tyr373Cys mutants, respectively.

By ANOVA, the effects of the Arg248Cys and Ser249Cys mutations on Intrinsic FRET, and thus dimer conformation, are highly statistically significant.

Discussion

In FRET studies of RTK dimerization, the measured FRET efficiencies depend on both RTK dimerization propensity and RTK dimer structure (particularly on the distances between the fluorescent proteins in the dimer). Unfortunately, this fact is sometimes not fully appreciated in FRET data interpretation. In addition, the read-out of other experimental techniques used in RTK research also depends on both the dimerization propensity and on structural factors. For instance, receptor phosphorylation, measured in Western blot experiments using anti-phospho-tyrosine antibodies, requires that the receptors are dimeric but also depends on the exact positioning and orientation of the kinase domains. The TDI mutations have been shown to increase FGFR3 phosphorylation (64), as compared with wild-type, but it is not known if the effect is due to increased dimerization or structural perturbations that promote phosphorylation. Similarly, cross-linking efficiencies, measured in Western blots using anti-receptor antibodies, depend both on the fraction of dimeric receptors and on the presence of suitable amine groups that are in close enough proximity for cross-linking to occur. Thus, a change in cross-linking due to a mutation may be due to either a change in dimerization propensity or a change in structure, or both.

In this study, we characterized the ligand-independent dimerization of three FGFR3 mutants linked to TDI in plasma membrane-derived vesicles using a FRET-based method. We overcome the limitations in data interpretation by separating structural effects from dimerization effects. This is accomplished by fitting a dimer model with two

adjustable parameters, the dimerization constant, K, and the structural parameter Intrinsic FRET, Ẽ, to the experimental data.

Modest changes in dimer stability due to the TDI mutations in the absence of ligand

Dimerization constants report on the propensity for dimer formation. For the wild-type receptor, we measured a dimerization free energy of $\Delta G = -3.4 \pm 0.1$ kcal/mol, which is consistent with previous FGFR3 experiments (26,43). Concurrent experiments on the Arg248Cys, Ser249Cys, and Tyr373Cys mutant constructs produced ΔG values of -4.2 ± 0.1, -3.7 ± 0.1, and -3.8 ± 0.1 kcal/mol, respectively. Thus, the mutations have a very modest effect on dimer stability, confirmed by statistical analysis.

Literature values for the energetic contributions of disulfide bonds to protein interactions vary substantially, with the most consensus values lying around 2-4 kcal/mol (84,85). Here, we measured that the Arg248Cys, Ser249Cys, and Tyr373Cys mutations stabilize the FGFR3 dimer by -0.8, -0.3, and -0.4 kcal/mol, respectively. These findings may suggest that disulfide bonds form with low probability within the unliganded TDI dimers, most likely due to structural constraints that make it difficult for disulfide bonds to form. This means that, in our experiments, we might probe two different mutant populations—one consisting of a disulfide bonded dimer structure and one consisting of a mutant dimer with a structure that is practically the same as the wild-type—and that our measurements of K and Ẽ are average values, not molecular characteristics of the disulfide bonded mutant dimers.

Modest structural effects due to the TDI mutations in the absence of ligand

Intrinsic FRET values report on the distances between the fluorescent proteins in the dimer, and are influenced by the mobility of the fluorescent proteins. We show that

the Arg248Cys and Ser249Cys TDI mutations cause statistically significant effects on the Intrinsic FRET, implying that there are differences in the structures of the wild-type and mutant dimers. Assuming free rotation of the fluorescent proteins, we calculate the average distance between the fluorescent proteins in the wild-type dimer as 53 ± 1 Å, compared with 45 ± 1 Å, 45 ± 1 Å, and 49 ± 1 Å for the Arg248Cys, Ser249Cys, and Tyr373Cys mutants, respectively. Therefore, the fluorescent proteins are likely closer to each other in the mutant dimers, suggesting a likely decrease in the separation between the TM domains.

Implications

Disulfide bonds in proteins or protein complexes are always envisioned as very strong, due to their covalent nature. Thus, one expects that disulfide bonds strongly stabilize protein folds and protein assemblies. In accordance with this view, it is believed that the effects of pathogenic cysteine mutations in RTKs are profound, with the disulfide bonds inducing constitutive dimerization. Yet, actual experimental measurements of disulfide bond-mediated stabilization for soluble proteins and dimers point to rather modest effects, on the order of -2 to -4 kcal/mol (84,85). In this study, we present, to our knowledge, the first quantitative measurement of the effect of cysteine mutations on membrane protein interactions. In particular, we study the TDI mutations in FGFR3, which are linked to a lethal phenotype and are thus expected to induce constitutive FGFR3 dimerization. Surprisingly, we see very modest effects on FGFR3 dimerization. Furthermore, we see indications of structural perturbations in the FGFR3 dimer due to the mutations. Thus, this study does not support the simple view that the TDI cysteine mutations cause pathologies by inducing constitutive FGFR3 dimerization.

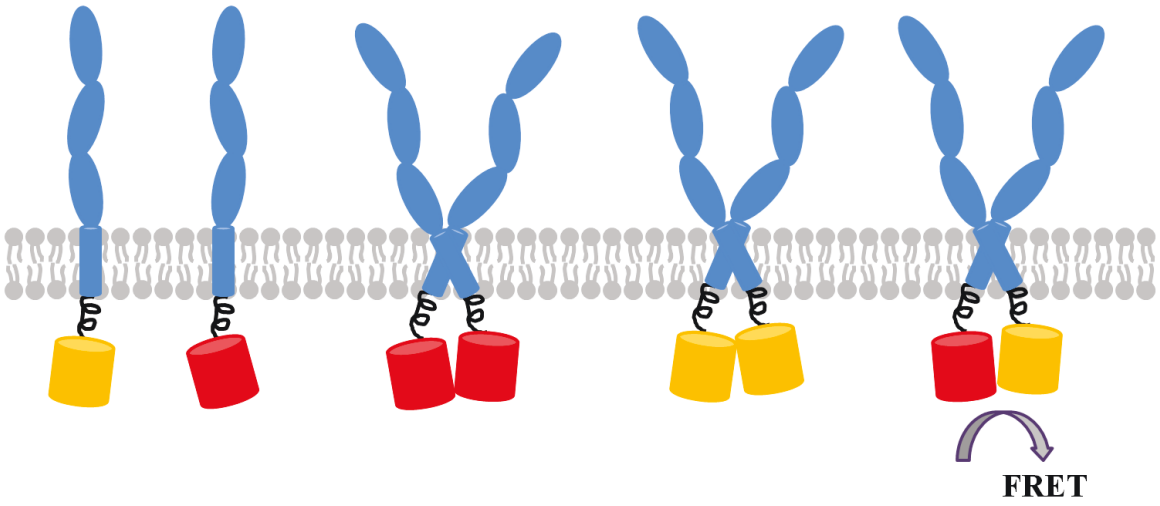

Figure 3-1. Cartoon representation of the species present in homodimer FRET experiments.

Receptors (in blue) are labeled with a FRET donor (YFP, shown as a yellow barrel) or a FRET acceptor (mCherry, red barrel). A sample of labeled receptors will consist of monomers and acceptor-acceptor, donor-donor, and acceptor-donor homodimers. The acceptor-donor homodimer is the only species that contributes to measured FRET efficiency. We use probability to account for the presence of acceptor-acceptor and donor-donor homodimers (Equation 3-7).

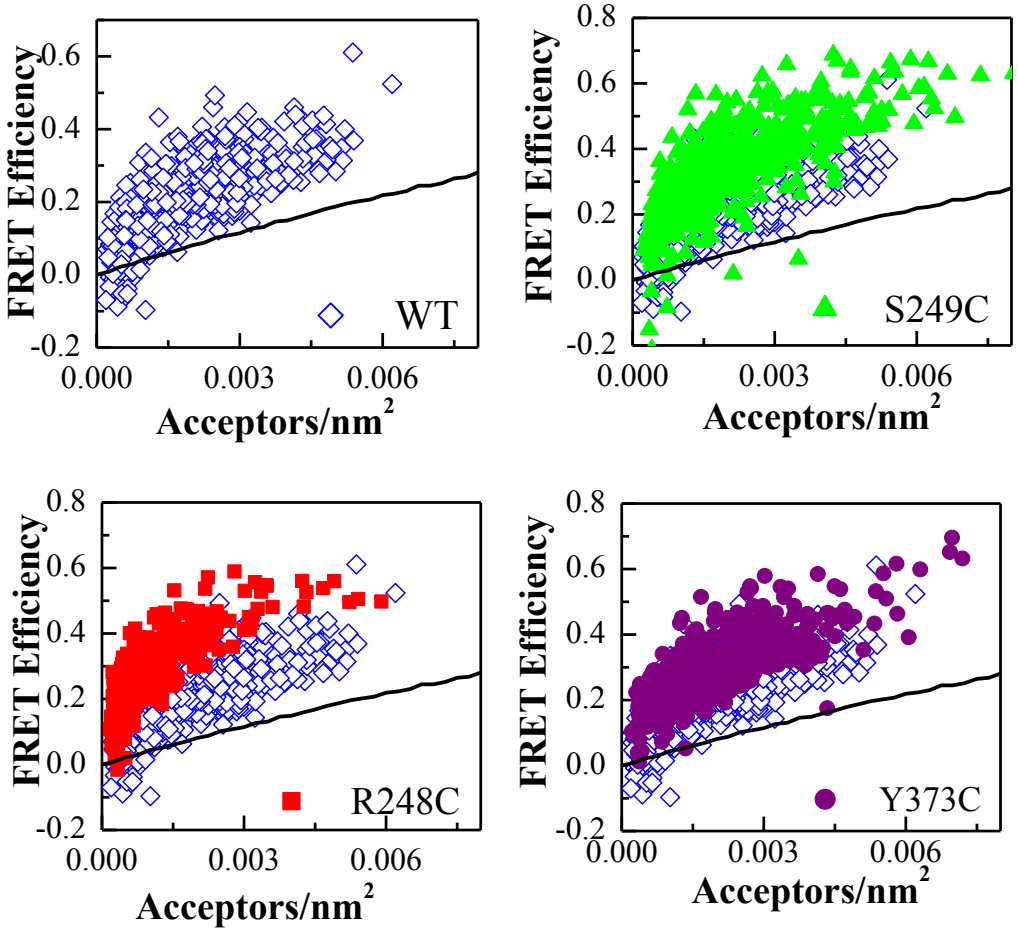

Figure 3-2. FRET efficiency versus acceptor concentration for wild-type FGFR3 and the TD mutants.

Wild-type FGFR3, FGFR3_R248C, FGFR3_S249C, and FGFR3_Y373C are shown with open blue diamonds, filled red squares, filled green triangles, and filled purple circles, respectively. Each data point represents a single vesicle and has a distinct donor concentration. The solid black line indicates the proximity FRET, known to occur due to random approach of donors and acceptors within distances of 100 Å in the membrane. The FRET data lie above this proximity line, indicating specific FGFR3 interactions. The FRET efficiencies measured for the mutant receptors are higher than those measured for

the wild-type receptors, indicating that the TDI mutations have an effect on FGFR3 dimerization.

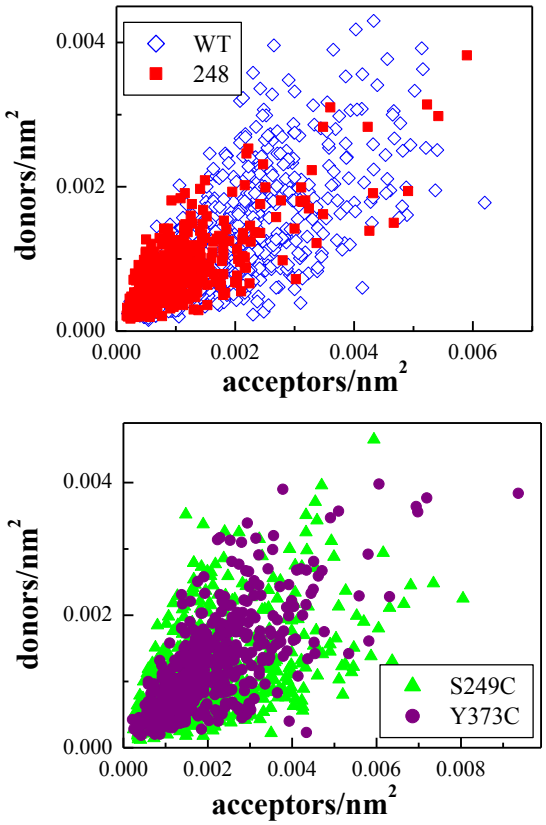

Figure 3-3. Donor concentration versus acceptor concentration for WT FGFR3 and the TD mutants.

Wild-type FGFR3, FGFR3_R248C, FGFR3_S249C, and Y373C are shown with open blue diamonds, filled red squares, filled green triangles, and filled purple circles, respectively. The wide spread of donor to acceptor concentrations explains the apparent wide spread of FRET efficiency observed in Figure 3-2.

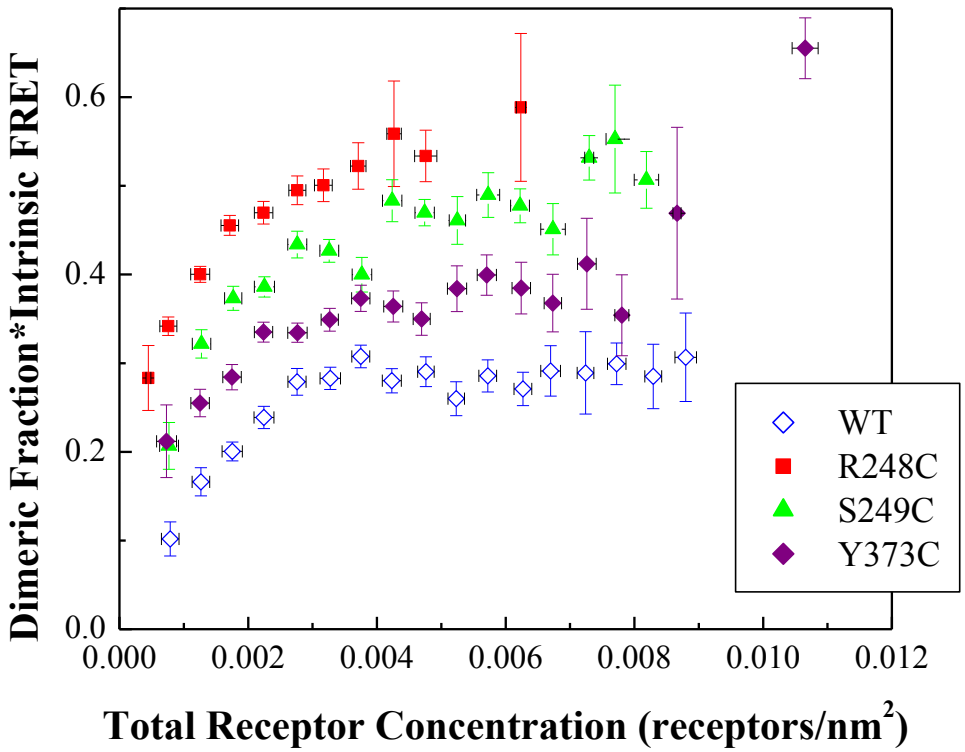

Figure 3-4. Dimeric fraction times Intrinsic FRET, versus total receptor concentration for WT FGFR3 and the TD mutants.

These data are obtained from the FRET data in Figure 3-2 using Equation 3-9, and are averaged within 5×10^{-4} receptors/nm^2 wide concentration bins. A reduced χ^2 analysis demonstrates that the mutant data sets are significantly different from the wild-type data set.

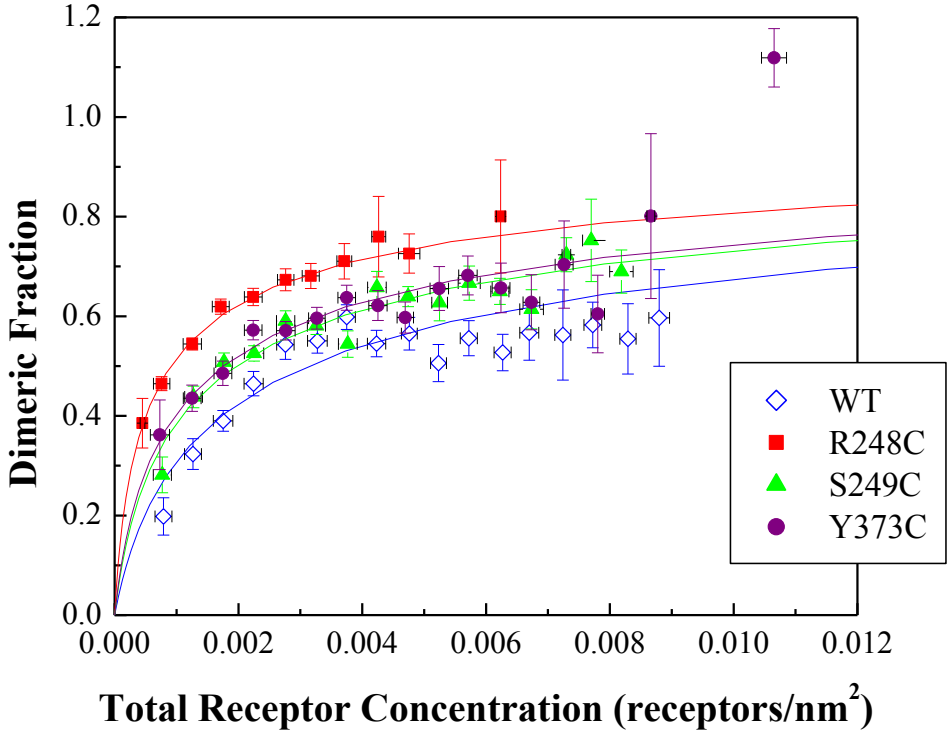

Figure 3-5. Dimeric fraction versus receptor concentration for WT FGFR3 and the TD mutants.

Averaged data are shown in $5x10^{-4}$ receptors/nm^2 wide bins. The solid line is the best fit to the homodimerization model, given by Equations 3-1 and 3-6, plotted for the optimized parameters in Table 3-1. A reduced χ^2 analysis demonstrates that the differences between the mutant and wild-type dimeric fractions are statistically significant.

	Wild-type	**FGFR3_R248C**	**FGFR3_S249C**	**FGFR3_Y373C**
K	290 ± 60	1110 ± 130	500 ± 100	590 ± 110
Ẽ	0.51 ± 0.04	0.74 ± 0.03	0.73 ± 0.03	0.62 ± 0.03
ΔG (kcal/mol)	-3.4 ± 0.1	-4.2 ± 0.1	-3.7 ± 0.1	-3.8 ± 0.1
ΔΔG (kcal/mol)		-0.8 ± 0.1	-0.3 ± 0.1	-0.4 ± 0.1
d (Å)	53 ± 1	45 ± 1	45 ± 1	49 ± 1

Table 3-1. Optimal parameters describing homodimerization of WT FGFR3 and the TD mutants.

The values of K and Ẽ are optimized in a two parameter fit of the homodimerization model to FRET data. Dimer stability, ΔG, is calculated according to Equation 3-3. The effect of the mutations on dimer stability, ΔΔG, is the difference between the wild-type and mutant dimer stabilities. The distance between fluorescent proteins, d, is calculated from Ẽ according to Equation 3-8.

CHAPTER FOUR Conformational Changes in FGFR1 and FGFR2 Homodimers in Response to the fgf Ligands that Regulate Embryonic Limb Development

Receptor-Ligand Interactions and Embryonic Limb Development

Activation of membrane-bound receptors through ligand binding is a common motif in cell signaling pathways (4,10-13,86,87). Despite the recurrence of this activation mechanism, exactly how a receptor is able to discriminate between its many ligands, and to produce differential signaling outcomes, remains an open question (14,22,71,86,88-90). Variations in receptor-ligand binding constants and spatiotemporal expression of both receptors and ligands provide some insight into this question (22,71,91), but fall short of a full explanation. Confounding factors include uniformity in the downstream signaling pathway of an activated receptor and co-expression of ligands (14,88,89). Conventional wisdom points toward the hypothesis that there are additional, unexplored mechanisms whereby receptors distinguish between their ligands.

The process of embryonic limb development is commonly employed as a model system in which to probe receptor-ligand interactions (89). This process is initiated when mesenchymal tissue accumulates under the ectoderm to form the limb bud. Signals from the mesenchyme induce formation of the apical ectodermal ridge (AER) from the ectodermal tissue. Subsequently, full limb development is regulated by both the mesenchyme and the AER. All steps in this process are primarily regulated through the FGFR subfamily of RTKs (22,88-94). FGFR1 is expressed exclusively in the mesenchyme, and FGFR2 is found only in the ectoderm/AER. The mesenchyme produces the fgf16 and fgf18 ligands, and the AER expresses the fgf4, fgf8, and fgf9 ligands. Ligands produced in the AER preferentially bind receptors in the mesenchyme,

and vice versa (88,90,92-96). Deletion of each of these five ligands, or a combination thereof, yields unpredictable disruptions to limb development, which can range in severity from lethality to anatomical abnormalities to no observable effects (22,89,92,93).

The five fgf ligands implicated in embryonic limb development come from a family of 18 fgfs (13,14,71). The fgf ligands exhibit high sequence and structural homology, and activate FGFRs by binding the DII and DIII immunoglobin-like domains of the EC domain of a receptor. Only two of the four FGFRs are involved in embryonic limb development, though all four FGFRs display similarities in sequence and structure. FGFR1 and FGFR2 exhibit a particularly high homology, and have been shown to be functionally redundant in some cases. In the context of so much apparent similarity, the mechanism by which FGFR1 and FGFR2 are able to distinguish between the five fgf ligands and orchestrate the specific process of limb development remains unclear (14,22,88,89).

Previous work in the lab leveraged the QI-FRET technique to measure changes in the conformation of the FGFR1, FGFR2, and FGFR3 homodimers in response to the activating ligands fgf1 and fgf2 (18). In those experiments, the IC domain of each receptor was substituted with a fluorescent protein (eYFP or mCherry), to allow for FRET detection of homodimer formation. Samples were saturated with each ligand, to ensure that all receptors existed in the fully liganded homodimer state, and the Intrinsic FRET was measured for each receptor-ligand pair. Intrinsic FRET is the FRET efficiency in a given dimer. It is a conformational parameter that depends only on the separation of fluorophores in a dimer, and is independent of the propensity for dimer formation. For all three receptors, the measured Intrinsic FRET was smaller in the presence of fgf1 as

compared to fgf2. This work contributes to a growing body of evidence that homodimer conformation might contribute to the mechanism by which receptors distinguish between their various activating ligands (71,97).

Here, we consider the question of how receptors differentiate between their activating ligands in the context of embryonic limb development. Our selection of receptors and ligands is based on previous studies in chick embryos (89,95,96) and mice (22,88,89,91-93). Limited studies in humans (94) verify the assumption that the same receptors and ligands regulate development of human limbs. We work with human FGFR1c and FGFR2c, where the IC domain of each receptor has been replaced with a flexible linker followed by a fluorescent protein, and the human fgf4, fgf8, fgf9, fgf16, and fgf18 activating ligands. We use the QI-FRET method to measure the Intrinsic FRET for each of the ten possible receptor-ligand pairs. We examine our results for clues as to how each FGFR differentiates between the five activating ligands present in embryonic limb development.

Fully Liganded Homodimer Model

In these experiments, we consider a special case of the homodimerization model presented in Chapter Three. Receptors are saturated with ligand, which shifts the equilibrium of Equation 3-1 such that all receptors exist as homodimers. That is, the association constant, K, is infinite, and the concentration of monomers, [M], is equal to zero. Experiments are performed in vesicles, so receptor concentration is constant (Equation 3-4), and dimer fraction, given by Equation 3-5, is equal to one.

Interpretation of Fully Liganded Homodimer FRET Data

Homodimer FRET data is interpreted as presented in Chapter Three. The measured FRET efficiency is corrected for the proximity FRET (77,82), to yield the dimer-specific FRET efficiency, E_D. In typical homodimer FRET experiments, we consider the quantity dimeric fraction times Intrinsic FRET, as given in Equation 3-9. In the case of fully liganded homodimers, f_D is equal to one, so Equation 3-9 reduces to:

$$\tilde{E} = \frac{E_D}{x_A} \tag{4-1}$$

where $\tilde{E}$ is the only unknown. We use Equation 4-1 to directly calculate the Intrinsic FRET in each vesicle.

Intrinsic FRET, or $\tilde{E}$, is the FRET efficiency in a given dimer, which depends on the separation and orientation of the two fluorophores. The fluorescent proteins are attached to the TM domain of the receptors via flexible $(GGS)_5$ linkers, which allows the fluorophores to rotate freely. Under this assumption of free fluorophore rotation, we use Equation 3-8 to calculate the distance between fluorophores in a given homodimer. Figure 4-1 is a cartoon representation of Intrinsic FRET, which helps demonstrate how the binding of different ligands might relate to changes in homodimer conformation. Here, we measure Intrinsic FRET values for fully liganded homodimers in order to compare homodimer conformations in response to various activating ligands.

Statistical Analysis

For each of the receptor-ligand pairs considered here, we analyze a few hundred vesicles. First, we sort vesicles by their Intrinsic FRET values (bin size of 0.05) to generate a histogram. Then, we fit a Gaussian distribution to the histogram. The mean of this Gaussian is the Intrinsic FRET for a given fully liganded homodimer. To estimate the error of our measure for Intrinsic FRET, we employ the bootstrap method. In this

method, a dataset is split into multiple subsets, each of which are fit separately. Then, the results of the fit for each subset (in this case, the mean Intrinsic FRET) are used to calculate an average and a standard deviation

We perform one-way analysis of variance (ANOVA) tests to compare the Intrinsic FRET values measured for a given receptor in the presence of each of the five activating ligands. We test the null hypothesis that the Intrinsic FRET values for all five fully liganded homodimers are the same. If $p < 0.05$, we reject that hypothesis and perform a multiple comparison post-test to identify statistically significant differences among the Intrinsic FRET values for the fully liganded homdimers.

Results

In these experiments, we examined the FGFR1 and FGFR2 homodimers in the presence of five different ligands: fgf4, fgf8, fgf9, fgf16, and fgf18. Both receptors and all five ligands have been shown to play critical roles in embryonic limb development. Each receptor-ligand pair has a unique function, but the molecular basis of how these receptor-ligand pairs vary, and thereby generate different outcomes, remains unclear. To begin to unravel the molecular differences between these receptor-ligand pairs, we measured the Intrinsic FRET, a parameter that reports on dimer conformation, for all ten receptor-ligand pairs. Specifically, we use Intrinsic FRET to assess and compare the homodimer conformation of each receptor in the presence of every ligand.

Experiments were performed with truncated receptors in cell-derived vesicles. We worked with plasmids coding for the EC and TM domains of the FGFR followed by a flexible linker and a fluorescent protein (eYFP or mCherry). The substitution of the IC domain with a fluorophore enables FRET detection of homodimer formation. The

plasmids were expressed in CHO cells, so that truncated receptors were trafficked to the membrane by the native cell machinery and underwent all relevant post-translation modifications. To obtain vesicles containing the fluorescently-labeled FGFR, these CHO cells were subjected to a gentle protocol that uses changes in osmotic pressure to induce vesicle production (43). The lipid and protein content of these vesicles is representative of the membranes of live cells (44). Vesicles were harvested and placed in a glass-bottomed chamber slide for further analysis.

Ligand was added to each sample at a saturating concentration of 5 μg/mL. This high concentration of ligand was selected because it exceeds the receptor-ligand binding constant by multiple orders of magnitude (98-101), ensuring that all receptors will exist as homodimers (that is, the equilibrium of Equation 3-1 will be pushed entirely to the [D] state). Samples were incubated at room temperature for 1 hour following ligand addition, to allow for the ligand binding and homodimer formation processes to reach equilibrium. This time allocation far exceeds the literature estimates for the kinetics of both the fgf binding and FGFR dimerization reactions (98,101). Vesicles were imaged according to the QI-FRET protocol, which yields the acceptor concentration, donor concentration, and FRET efficiency in each vesicle. We prepared a minimum of three samples and imaged between 200 and 500 vesicles for each of the ten possible receptor-ligand pairs

FGFR1 and FGFR2 form fully liganded homodimers in the presence of fgf4, fgf8, fgf9, fgf16, and fgf18

Here, we consider the FGFR1 and FGFR2 homodimers in the presence of the five ligands—fgf4, fgf8, fgf9, fgf16, and fgf18—that regulate embryonic limb development.

QI-FRET results for FGFR1 and FGFR2 are displayed in Figure 4-2 and Figure 4-3, respectively, with panels A through E corresponding to fgf4, fgf8, fgf9, fgf16, and fgf18.

The panel for each receptor-ligand pair consists of four plots. In the top half of the panel, we display raw data from QI-FRET experiments. In the upper left-hand corner, we plot measured FRET efficiency as a function of acceptor concentration. Each point represents a single vesicle. The solid black line indicates the proximity FRET, or the FRET efficiency that arises due to random close approach of receptors in the two-dimensional membrane. For each of the receptor-ligand pairs examined, the measured FRET efficiencies exceed proximity FRET, suggesting specific receptor-receptor interactions in the presence of ligand. In the upper right-hand corner, we plot donor concentration versus acceptor concentration. Both concentrations affect measured FRET efficiency and are accounted for when calculating the Intrinsic FRET in each vesicle.

Next, measured FRET efficiencies are corrected for proximity FRET as described previously (77), yielding the dimer-specific FRET efficiencies, E_D. In the lower left-hand corner, we plot E_D as a function of total receptor concentration. For all of the receptor-ligand pairs studied here, dimer-specific FRET efficiency is constant as a function of receptor concentration, indicating that all receptors exist as fully liganded homodimers. This observation verifies the assumption that the saturating ligand conditions shift the equilibrium of Equation 3-1 entirely to the dimer state.

Finally, the Intrinsic FRET is calculated for each vesicle according to Equation 4-1. These results are binned to generate a histogram, which is displayed in the lower right-hand corner. The blue bars represent binned experimental data, and the solid red

line is the best fit Gaussian distribution. The mean of this Gaussian distribution is the Intrinsic FRET for the receptor-ligand pair being considered.

For the FGFR1 homodimer bound to the activating ligands fgf4, fgf8, fgf9, fgf16, and fgf18, we measure Intrinsic FRET as 0.506 ± 0.001, 0.417 ± 0.009, 0.494 ± 0.010, 0.432 ± 0.010, and 0.510 ± 0.002, respectively. The analogous values for the FGFR2 homodimer are 0.644 ± 0.009, 0.580 ± 0.007, 0.651 ± 0.010, 0.632 ± 0.004, and 0.646 ± 0.004. Equation 3-8 relates Intrinsic FRET to the distance, d, between fluorophores in a homodimer. We use that relation to estimate the inter-fluorophore distance in each fully liganded homomdimer. The Intrinsic FRET and inter-fluorophore distance for all ten receptor-ligand pairs examined here are tabulated in Table 4-1.

Conformational changes in the FGFR1 and FGFR2 homodimers in the presence of some ligands

We perform an ANOVA test to compare the Intrinsic FRET values for the FGFR1 homodimer in the presence of each of the five activating ligands. The p-value for the initial ANOVA test is 4.5×10^{-8}, so we reject the null hypothesis that the Intrinsic FRET for all five liganded FGFR1 homodimers is the same. The multiple comparison post-test indicates that the FGFR1 homodimer conformations in the presence of fgf8 and fgf16 are statistically the same as each other and different from the homodimer conformations in the presence of fgf4, fgf9, and fgf18, which form a second statistical group.

We follow the same protocol to compare Intrinsic FRET values for the FGFR2 homodimer. We reject the null hypothesis that the five FGFR2 homodimer conformations are the same ($p = 1.8 \times 10^{-6}$). The post-test reveals that Intrinsic FRET for the liganded

FGFR2 homodimers in the presence of fgf4, fgf9, fgf16, and fgf18 are statistically the same as each other, and different from the Intrinsic FRET in the presence of fgf8.

The FGFR1 and FGFR2 Intrinsic FRET values and results of both ANOVA tests are displayed in Figure 4-4.

Discussion

In these experiments, we measure changes in the conformation of the FGFR1 and FGFR2 homodimer, seen through changes in Intrinsic FRET, in response to five activating ligands (see Figure 4-4). This result is another piece of evidence in support of the hypothesis that homodimer conformation is a key component of how a receptor distinguishes between ligands (71,97). However, our results do not provide much insight into the mechanistic underpinnings of receptor-ligand interactions in embryonic limb development. Differences in measured Intrinsic FRET do not depend on the tissue of ligand origin. Furthermore, they are small as compared to those measured for FGFR1, 2, and 3 in response to fgf1 and 2 (18), and do not follow any other obvious trend, including magnitude of the receptor-ligand binding constant (99,101).

It is worth noting the possibility that receptor-ligand pairs with the same Intrinsic FRET might have very different homodimer conformations. As diagrammed in Figure 4-1, Intrinsic FRET reports on changes in homodimer conformation through the separation of fluorophores. Since fluorescent proteins are attached to the TM domain of each receptor by flexible linkers, Intrinsic FRET is believed to be most sensitive to changes in the separation of the C-termini of the TM domains. TM domain conformation depends on both helix separation and rotation, both of which have been shown to influence signaling (27,102). Intrinsic FRET cannot capture rotational changes in TM

helix orientation or overall homodimer conformation, which may explain why so many of the receptor-ligand pairs studied here are indistinguishable from each other.

Additional experiments should be performed to address the questions left unanswered by this work. First, the possibility of multiple homodimer conformations should be more completely explored. RTKs are hypothesized to have multiple dimerization interfaces. This idea is supported by work with a diverse array of techniques, including traditional biochemistry (102), fluorescence (30,103), nuclear magnetic resonance spectroscopy (27), and molecular dynamics simulations (104) . These types of experiments should be replicated, in order to identify the possible dimerization interfaces of FGFR1 and FGFR2. Mutagenesis and additional QI-FRET experiments can confirm the functional in/significance of these interfaces and may allow for direct correlation between Intrinsic FRET and homodimer conformation for each receptor-ligand pair.

A second set of experiments should focus on tying the physical models of receptor activation generated by QI-FRET experiments to biological outcomes. In previous work, phosphorylation of FGFR3 was shown to scale linearly with Intrinsic FRET (18). Thus, Western blots should be performed, in order to assess the phosphorylation of both FGFR1 and FGFR2 in response to the five activating ligands.

Together, QI-FRET experiments, investigation of dimerization interfaces, and Western blots may produce further insight into the molecular mechanism by which receptors distinguish between their activating ligands during embryonic limb development.

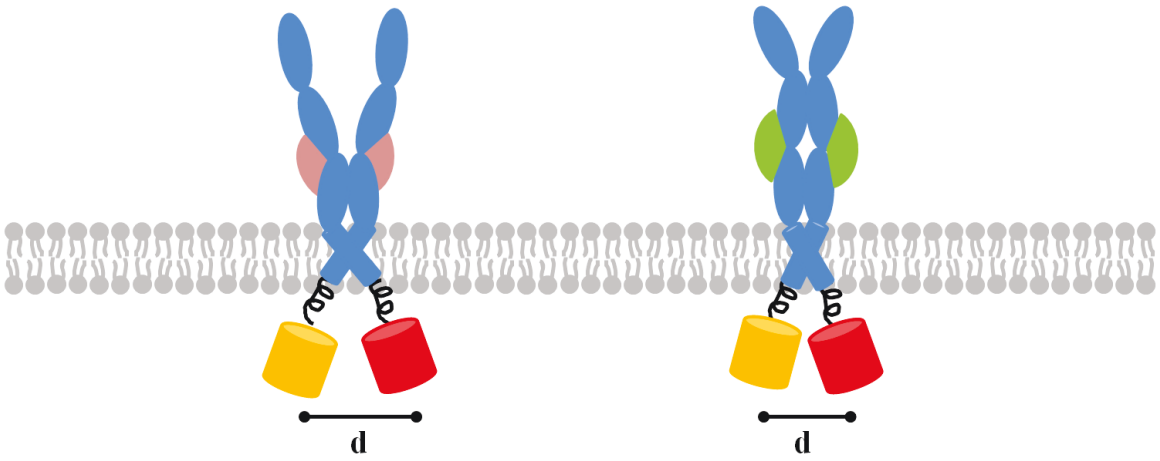

Figure 4-1. Cartoon representation of changes in Intrinsic FRET in liganded homodimers. RTK homodimer conformation can change in response to the binding of different ligands. We probe homodimer conformation through Intrinsic FRET, or the FRET efficiency in a given homodimer. Intrinsic FRET is a parameter that depends primarily on the distance, d, between fluorophores in a homodimer (see Equation 3-8).

A

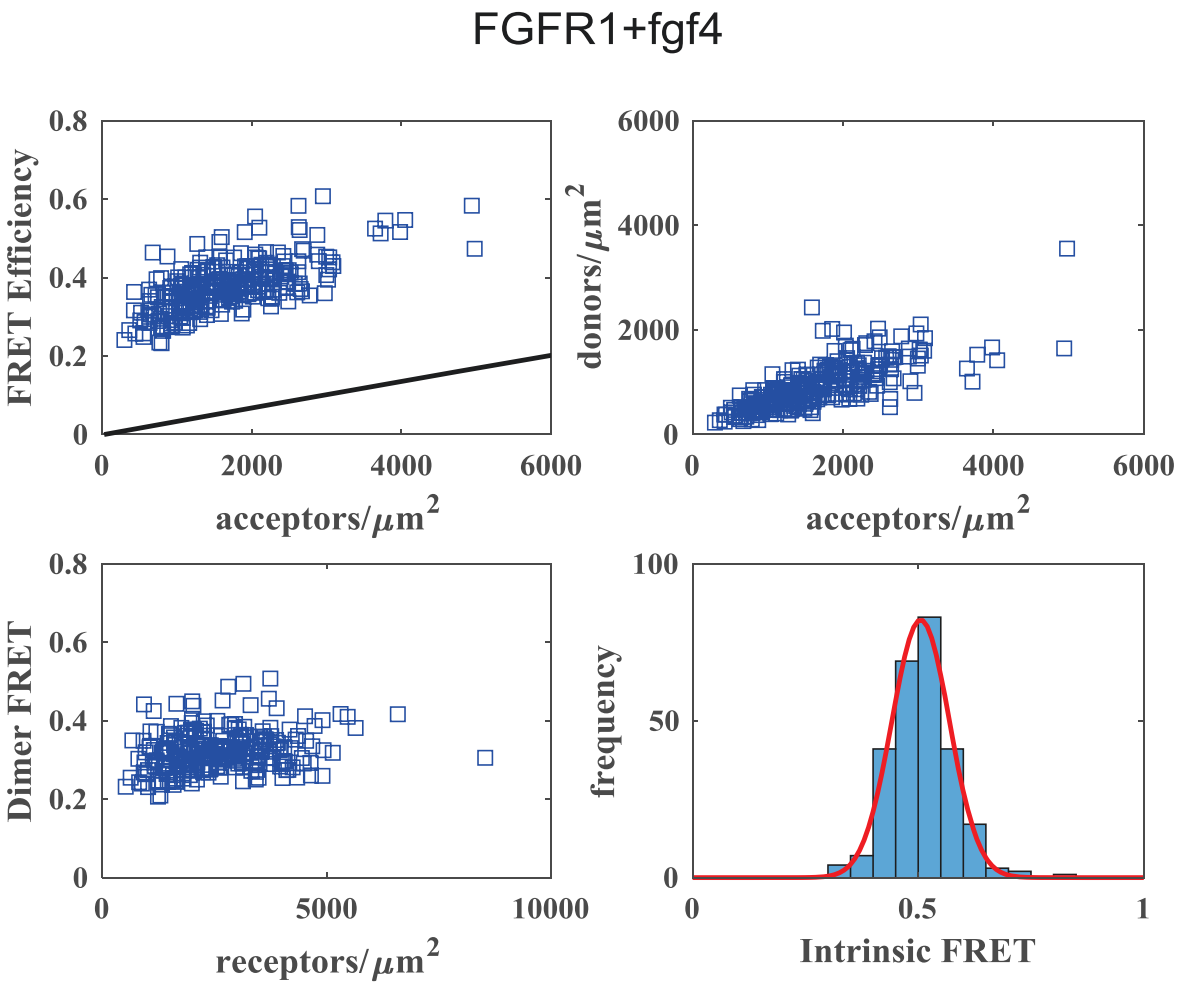
FGFR1+fgf4
FRET Efficiency
acceptors/μm^2
donors/μm^2
acceptors/μm^2
Dimer FRET
receptors/μm^2
frequency
Intrinsic FRET

B

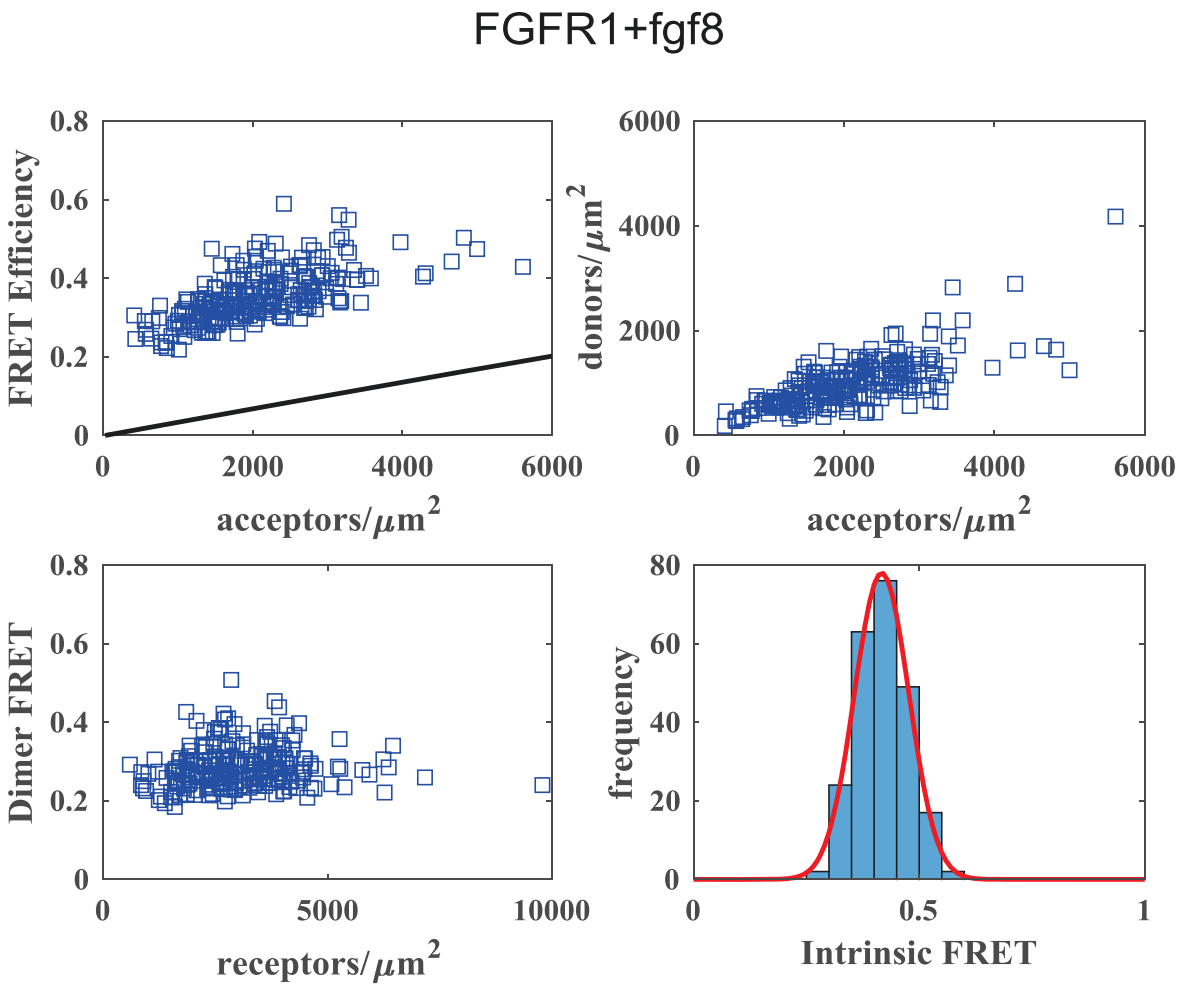
FGFR1+fgf8
FRET Efficiency
acceptors/μm^2
donors/μm^2
acceptors/μm^2
Dimer FRET
receptors/μm^2
frequency
Intrinsic FRET

C

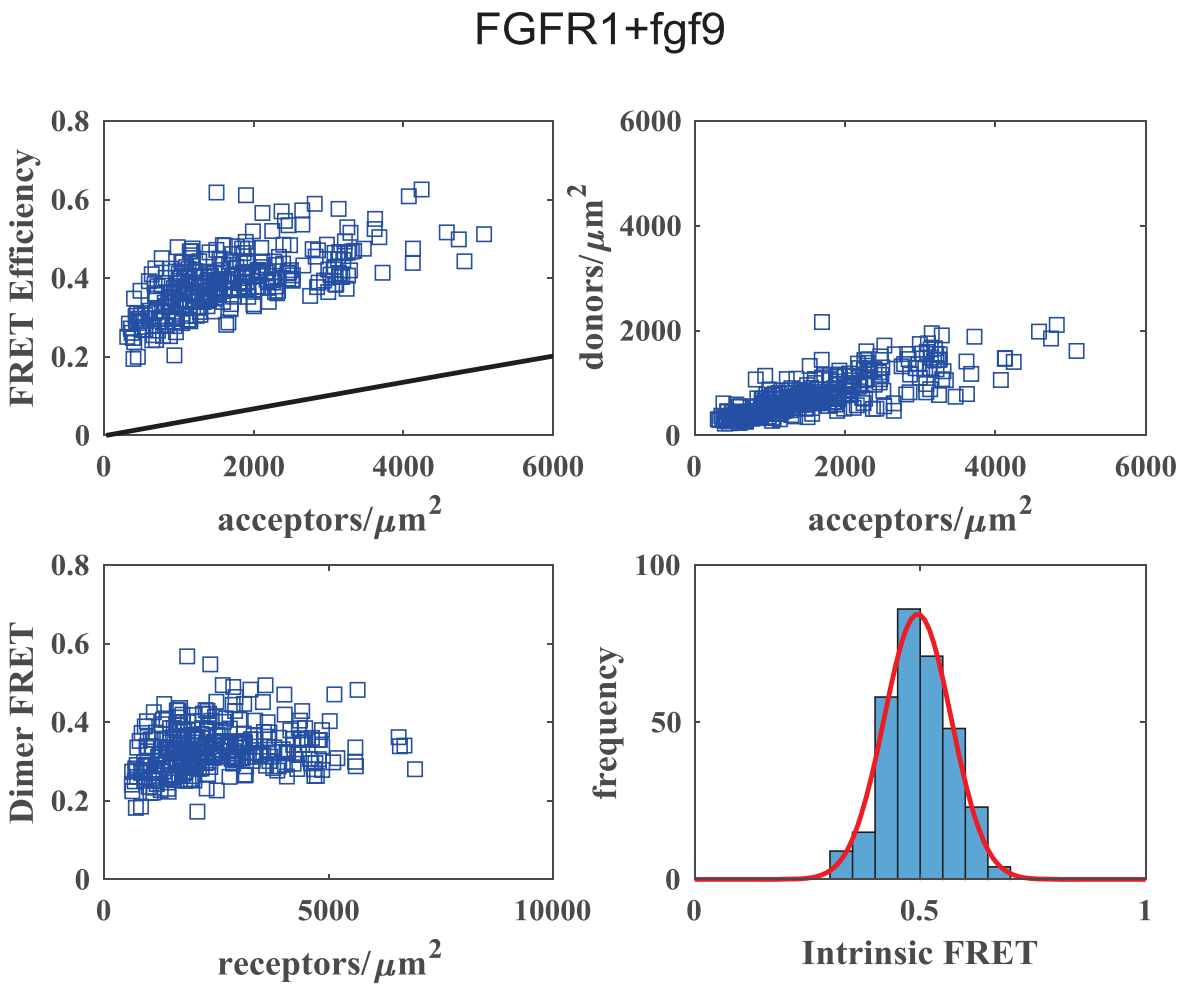
FGFR1+fgf9
FRET Efficiency
acceptors/μm^2
donors/μm^2
acceptors/μm^2
Dimer FRET
receptors/μm^2
frequency
Intrinsic FRET

D

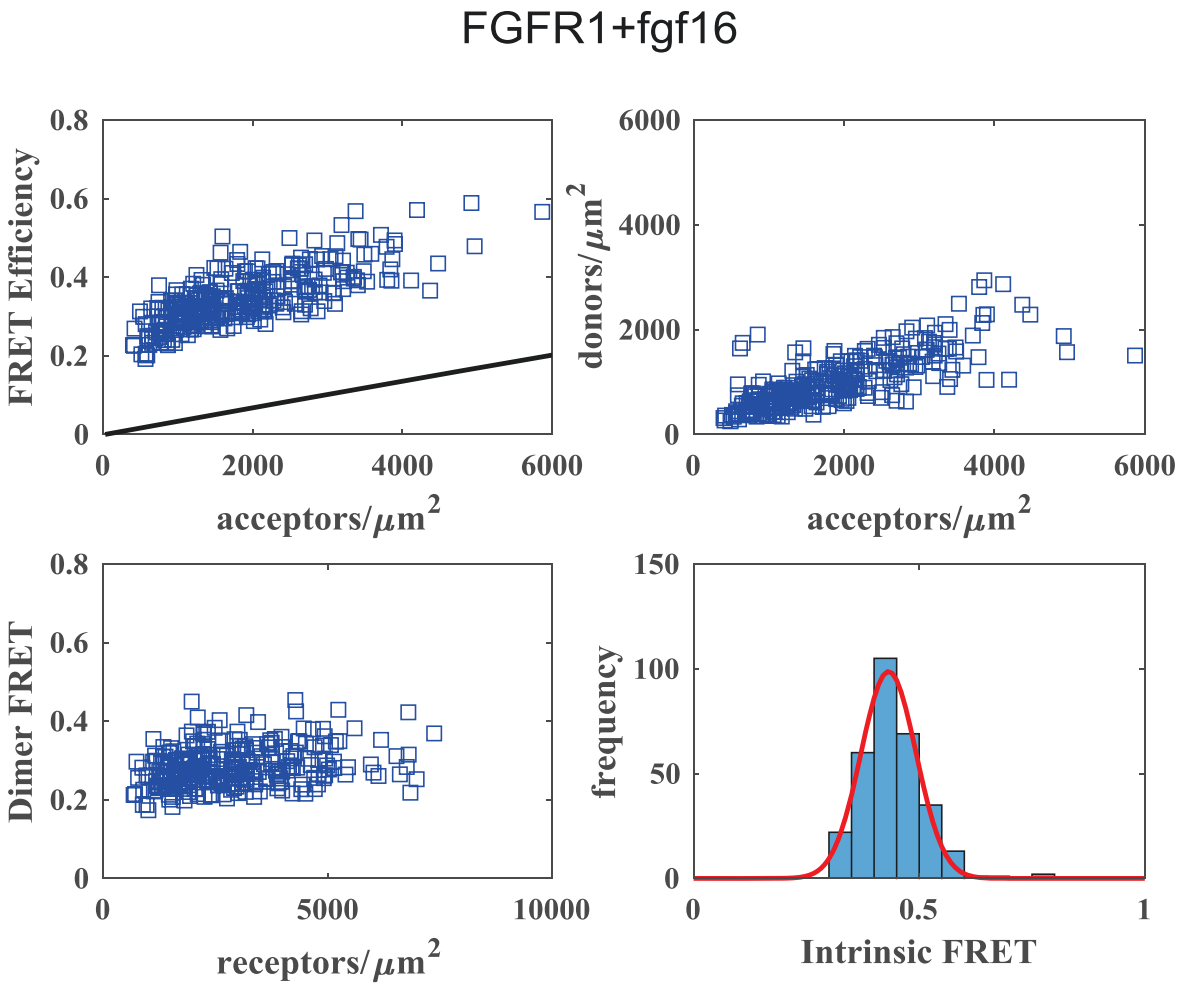
FGFR1+fgf16
FRET Efficiency
acceptors/μm^2
donors/μm^2
acceptors/μm^2
Dimer FRET
receptors/μm^2
frequency
Intrinsic FRET

E

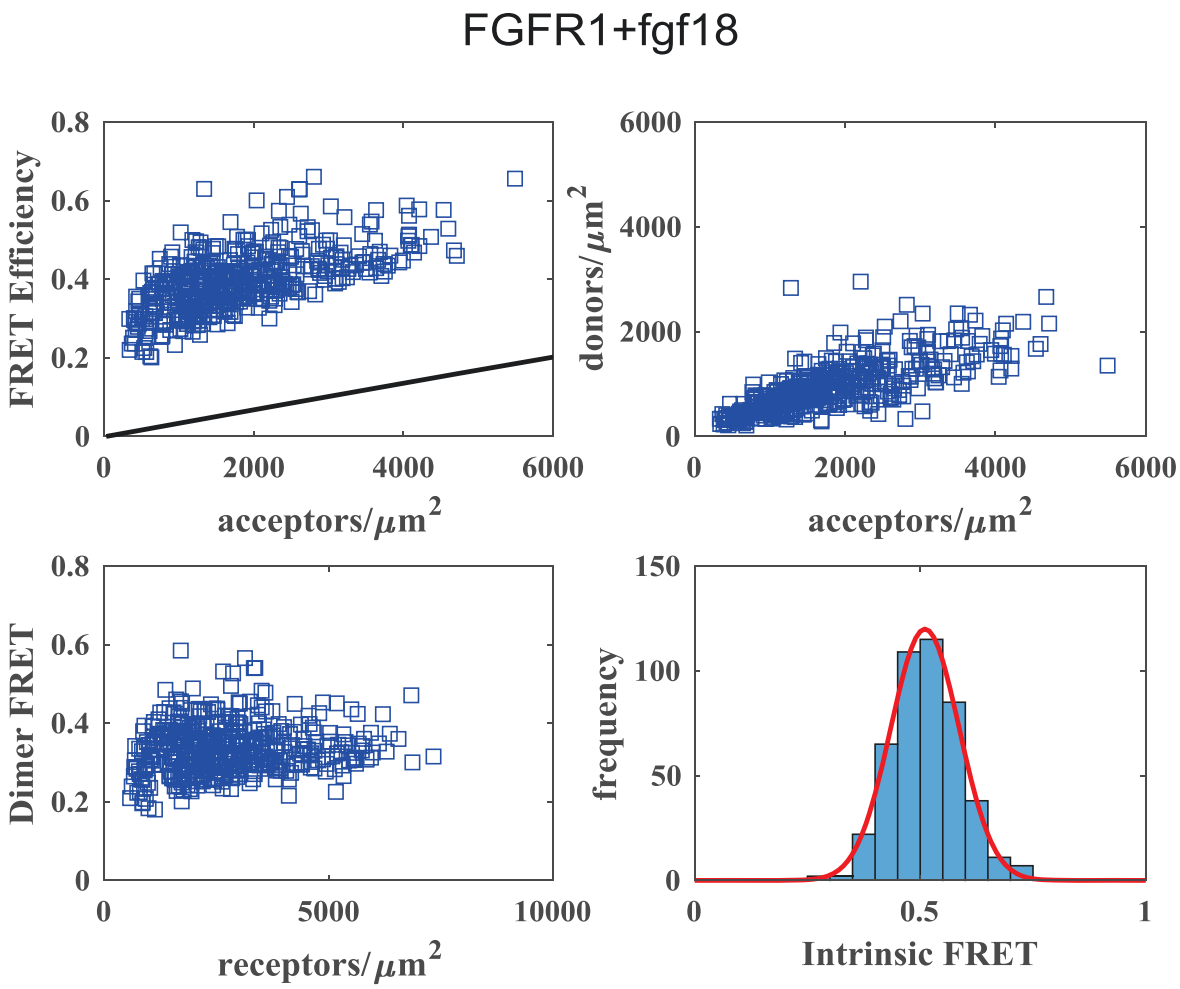

Figure 4-2. FGFR1 homodimerization in the presence of five activating ligands. Results for QI-FRET measurements of FGFR1 activated by fgf4, fgf8, fgf9, fgf16, and fgf18 are shown in panels A through E, respectively. In the upper left-hand corner, FRET efficiency is plotted as a function of acceptor concentration. The solid black line denotes proximity FRET. Each point represents a single vesicle. The upper right-hand corner shows donor versus acceptor concentration in each vesicle. We correct measured FRET efficiency for proximity FRET (77) to find the dimer-specific FRET efficiency. In the lower left-hand corner, we plot measured FRET efficiency as a function of receptor

concentration. Finally, we calculate the Intrinsic FRET in each vesicle (Equation 3-8) and bin these values to generate the histogram in the lower right-hand corner. The solid red line is a Gaussian distribution fit to the histogram.

A

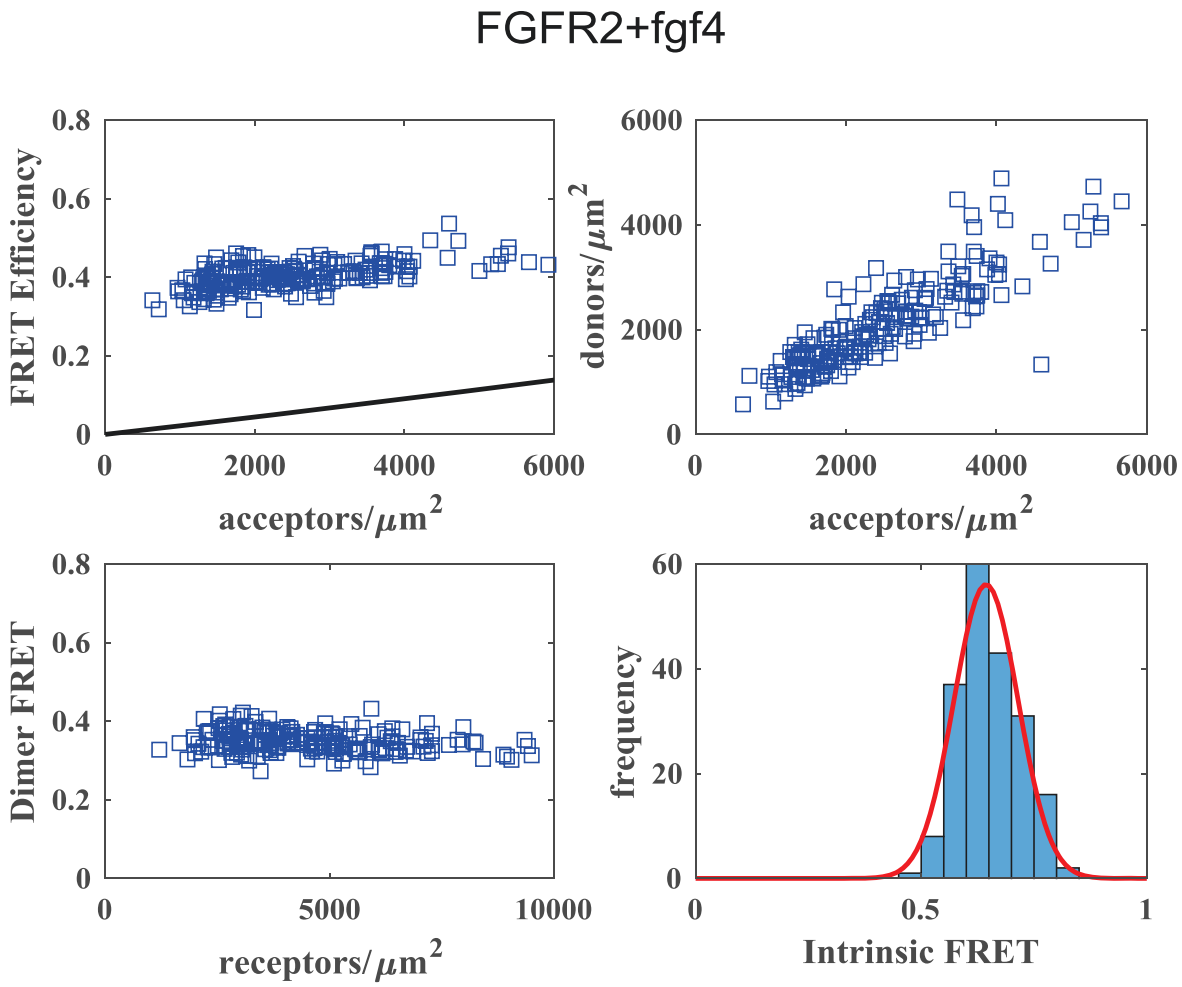
FGFR2+fgf4
FRET Efficiency
acceptors/μm^2
donors/μm^2
acceptors/μm^2
Dimer FRET
receptors/μm^2
frequency
Intrinsic FRET

B

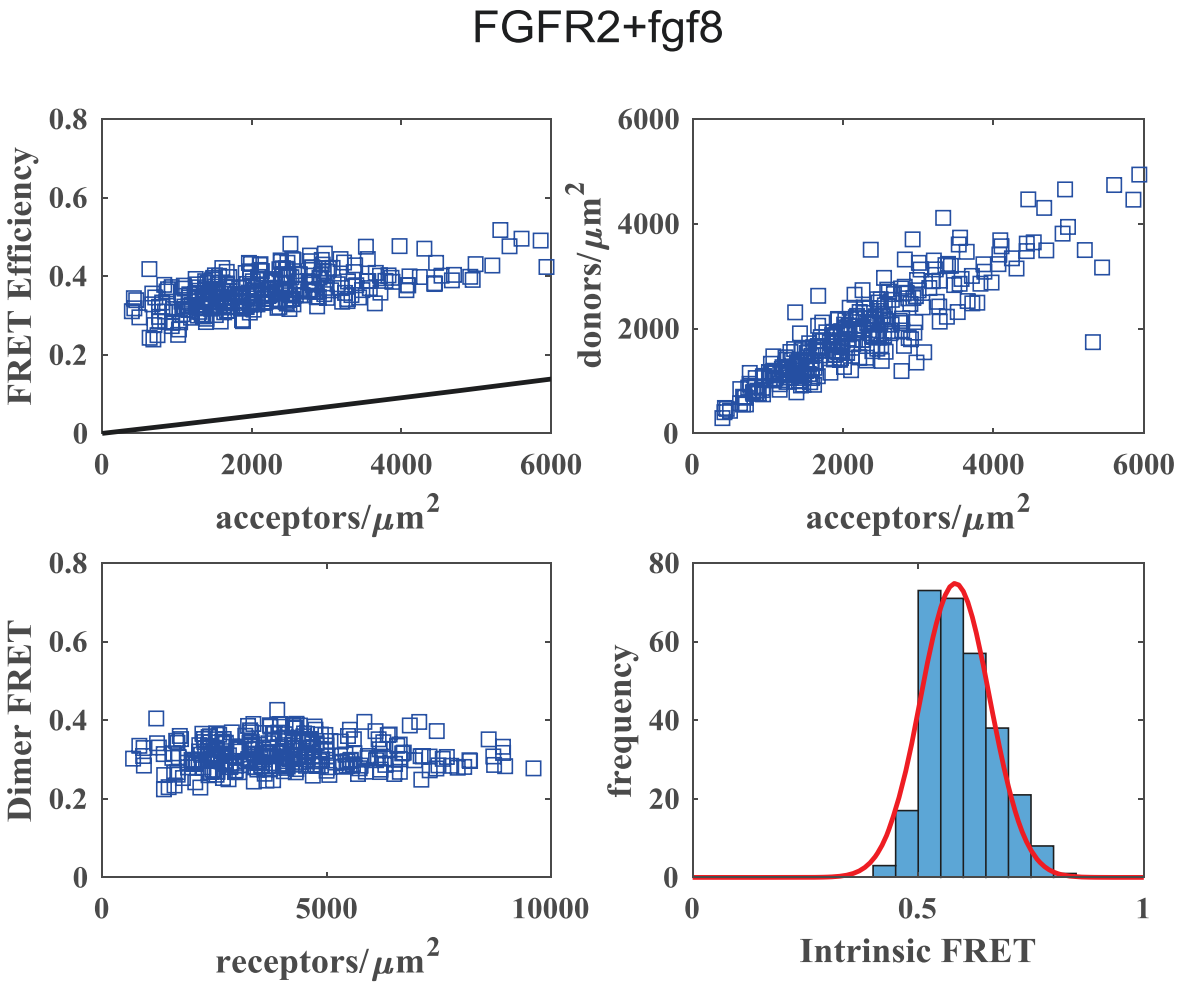
FGFR2+fgf8
FRET Efficiency
acceptors/μm^2
donors/μm^2
acceptors/μm^2
Dimer FRET
receptors/μm^2
frequency
Intrinsic FRET

C

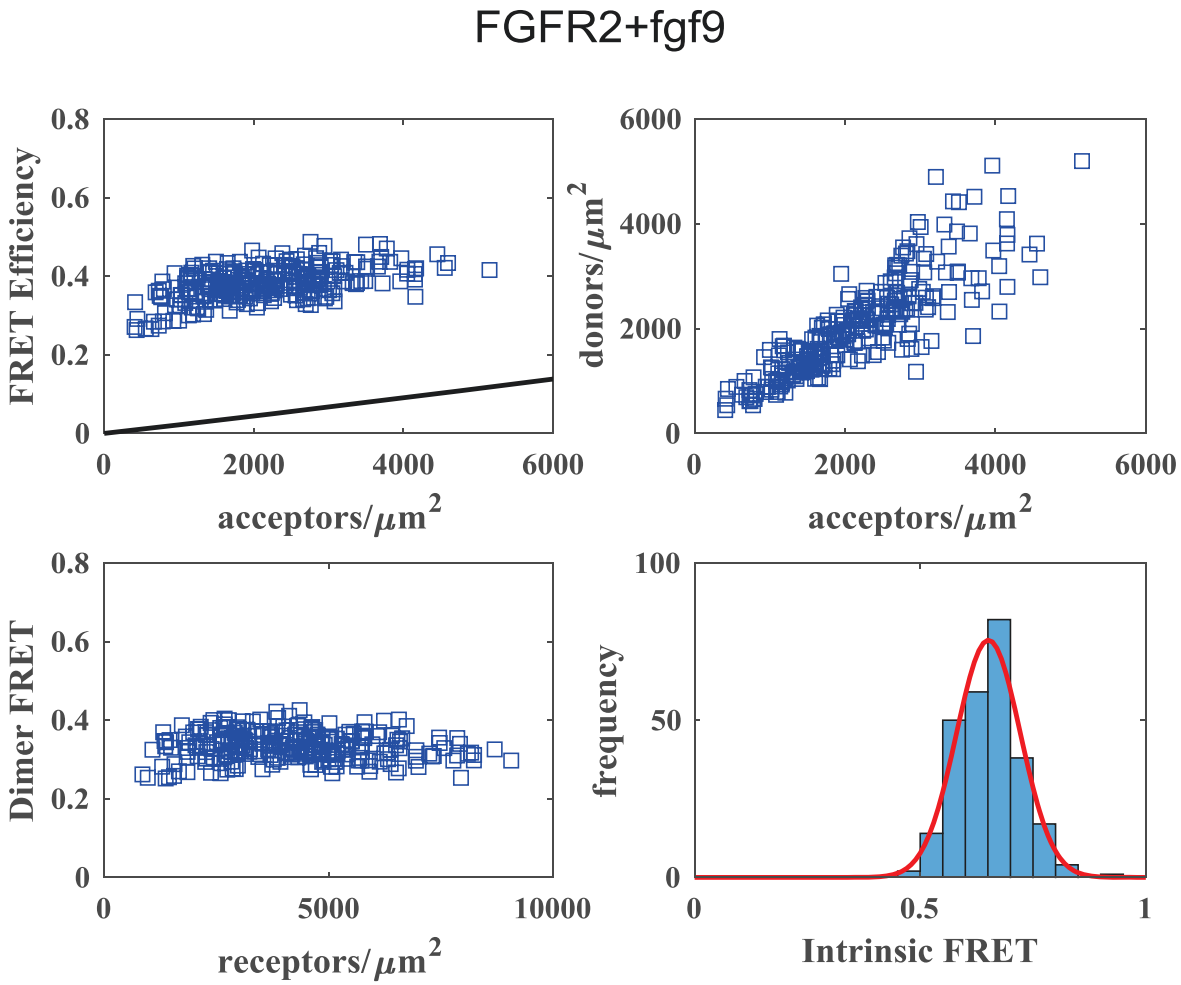
FGFR2+fgf9
FRET Efficiency
acceptors/μm^2
donors/μm^2
Dimer FRET
receptors/μm^2
frequency
Intrinsic FRET

D

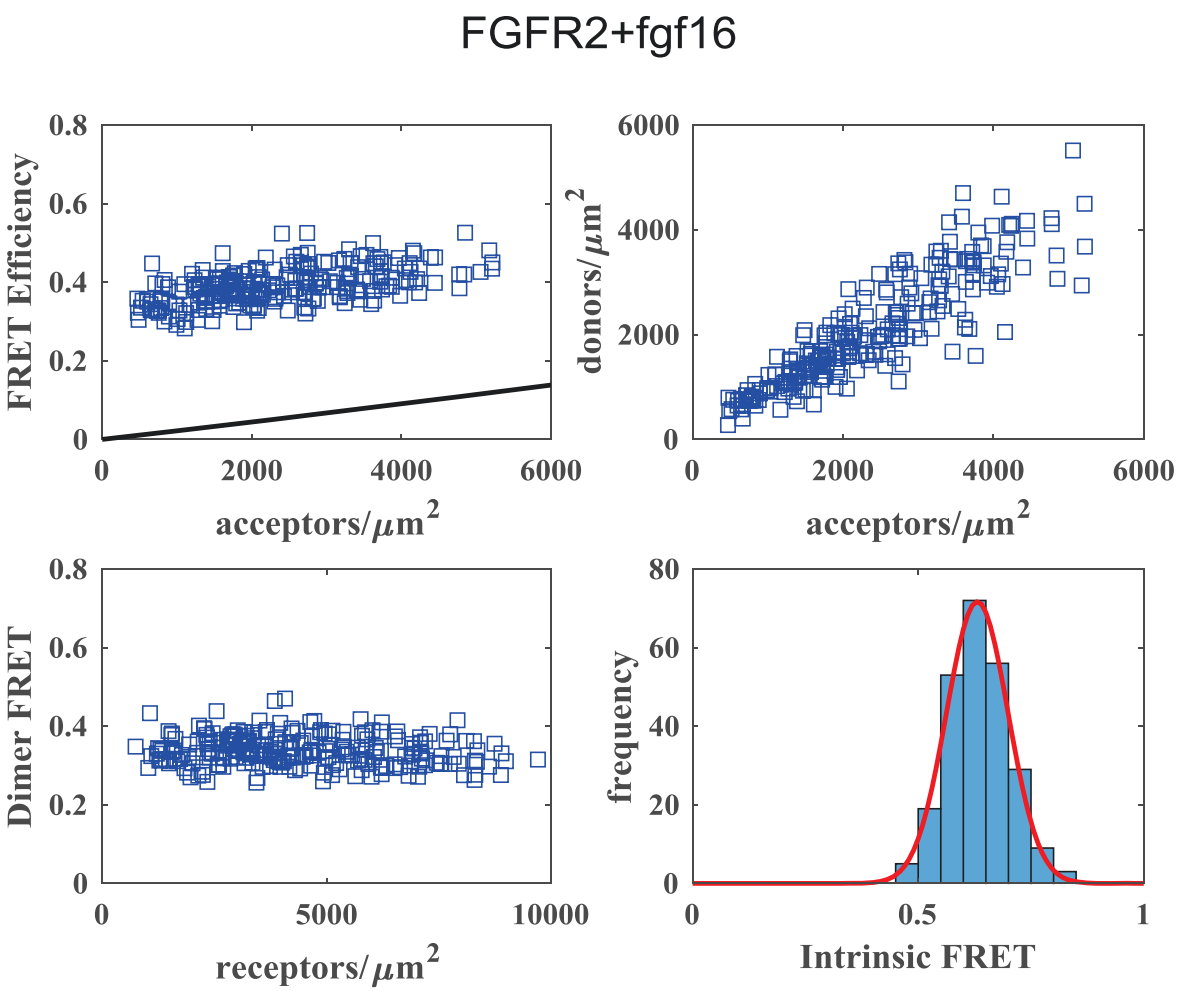
FGFR2+fgf16
FRET Efficiency
acceptors/μm^2
donors/μm^2
acceptors/μm^2
Dimer FRET
receptors/μm^2
frequency
Intrinsic FRET

E

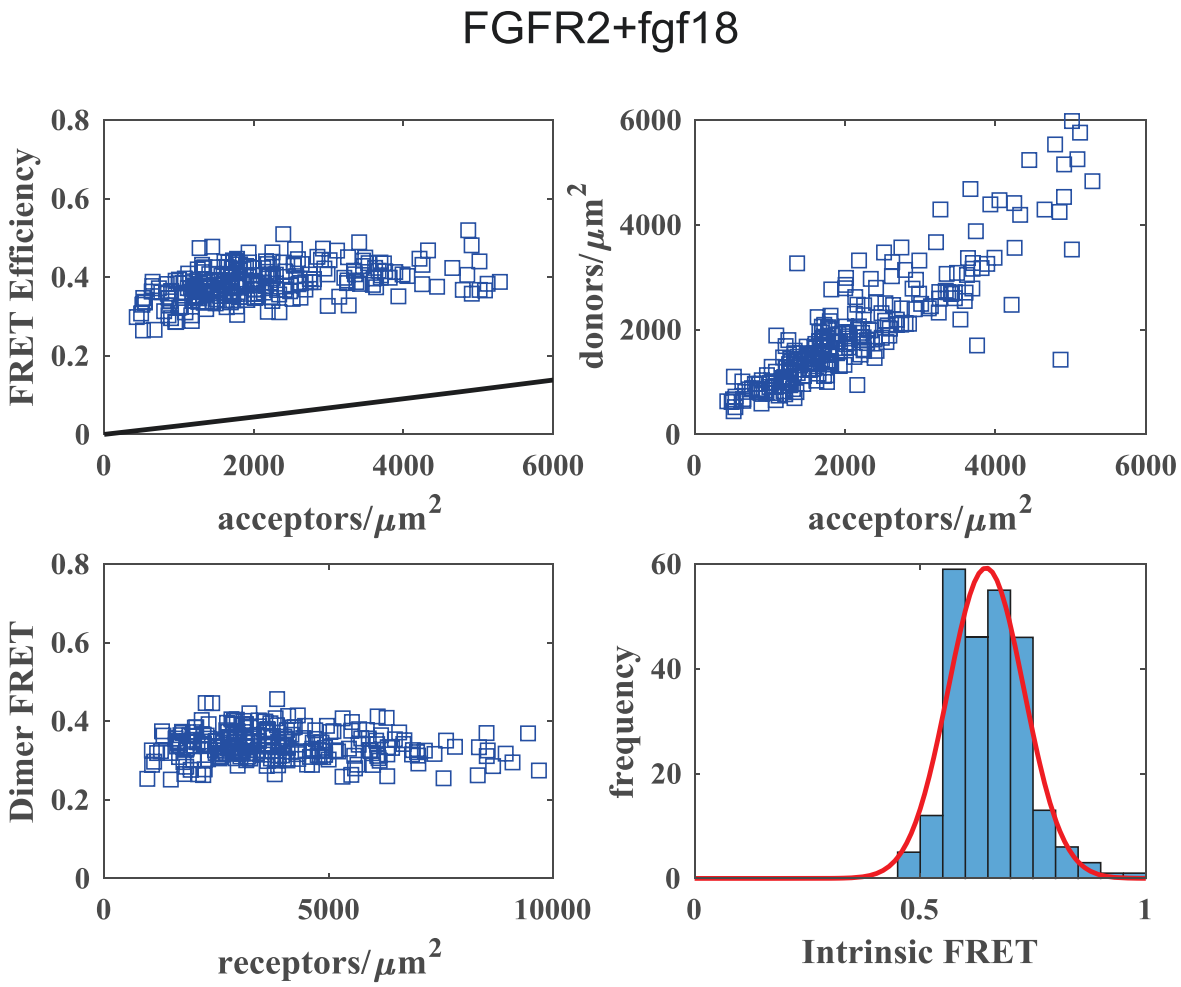

Figure 4-3. FGFR2 homodimerization in the presence of five activating ligands. The results for QI-FRET measurements of FGFR2 and the five ligands. With the exception of receptor identity, this figure is identical to Figure 4-2. See the legend of that figure for more details about each panel.

A

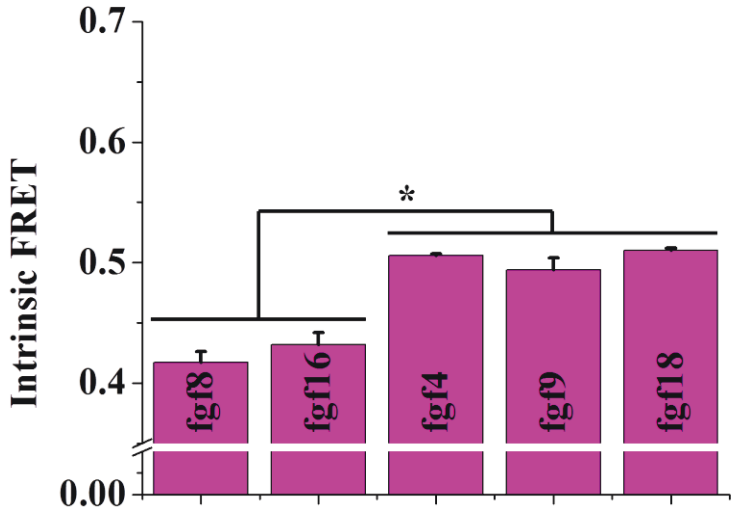

B

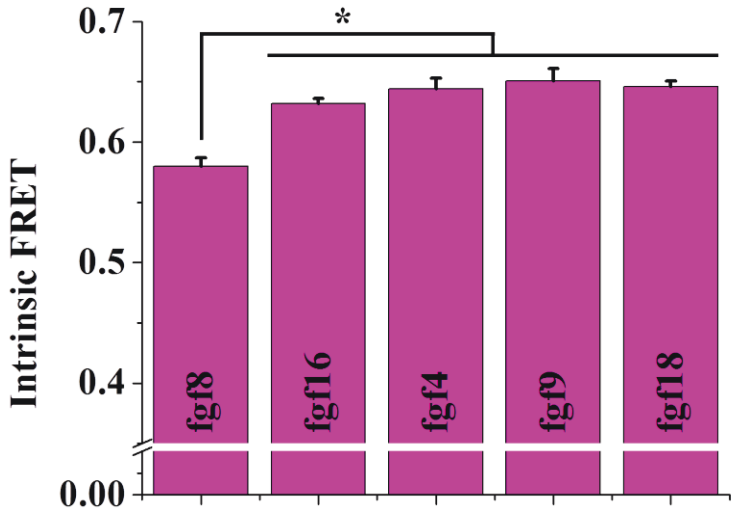

Figure 4-4. Comparison of FGFR1 and FGFR2 Intrinsic FRET in the presence of five activating ligands.

Intrinsic FRET, which reports on homodimer conformation, is graphed for (A) FGFR1 and (B) FGFR2 in the presence of the five ligands that regulate embryonic limb development. ANOVA tests are employed to compare Intrinsic FRET for each receptor in the presence of the five ligands. Results are denoted on the bar graph using groups and asterisks.

		Intrinsic FRET (Ẽ)	distance (Å)
FGFR1	**fgf4**	0.506 ± 0.001	52.9 ± 0.1
	fgf8	0.417 ± 0.009	56.1 ± 0.7
	fgf9	0.494 ± 0.010	53.3 ± 0.7
	fgf16	0.432 ± 0.010	55.6 ± 0.7
	fgf18	0.510 ± 0.002	52.7 ± 0.2
FGFR2	**fgf4**	0.644 ± 0.009	48.1 ± 0.6
	fgf8	0.580 ± 0.007	50.3 ± 0.5
	fgf9	0.651 ± 0.010	47.9 ± 0.7
	fgf16	0.632 ± 0.004	48.5 ± 0.3
	fgf18	0.646 ± 0.005	48.1 ± 0.4

Table 4-1. FGFR1 and FGFR2 Intrinsic FRET and inter-fluorophore distance in the presence of five activating ligands.

Intrinsic FRET for FGFR1 (top half of table) and FGFR2 (bottom half) in response to the five ligands that regulate embryonic limb development. Inter-fluorophore distance is calculated, under the assumption of free fluorophore rotation, using Equation 3-8.

CHAPTER FIVE A New Method to Study Heterodimerization of Membrane Proteins and its Application to Fibroblast Growth Factor Receptors

This research was originally published in the Journal of Biological Chemistry. Nuala Del Piccolo, Sarvenaz Sarabipour, and Kalina Hristova. A New Method to Study Heterodimerization of Membrane Proteins and its Application to Fibroblast Growth Factor Receptors. *Journal of Biological Chemistry*. 2016; Papers in Press. © the American Society for Biochemistry and Molecular Biology.

The text reproduced here has been revised to match the style of this thesis.

RTK Heterodimerization and the FGFRs

Receptor tyrosine kinases (RTKs) regulate many key biological processes, including cell survival, growth, differentiation, and migration. There are 58 different RTKs, classified into 20 families based on sequence similarity. An archetypal RTK consists of a ligand-binding extracellular (EC) domain, a single-pass transmembrane (TM) domain, and an intracellular (IC) kinase domain (4,11,13,14,16). These receptors are activated upon dimerization, which is known to be a reversible process (105,106). Dimer formation is required (although not sufficient) for function (4,18,19,105,107,108), as it brings the two kinases into close proximity, enabling cross-phosphorylation on specific tyrosines. Phosphorylated RTKs trigger many intracellular signaling cascades, including the MAPK, PI3K, PKC, and STAT pathways. These pathways, in turn, determine cell fate and function (4,11,13,14,16,91,109).

RTKs play a fundamental role in human development. They are also critical players in the induction and progression of many cancers (4,11,13-16,91,110). Thus, significant efforts have been dedicated to the development of RTK-specific therapies

with high specificity and low toxicity. One class of anti-cancer drugs on the market specifically aims to inhibit RTK dimerization, as it is an important regulator of function. The best known example of these drugs is Herceptin, an antibody raised against the extracellular domain of HER2, an RTK that is often overexpressed in breast cancer (15,111). While Herceptin treatment can significantly improve patient outcomes in some cases, the performance of this treatment and other RTK-targeted molecular therapies has not reached expectations (16,111,112). This may be partly due to gaps in basic knowledge about RTK interactions in the plasma membrane.

RTKs readily form homodimers, but they also participate in hetero-interactions with other RTKs, often other members of the same family. Heterodimerization between RTKs is believed to be a means of signal amplification and diversification. RTK heterodimers have been shown to enhance receptor activation and downstream signaling, as compared to homodimers (4,11,15,16,30,113). For instance, the ErbB2•ErbB3 heterodimer is known as the most biologically active and the most pro-tumorigenic of all ErbB homodimers and heterodimers (15,16). Yet, our understanding of RTK heterodimerization is only rudimentary, in part due to a paucity of methods that provide quantitative information about heterodimer formation (21,113,114). Indeed, prior work has relied primarily on qualitative methods such as immunoprecipitation. Thus, the extent of heterodimerization between members of an RTK family remains unknown. Often, even the identities of RTK partners that engage in hetero-interactions are unknown, and this can significantly impede the design of high efficacy therapeutics that target RTK dimerization.

Here, we introduce a novel Förster Resonance Energy Transfer (FRET)-based technique that overcomes the limitations of previous methods employed to study heterodimers in the plasma membrane. To demonstrate the utility of the method, we apply it to study heterodimerization within the Fibroblast Growth Factor Receptor (FGFR) family of RTKs. We use truncated receptors in which the IC domains have been substituted with fluorescent proteins, to allow for FRET detection. Measurements are performed in plasma membrane vesicles, derived from live cells using an osmotic stress buffer (43). As the receptors are expressed in cells prior to vesicle production, they undergo all post-translational modifications. FRET is measured with the Quantitative Imaging-FRET (QI-FRET) method (54,55), which yields donor and acceptor concentrations, in addition to FRET efficiencies, in each vesicle.

The FGFRs regulate the development of the skeletal system (13,23,91,109,115,116). There are four FGFRs—FGFR1, FGFR2, FGFR3, and FGFR4. Here we focus on FGFR1, FGFR2, and FGFR3, three receptors that have been implicated in many growth disorders (4,11,13,14,18,69,91,116,117). While originally believed to form dimers only in response to ligand (fgf) binding, FGFRs have been shown to interact and form homodimers even in the absence of ligand (18,26,34,118-120). FGFR homodimerization seems to prime the receptors for efficient activation by the ligand, and thus unliganded FGFR dimers appear to be important intermediates in the signal transduction process (18,120).

The propensities for homodimer formation have been quantified for full-length FGFR1, FGFR2, and FGFR3, in the absence of ligand (18). The truncated FGFRs also form homodimers, with propensities that are similar to or lower than full-length FGFRs

(18,34,118,119). We seek to determine the heterodimerization propensities of the truncated FGFR1, FGFR2, and FGFR3, and compare them to the homodimerization propensities, in the absence of ligand.

We further seek to examine FGFR heterodimer formation in the presence of two different pathogenic point mutations in FGFR3: G380R and A391E. The G380R mutation in the TM domain of FGFR3 is found in 98% of all Achondroplasia cases. Achondroplasia is the most common form of human dwarfism and is characterized by short stature and premature endochondral ossification of long bones (21,23,67,69,109,115,116,119). The A391E mutation, also in the TM domain of FGFR3, causes Crouzon syndrome with acanthosis nigricans. This developmental disorder is characterized by premature ossification of skull bones accompanied by a skin disorder (24,94,116,118,121,122). While both mutations introduce a charged amino acid into the TM domain of the same receptor, the resulting phenotypes are substantially different. It has been hypothesized that this difference in phenotype might be explained by disparate perturbations to FGFR heterodimers (24,116). To directly test this hypothesis, we examine the FGFR1•FGFR3, FGFR2•FGFR3, and wild-type\mutant FGFR3 heterodimers in the presence of both mutations using the new quantitative FRET method, and we compare the results to those of the wild-type using statistical methods.

Heterodimerization Model

RTK lateral association can be described by monomer-dimer equilibrium models (11,114,123). Here, we consider dimer formation when two receptors, X and Y, are capable of forming both heterodimers and homodimers (see Figure 5-1). In this case, the equilibrium between monomers and dimers is described by three reactions (124):

$$[X] + [X] \overset{K_X}{\leftrightarrow} [XX] \qquad [Y] + [Y] \overset{K_Y}{\leftrightarrow} [YY] \qquad [X] + [Y] \overset{K_{XY}}{\longleftrightarrow} [XY] \tag{5-1}$$

where K_X and K_Y are the two macroscopic homodimer association constants and K_{XY} is the macroscopic heterodimer association constant. The bracket notation indicates two-dimensional species concentration. The three association constants can be written as:

$$K_X = \frac{[XX]}{[X]^2} \qquad K_Y = \frac{[YY]}{[Y]^2} \qquad K_{XY} = \frac{[XY]}{[X][Y]} \tag{5-2}$$

and these relationships are the first key component describing the complex heterodimerization process. The association constants can be used to calculate dimer stability using Equation 3-3. The number of receptors in a cell-derived vesicle is constant over time, and we write the equations of mass conservation as:

$$[X_{total}] = [X] + 2[XX] + [XY] \qquad [Y_{total}] = [Y] + 2[YY] + [XY] \tag{5-3}$$

where $[X_{total}]$ and $[Y_{total}]$ are the total concentrations of each receptor species in a given vesicle. If we rearrange the first two statements in Equation 5-2 to solve for [XX] and [YY] and substitute into Equation 5-3, we have:

$$[X_{total}] = [X] + 2K_X[X]^2 + [XY] \qquad [Y_{total}] = [Y] + 2K_Y[Y]^2 + [XY] \tag{5-4}$$

These equations constitute the second key component describing heterodimerization. Using the quadratic formula (125) to solve Equations 5-4 for [X] and [Y], and then substituting into the third statement in Equation 5-2, we arrive at a single equation describing heterodimerization:

$$0 = K_{XY}\left(\frac{2([XY]-[X_{total}])}{1+\sqrt{1-8K_X([XY]-[X_{total}])}}\right)\left(\frac{2([XY]-[Y_{total}])}{1+\sqrt{1-8K_Y([XY]-[Y_{total}])}}\right) - [XY] \tag{5-5}.$$

This equation is implicit and must be solve numerically. To achieve this, we can employ MATLAB's function "fsolve" in the default setting, which utilizes the trust-region-dogleg algorithm. Solving Equation 5-5 in this manner produces theoretical predictions for the

concentration of heterodimers, which depend on the homodimer association constants, K_X and K_Y, and on the total receptor concentrations, $[X_{total}]$ and $[Y_{total}]$. The total dimer fraction, f_D, is:

$$f_D = \frac{2([XX]+[YY]+[XY])}{[X_{total}]+[Y_{total}]} \quad (5\text{-}6).$$

This value is also equivalent to the sum of the two homodimer fractions, $f_{D,XX}$ and $f_{D,YY}$, and the heterodimer fraction, $f_{D,XY}$:

$$f_{D,XX} = \frac{2[XX]}{[X_{total}]+[Y_{total}]} \quad f_{D,YY} = \frac{2[YY]}{[X_{total}]+[Y_{total}]} \quad f_{D,XY} = \frac{2[XY]}{[X_{total}]+[Y_{total}]} \quad (5\text{-}7).$$

Interpretation of Heterodimer FRET Data

Next, we turn to solving the heterodimerization problem in the context of FRET experiments. If the two receptors form heterodimers, and if one receptor is labeled with the donor and the other is labeled with the acceptor, FRET will occur. The FRET efficiency can be measured with the QI-FRET method as described (54,55). The measured FRET efficiency can then be corrected for the so-called proximity FRET, to yield the interaction-specific FRET efficiency, E_D. Proximity FRET is a non-negligible FRET efficiency that arises even in the absence of specific interactions, due to the random approach of donors and acceptors within the two-dimensional membrane. We have extensively modeled and measured this phenomenon in previous work, and it mainly depends on acceptor concentration (77,82). The corrected FRET efficiency, E_D, is due to heterodimerization only. FRET efficiency is based on the change in donor fluorescence, so E_D can be written in terms of the concentration of the acceptor-donor complex (that is, the heterodimer) and the concentration of the donor (121,126,127):

$$E_D = \frac{[XY]\tilde{E}}{[donor]} \quad (5\text{-}8)$$

where $\tilde{E}$ is the Intrinsic FRET, or the FRET efficiency in a given dimer. Intrinsic FRET is the maximum E_D; that is, if all receptors in a vesicle were found in heterodimers, E_D would be equal to $\tilde{E}$. In the general case, $\tilde{E}$ depends on the relative positioning of the two fluorescent proteins (i.e. the separation and orientation of the fluorophores) in the dimer. Since the fluorophores are attached to the receptors via long flexible linkers, we can assume that they rotate freely, and thus Intrinsic FRET depends mainly on fluorescent protein separation. Under the assumption of free rotation, Intrinsic FRET can be written using Equation 3-8. Given an Intrinsic FRET value, Equation 3-8 can be solved for d to estimate fluorophore separation in a given dimer.

Using QI-FRET, we can measure three values per vesicle: donor concentration, acceptor concentration, and FRET efficiency (54,55). Since one receptor is labeled with the donor and the other receptor is labeled with the acceptor, the receptor concentrations, $[X_{total}]$ and $[Y_{total}]$, can be directly measured as the donor concentration and acceptor concentration. To calculate heterodimer concentration from experimental data, we rearrange Equation 5-8 to obtain:

$$[XY] = \frac{E_D[donor]}{\tilde{E}} \tag{5-9}$$

and this relationship is substitute into Equation 5-5 to yield:

$$0 = K_{XY}\left(\frac{2(\frac{E_D[donor]}{\tilde{E}}-[X_{total}])}{1+\sqrt{1-8K_X(\frac{E_D[donor]}{\tilde{E}}-[X_{total}])}}\right)\left(\frac{2(\frac{E_D[donor]}{\tilde{E}}-[Y_{total}])}{1+\sqrt{1-8K_Y(\frac{E_D[donor]}{\tilde{E}}-[Y_{total}])}}\right)-\frac{E_D[donor]}{\tilde{E}} \tag{5-10}.$$

The quantities $[X_{total}]$, $[Y_{total}]$, E_D, and [donor] are measured experimentally. When K_X and K_Y are known, Equation 5-10 can be fit to experimental FRET data to find the unknowns K_{XY} and $\tilde{E}$, the two parameters describing heterodimer formation.

Statistical Analysis

A two-step process is used to fit the heterodimerization model to the experimental FRET data, ultimately identifying the optimal values for the unknowns K_{XY} and $\tilde{E}$. First, $\tilde{E}$ is fixed and non-linear least squares (128) (specifically, MATLAB's "nlinfit") is used to find K_{XY}. This process is repeated at discreet values of $\tilde{E}$ with a step of 0.01. Second, the mean square error (MSE) is calculated (128) for each of the resulting ($\tilde{E}$, K_{XY}) pairs as:

$$MSE = \frac{\sum_{i=1}^{n}(E_{D\,exper,i} - E_{D\,theor,i})^2}{n} \tag{5-11}$$

where E_D is the interaction-specific FRET efficiency. The experimental value, $E_{D_{exper,i}}$, is measured in each vesicle using the QI-FRET method (54,55). The theoretical value, $E_{D_{theor,i}}$, is calculated by solving Equation 5-5 for [XY] using the receptor concentrations in a given vesicle, then substituting into Equation 5-9 and solving for E_D. n is the total number of vesicles in a given dataset. The lowest MSE corresponds to the optimal parameters. A plot of the MSE as a function of $\tilde{E}$ is U-shaped. The minimum MSE was identified (using MATLAB's "min") and the ($\tilde{E}$, K_{XY}) pair corresponding to this minimum is taken as the optimal set of parameters.

We note that we use this two-step process because MATLAB's nlinfit could not fit for both parameters simultaneously, as one of the parameters was consistently imaginary. To confirm that this issue arises from the equations and not the data, we generated simulated heterodimer datasets where we fixed K_{XY} and $\tilde{E}$ and then attempted to use nlinfit to retrieve both parameters simultaneously. Despite the fact that this data is error-free and fits the model perfectly, nlinfit continued to produce imaginary parameter values. Employing the iterative approach, on the other hand, allowed us to successfully retrieve both parameters.

Next, we use the bootstrap method (125) to estimate the errors on these parameters. In the bootstrap method, a given set of data is split into multiple synthetic datasets and the fitting process is performed on each subset. The optimal parameters from the subsets are used to calculate parameter means and standard deviations.

One-way analysis of variance (ANOVA) tests are performed to compare the association constants and Intrinsic FRET values for wild-type homodimers and heterodimers. First, the bootstrap method is used to refit the previously published homodimer data (18,34), in order to make the homodimer and heterodimer datasets comparable. Then, the optimal parameters from these fits are compared to K and $\tilde{E}$ for the wild-type heterodimers using one-way ANOVA tests (MATLAB's "anova1"). We test the null hypothesis that the three homodimers and three heterodimers are all equivalent. In the case of $p < 0.05$, we reject the null hypothesis and perform a multiple comparison test (MATLAB's function "multcompare") to determine which homodimers and/or heterodimers are significantly different from the others.

Finally, K_{XY} and $\tilde{E}$ are compared using unpaired t-tests (MATLAB's "ttest2"), in order to determine the effect of the two pathogenic point mutations. Each mutant heterodimer is compared to the corresponding wild-type heterodimer, and the wild-type\mutant FGFR3 heterodimers are each compared to the wild-type FGFR3 homodimer. We test the null hypothesis that the two dimers being compared are not significantly different from each other. The resulting p-values are recorded, where $p < 0.05$ indicates that the two groups are significantly different, and $p < 0.005$ indicates a very significant difference.

Results

Predictions of the model

Equation 5-5 predicts the heterodimer concentration [XY], based on each receptor's concentration and the two homodimer association constants. Solving Equation 5-5 can be a challenging problem. In previous work (30,121,129,130), the ratio of receptor concentrations, $[X_{total}]$:$[Y_{total}]$, was held constant so that all equations can be written as a function of just one receptor concentration, substantially simplifying the mathematical analysis. However, our experiments are performed in a cellular system, which means that the concentration of each receptor, and thus the ratio $[X_{total}]$:$[Y_{total}]$, cannot be controlled. Instead, we must consider and solve Equation 5-5 as a function of both $[X_{total}]$ and $[Y_{total}]$. In this general case, the theoretical solution is a surface instead of a line. Additionally, since heterodimerization is described by a coupled system of equations, the formation of any dimer species—[XX], [YY], or [XY]—is dependent on the formation propensity of the other two.

Figure 5-2 illustrates both of these characteristics using a series of graphs generated over a wide range of possible individual receptor concentrations. In these predictions, the homodimer association constants K_X and K_Y are varied by an order of magnitude, while keeping K_{XY} fixed in all cases. In the left-hand panels, the theoretical total dimer fraction, f_D, is represented by a cyan surface with contour lines. The total dimer fraction plots can be asymmetrical depending on the relative values of the homodimer association constants. The right-hand panels depict the contribution of each dimer species to the total dimer fraction, where the fractional contribution of [XX], [YY], and [XY] are displayed as violet, pink, and white surfaces, respectively. The features of

these theoretical solutions are in accordance with the law of mass action. Homodimer fraction is low when the concentration of a given receptor is low and increases with its concentration, and heterodimer fraction approaches zero as either $[X_{total}]$ or $[Y_{total}]$ (or both) go to zero. Note that the heterodimerization fraction decreases from panel A to panel D, despite the fact that K_{XY} is the same in all cases. This decrease is due to the relative increases in K_X and K_Y, i.e, due to the depletion of monomers as homodimerization increases. These predictions illustrate the complex manner in which receptor concentrations and association constants determine each dimer's concentration.

FGFR1, FGFR2, FGFR3, FGFR3_G380R, and FGFR3_A391E form all possible heterodimers

We use the model described above to study the heterodimerization of truncated FGFRs, consisting of the EC and TM domains of a receptor followed by flexible linkers and fluorescent proteins. First, we consider the hetero-interactions between wild-type FGFR1, FGFR2, and FGFR3. Then, we examine these hetero-interactions when FGFR3 carries the point mutations for Achondroplasia (FGFR3_G380R) or Crouzon syndrome with acanthosis nigricans (FGFR3_A391E). We investigate three possible wild-type FGFR heterodimers: FGFR1•FGFR2, FGFR1•FGFR3, and FGFR2•FGFR3; and six possible mutant heterodimers: FGFR1•FGFR3_G380R, FGFR2•FGFR3_G380R, FGFR3•FGFR3_G380R, FGFR1•FGFR3_A391E, FGFR2•FGFR3_A391E, and FGFR3•FGFR3_A391E.

For each heterodimer studied, Chinese Hamster Ovary (CHO) cells are co-transfected with plasmids encoding the two receptor constructs, each labeled with either the donor or the acceptor (and then the labeling scheme is reversed). Twenty-four hours

post-transfection, cells are exposed to an osmotic stress buffer (43) that produces plasma membrane-derived vesicles. These vesicles are collected and then imaged using the QI-FRET method (54,55). In brief, a confocal microscope is used to image the cross-section of each vesicle in the donor, FRET, and acceptor channels (see Figure 2-3 for a representative vesicle). The microscope is calibrated using solutions of free fluorescent protein, so that fluorescence intensity and protein concentration can be directly related, enabling quantitative analysis of images (53). Ultimately, three quantities are measured in each vesicle: donor concentration, acceptor concentration, and FRET efficiency.

Figure 5-3 displays the raw data for the nine FGFR heterodimers examined here. The left-hand panels show the FRET efficiency as a function of acceptor concentration. The dark blue right-pointing triangles, purple up-pointing triangles, green left-pointing triangles, light blue diamonds, and black squares represent the FGFR1, FGFR2, FGFR3, FGFR3_G380R, and FGFR3_A391E homodimer FRET data, respectively (previously published (18,34,118,119)). In each case, the heterodimer data are represented by red circles. Each point corresponds to a single vesicle. The solid black line represents the proximity FRET, or the FRET efficiency expected due to non-specific close approach of labeled receptors (77,82). For all wild-type and mutant FGFR heterodimers, measured FRET efficiencies exceed proximity FRET, indicating that specific heterodimeric interactions occur in all cases.

While FRET is plotted in Figure 5-3 as a function of acceptor concentration, it also depends on the donor concentration, and thus both concentrations are taken into account in the analysis. The right-hand panels in Figure 5-3 plot the donor concentration versus the acceptor concentration for all vesicles analyzed in the heterodimer FRET

experiments, again using red circles. The substantial variation of the ratio between acceptors and donors occurs because, in a transient transfection experiment, every cell will produce a different amount of each receptor. This variation explains the seemingly wide spread of FRET efficiencies seen in the FRET efficiency versus acceptor concentration plots. As discussed previously, a wide range of donor to acceptor ratios, as well as a wide range of concentrations, is an advantage in the QI-FRET methodology, as it ensures a robust fit of a dimerization model to FRET data (55).

FGFR heterodimer stabilities and Intrinsic FRET values can be quantified

We fit the heterodimerization model (Equation 5-10) to the experimental FRET measurements for each heterodimer pair. We have previously reported all relevant homodimer association constants (18,34,118,119). We list those values in Table 5-1 and we use them as K_X and K_Y in Equation 5-10. This analysis yields the optimal K_{XY} and $\tilde{E}$. The apparent association constant, K_{XY}, reveals the propensity for heterodimer formation and is used to calculate dimer stability, ΔG_{XY} (Equation 3-3). Intrinsic FRET, or $\tilde{E}$, is a structural parameter that depends on the positioning of the fluorescent proteins in the dimer, but not on the propensity for dimer formation. Note that both K_{XY} and $\tilde{E}$ determine the magnitude of the measured FRET efficiencies, and thus both parameters need to be determined and accounted for, in order to correctly interpret results. In Table 5-1, we report the optimal K_{XY} and $\tilde{E}$ parameters, along with the calculated dimer stabilities and estimated distances between fluorescent proteins for all nine heterodimers.

In Figure 5-4 and Figure 5-5, we compare experimentally determined values to the optimized heterodimer model for each heterodimer pair. In Figure 5-4, the heterodimer concentration [XY] is plotted as a function of both receptor concentrations,

with model values (Equation 5-5) and experimentally determined measurements (Equation 5-9) shown as a yellow surface with contour lines and open blue (above surface) and red (below) circles, respectively. In Figure 5-5, the total dimer fraction, calculated using Equation 5-6, is plotted as a function of the concentration of the two receptors. Model values are displayed as a cyan surface with contour lines, and experimentally determined measurements are plotted using purple circles.

The wild-type FGFR1•FGFR2, FGFR1•FGFR3, and FGFR2•FGFR3 heterodimer stabilities are -4.5 ± 0.1, -4.8 ± 0.1, and -4.1 ± 0.2 kcal/mol, respectively (Table 5-1 and Figure 5-6). ANOVA tests are performed to compare ΔG values of homodimers and heterodimers. The stabilities of the FGFR2 and FGFR3 homodimers are statistically the same as each other, but different from those of FGFR1 and all the heterodimers. Additionally, the stabilities of FGFR1•FGFR2 and FGFR1•FGFR3 are statistically the same as each other, but different from the stability of FGFR2•FGFR3. The ΔG for FGFR1•FGFR3 is also different from that of FGFR1.

We also use ANOVA to compare wild-type Intrinsic FRET values. We find that Intrinsic FRET is statistically the same for all three wild- type homodimers and the FGFR1•FGFR2 and FGFR2•FGFR3 heterodimers. The Intrinsic FRET of the FGFR1•FGFR3 heterodimer is smaller than that of the other five dimers, and this difference is significant. In our experiments, the fluorescent proteins are attached to the TM domain of each FGFR via flexible linkers, so Intrinsic FRET predominantly depends on the distance between the fluorescent proteins in the dimers, d. Using Equation 3-8, we calculate this distance under the assumption of free fluorescent protein rotation (an assumption that may not be correct). The relative positioning of the fluorescent proteins,

and thus the general dimer architecture, is similar for five of the dimers. In contrast, the inter-fluorophore distance is larger in the FGFR1•FGFR3 heterodimer, suggesting an increase in the separation of the TM domain C-termini relative to the other dimers.

We further examine six mutant FGFR heterodimers (Table 5-2 and Figure 5-6). The Achondroplasia heterodimers FGFR1•FGFR3_G380R, FGFR2•FGFR3_G380R, and FGFR3•FGFR3_G380R have stabilities of -5.2 ± 0.1, -4.7 ± 0.3, and -5.2 ± 0.1 kcal/mol, respectively. The Crouzon syndrome heterodimers FGFR1•FGFR3_A391E, FGFR2•FGFR3_ A391E, and FGFR3•FGFR3_ A391E have stabilities of -5.3 ± 0.2, -4.5 ± 0.2, and -5.1 ± 0.1 kcal/mol, respectively.

To compare the wild-type and mutant heterodimers, t-tests are performed on the dimer stability and Intrinsic FRET values. The difference between wild-type and mutant dimer stabilities, $\Delta\Delta G_{XY}$, is calculated to assess the effects of mutations on the thermodynamics of dimer formation. Analogously, the difference in Intrinsic FRET values, $\Delta\tilde{E}$, is computed to estimate any alteration in dimer architecture.

First, we consider the FGFR1•FGFR3 heterodimer. The Achondroplasia and Crouzon syndrome mutations both stabilize this heterodimer, by -0.4 ± 0.1 and -0.5 ± 0.1 kcal/mol, respectively. Additionally, the Achondroplasia mutation increases the Intrinsic FRET value.

Next, we turn to the FGFR2•FGFR3 heterodimer. We find that the Achondroplasia mutation stabilizes the dimer by -0.6 ± 0.1 kcal/mol and has no effect on Intrinsic FRET. The differences between the wild-type and Crouzon syndrome FGFR2•FGFR3 heterodimers are not statistically significant.

The wild-type\mutant FGFR3 heterodimer is slightly different from those described thus far, which all form between two different FGFRs. This heterodimer forms between a wild-type FGFR3 and a FGFR3 with a pathogenic point mutation (either G380R or A391E), and comparisons are made to the wild-type FGFR3 homodimer. The Achondroplasia mutation stabilizes the dimer by -1.8 ± 0.1 kcal/mol. The Crouzon syndrome mutation also has a stabilizing effect, with a $\Delta\Delta G_{XY}$ of -1.7 ± 0.1 kcal/mol. Both mutations also decrease the Intrinsic FRET value, suggesting that the fluorescent proteins are further apart in the wild-type\mutant FGFR3 heterodimers than in the wild-type FGFR3 homodimer.

Discussion

We introduce a new methodology to study RTK heterodimerization

Membrane proteins are notoriously challenging to study (7), and detailed information about membrane protein interactions and structure is elusive, despite active research in the field (8,131-133). The need for new basic knowledge is underscored by the fact that approximately 60% of all FDA-approved therapeutics target membrane proteins (6). Biophysical information about drug targets can yield better mechanistic understanding of their function, and ultimately allows for more accurate prediction of drug action and function.

Recently, advances in microscopy have complemented the biochemical assays traditionally used in membrane protein research, producing new insights about membrane protein function (46,54,77,105,106,108,134,135). In this paper, we build on our previous work to develop and implement a quantitative FRET assay for examining RTK heterodimers. The method yields the apparent heterodimer association constant, K_{XY}, and

a conformational parameter (Intrinsic FRET, or Ẽ), which has been previously used to assess if structural changes occur in RTK dimers due to ligand binding or mutations (18,19,34,118,119).

Compared to biochemical methods, FRET offers unique advantages for examining heterodimers. We label one receptor with a FRET donor and the other with a FRET acceptor, so heterodimers have both a donor and acceptor, while homodimers have either two donors or two acceptors. Thus, FRET occurs only when heterodimers form. Methods such as SDS-PAGE and Western blotting, on the other hand, struggle to distinguish between RTK homodimers and heterodimers. Challenges arise because receptors are similar in size, so the two complexes cannot be distinguished on a gel. While immunoprecipitation can report on heterodimer formation, it is limited to qualitative observations and requires the removal of the receptors from the native membrane. Furthermore, in many biochemical methods, the propensity for dimer formation and the structure of that dimer are both known to affect experimental read-outs, but their respective contributions usually cannot be separated. The FRET technique described here can report on heterodimer formation in an intact membrane and can uncouple thermodynamic from structural information. However, the receptors are attached to bulky fluorescent proteins, which may perturb interactions in some cases. Furthermore, heterodimerization propensities can only be determined when the homodimerization propensities have already been measured. Finally, no FRET will be detected if the distance between the two fluorophores in the dimer complex exceeds 100 Å, even if a stable dimer forms.

Similar FRET techniques have been discussed in the literature (30,121,136), but the methodology presented here improves on previous work in multiple ways. Experiments are performed in cell-derived vesicles that capture many features of the native environment (43,44). These vesicles closely mimic the diverse lipid and protein content of the plasma membrane (44). The receptors are transiently expressed in the cells prior to vesiculation, so they undergo all relevant post-translational modifications, including glycosylation. In contrast, the previous heterodimerization studies were performed in synthetic lipid vesicles and limited to TM domain peptides.

In previous work on heterodimerization in membranes, the ratio between receptors has been held constant to simplify data analysis (30,121,129,130,136). The approach that we present has no such limitations and is applicable in cases where the ratio between receptors cannot be controlled, as in cellular studies. The new method is quantitative, yielding heterodimer association constants, despite being performed in a complex system that mimics the native environment. Thus, this FRET method can have broad utility in membrane protein research, as it can be used to study the heterodimerization propensity of any two membrane proteins.

Wild-type FGFR homodimers and heterodimers have similar stabilities and Intrinsic FRET values

Biochemical methods have previously shown that FGFR heterodimers form and are enzymatically active in cells, in the presence of ligand (21,117,137,138), but the thermodynamics of the association process have not been quantified. Furthermore, FGFR heterodimerization in the absence of ligand has never been investigated. Here, we observe unliganded FGFR heterodimers and for the first time measure the

thermodynamic stability of these heterodimers in the plasma membrane. In the absence of ligand, the propensity for heterodimer formation is similar to or larger than that of homodimers (see Table 5-1 and Figure 5-6). When combined with information about the cell's receptor concentrations, such dimer stabilities can empower prediction of homodimer and heterodimer populations. Therefore, this work can further our understanding of FGFR signaling, which is regulated by the formation of different dimers with unique functions (117,137,138).

In this set of experiments, we work with receptors that lack the IC domain, which is replaced with a fluorescent protein on a flexible linker. These truncated receptors can be expressed in a broad concentration range, a requirement for a successful fit of the model to the data, thereby facilitating method development (55). Additionally, the truncation of the receptors increases the likelihood that fluorophores attached to FGFRs in a heterodimer will undergo FRET. RTKs are known to have long unstructured C-terminal tails, and in some cases, this means that fluorescent proteins attached to full-length receptors in a dimer are too far apart to undergo FRET (139).

Contacts between IC domains generally promote, and never inhibit, RTK dimer formation (18,19,140-143). Indeed, full-length RTKs have been shown to have stronger propensities for lateral interactions than RTK constructs that lack the IC domain (18). In our previous work with FGFR dimer formation, we measured the contribution of the IC domain to FGFR1, FGFR2, and FGFR3 homodimerization as ~0, -2, and -3 kcal/mol, respectively (18). We expect heterodimer behavior to be similar. Accordingly, our finding that the truncated FGFRs engage in heterodimeric interactions suggests that full-length receptors will also form heterodimers. Furthermore, we expect that the stability of

full-length FGFR heterodimers is likely similar to or larger than that measured for truncated FGFR heterodimers.

The Achondroplasia and Crouzon syndrome mutations show their largest effects on the stability of the FGFR3 dimer

Table 5-2 summarizes the changes observed in the FGFR heterodimers due to the Achondroplasia and Crouzon syndrome mutations. The thermodynamics of heterodimerization are perturbed in five of six cases. The largest effects are measured on the dimer stability in the wild-type\mutant FGFR3 dimer. Indeed, the Achondroplasia and Crouzon syndrome mutations stabilize this heterodimer by -1.8 ± 0.1 and -1.7 ± 0.1 kcal/mol, respectively. These stabilizations are comparable to those measured for the mutant FGFR3 homodimers (118,119), suggesting that both mutant homodimers and mutant heterodimers may be important signaling entities in the two developmental disorders. The effects on the FGFR1•FGFR3 and FGFR2•FGFR3 heterodimers, on the other hand, are relatively small. The Achondroplasia mutation stabilizes these two heterodimers by -0.4 ± 0.1 and -0.6 ± 0.1 kcal/mol, respectively. The Crouzon syndrome mutation stabilizes FGFR1•FGFR3 by -0.5 ± 0.1 kcal/mol and has no effect on FGFR2•FGFR3. These stabilizations rank among the smaller ΔΔG values that we have measured for pathogenic point mutations in FGFRs (34,118,119), although these changes might still contribute to the development of the skeletal disorders studied here.

For three of the mutant heterodimers, we observe a statistically significant change in Intrinsic FRET, most likely due to a change in the separation of the fluorescent proteins in the heterodimer. While the details of how RTK dimer architecture relates to function remain obscure, it is clear that TM domain structure plays a fundamental role in

determining signaling properties (102,103). It is possible that the structural effects (observed as changes in Intrinsic FRET) captured in these experiments influence cross-phosphorylation in the heterodimer and potentially contribute to the two phenotypes.

It has been suggested that the phenotypical differences observed between Achondroplasia and Crouzon syndrome with acanthosis nigricans might be explained if one of the mutations primarily affects homodimerization, while the other mostly influences heterodimerization (24,116). Our results are inconsistent with this idea, instead suggesting that both mutations have their dominant effects on the FGFR3 homodimer.

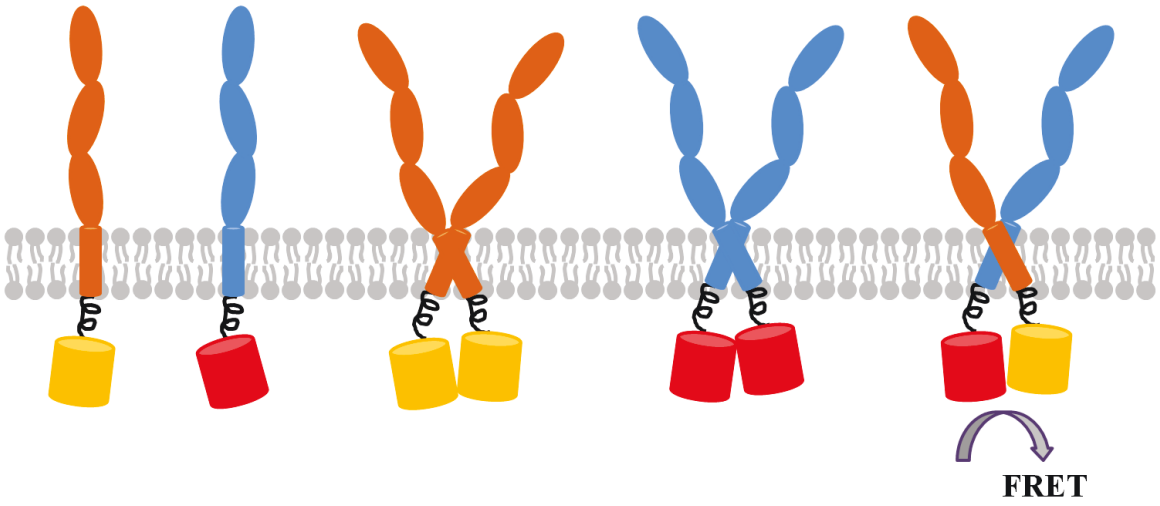

Figure 5-1. A cartoon representation of the receptor species present in heterodimer FRET experiments.

Receptors X and Y are shown in orange and blue. The IC domains of the receptors are replaced with the fluorescent proteins YFP and mCherry, depicted as yellow and red barrels, to allow for FRET detection of heterodimer formation. Three possible dimers can form, in accordance with the law of mass action. From left to right, we show the receptor monomers X and Y, the homodimers XX and YY, and the heterodimer XY. Equations 5-1 and 5-2 in the Heterodimerization Model section describe the coupled equilibria between the dimers and the monomers. The heterodimer is the only species with both YFP and mCherry and therefore is the only contributor to measured FRET efficiency. All possible species must be accounted for when quantitatively interpreting heterodimer formation from experimental data.

A

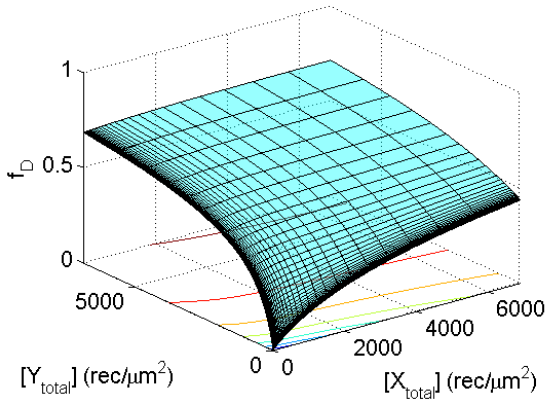
1
0.5
0
f_D
5000
0
0
2000
4000
6000
[Y_{total}] (rec/μm^2)
[X_{total}] (rec/μm^2)

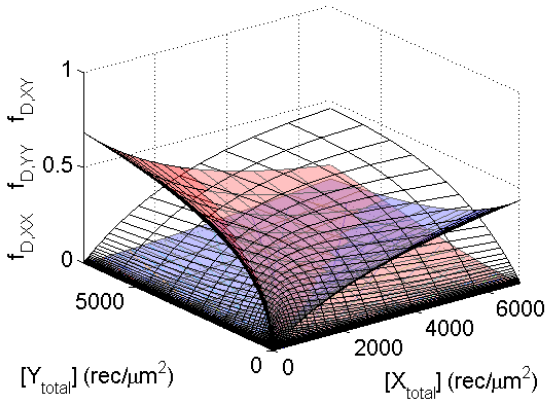
1
0.5
0
$f_{D,XX}$ $f_{D,YY}$ $f_{D,XY}$
5000
0
0
2000
4000
6000
[Y_{total}] (rec/μm^2)
[X_{total}] (rec/μm^2)

B

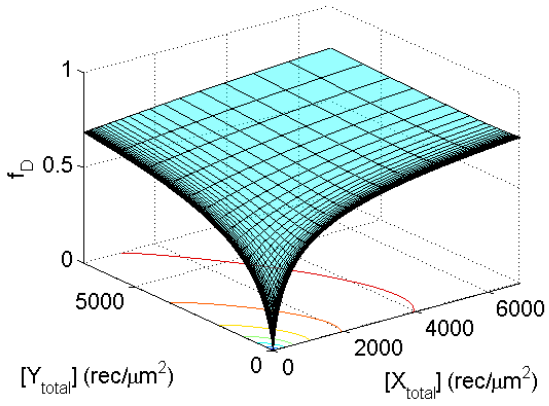
1
0.5
0
f_D
5000
0
0
2000
4000
6000
[Y_{total}] (rec/μm^2)
[X_{total}] (rec/μm^2)

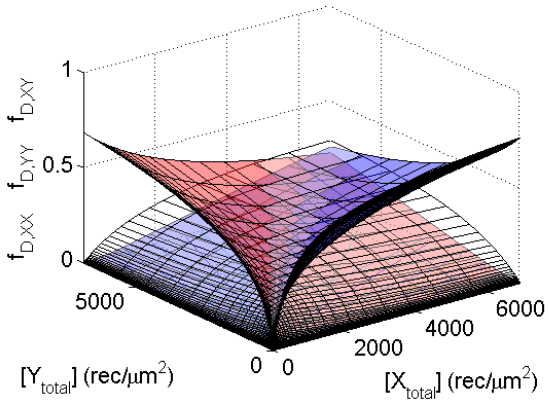
1
0.5
0
$f_{D,XX}$ $f_{D,YY}$ $f_{D,XY}$
5000
0
0
2000
4000
6000
[Y_{total}] (rec/μm^2)
[X_{total}] (rec/μm^2)

C

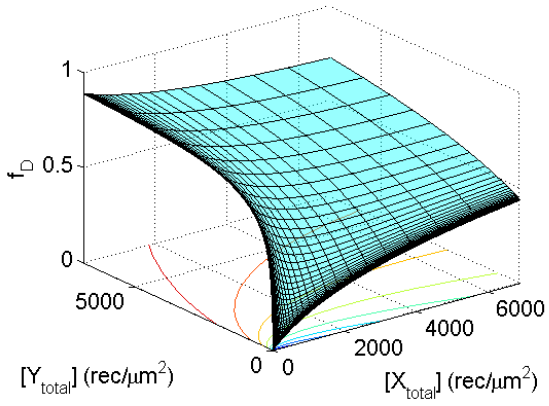
1
0.5
0
f_D
5000
0
0
2000
4000
6000
[Y_{total}] (rec/μm^2)
[X_{total}] (rec/μm^2)

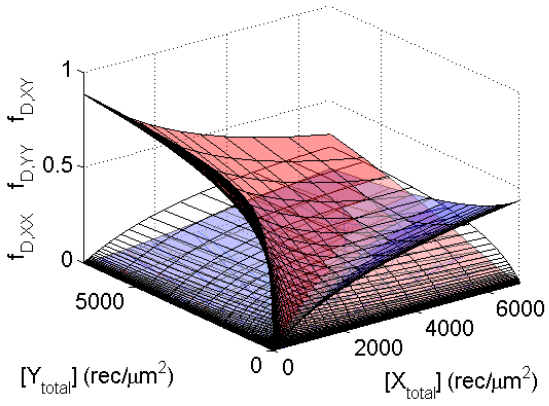
1
0.5
0
$f_{D,XX}$ $f_{D,YY}$ $f_{D,XY}$
5000
0
0
2000
4000
6000
[Y_{total}] (rec/μm^2)
[X_{total}] (rec/μm^2)

D

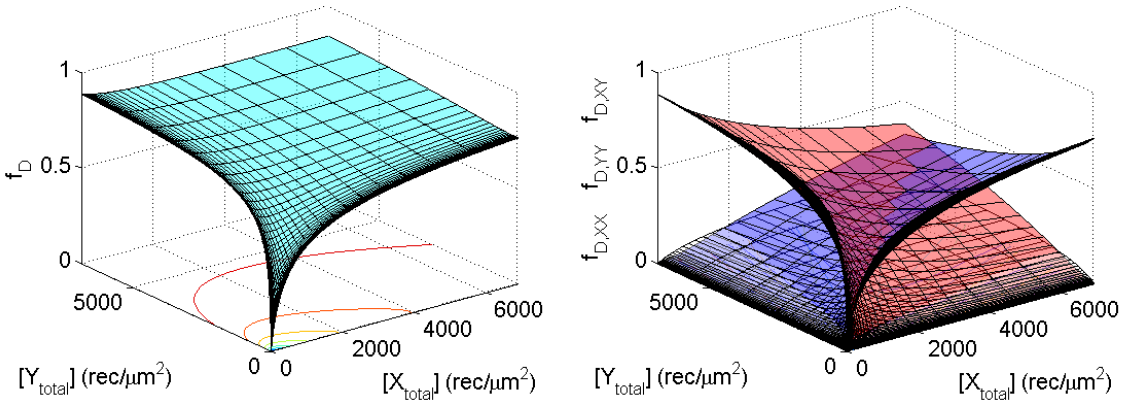

Figure 5-2. Theoretical predictions of the heterodimerization model, as a function of the concentration of the two receptors.

This model is based on a coupled system of equations describing the formation of the homodimers XX and YY and the heterodimer XY (see Equations 5-1 & 5-2), as well as the mass conservation of the receptors (Equations 5-3 & 5-4). The solution of this system is the heterodimerization model (Equation 5-5), and predictions from this equation are graphed here. The dimer fraction depends on the concentration of each receptor species ($[X_{total}]$ and $[Y_{total}]$) and all three association constants (K_X, K_Y, and K_{XY}). K_X and K_Y are increased from top to bottom. The left-hand panels display total dimer fraction (Equation 5-6) as a cyan surface with contour lines, and the right-hand panels display the fractional contribution of each dimer species [XX], [YY], and [XY] (Equation 5-7) as violet, pink, and white surfaces, respectively. In these plots, we assume a heterodimer association constant of $850*10^{-6}$ um^2/rec (ΔG_{XY} = -4.0 kcal/mol). The homodimer association constants are varied by an order of magnitude from (a) $K_{X,1} = 100*10^{-6}$ um^2/rec and $K_{Y,1} = 500*10^{-6}$ um^2/rec to (b) $K_{X,2} = 10*K_{X,1}$ and $K_{Y,2} = K_{Y,1}$ to '(c) $K_{X,3} = K_{X,1}$ and $K_{Y,3} = 10*K_{Y,1}$ to (d) $K_{X,4} = 10*K_{X,1}$ and $K_{Y,4} = 10*K_{Y,1}$.

A

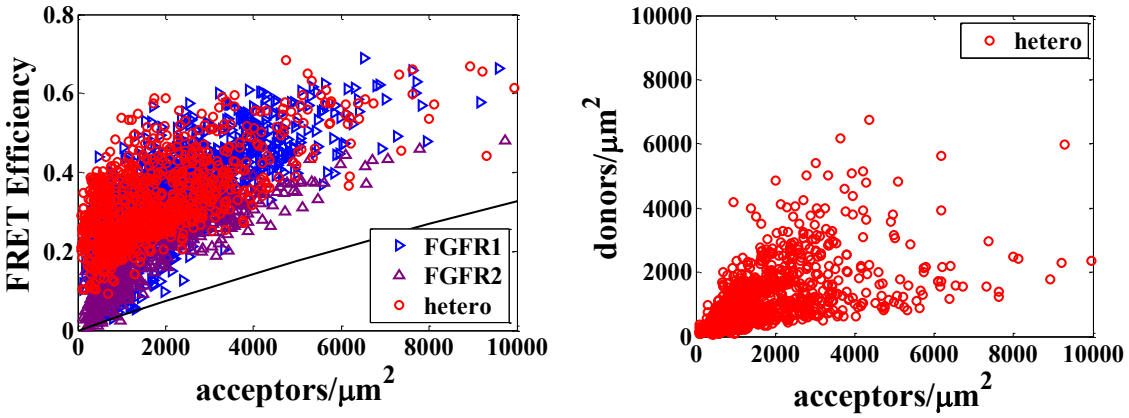
FRET Efficiency
acceptors/μm2
FGFR1
FGFR2
hetero
donors/μm2
acceptors/μm2
hetero

B

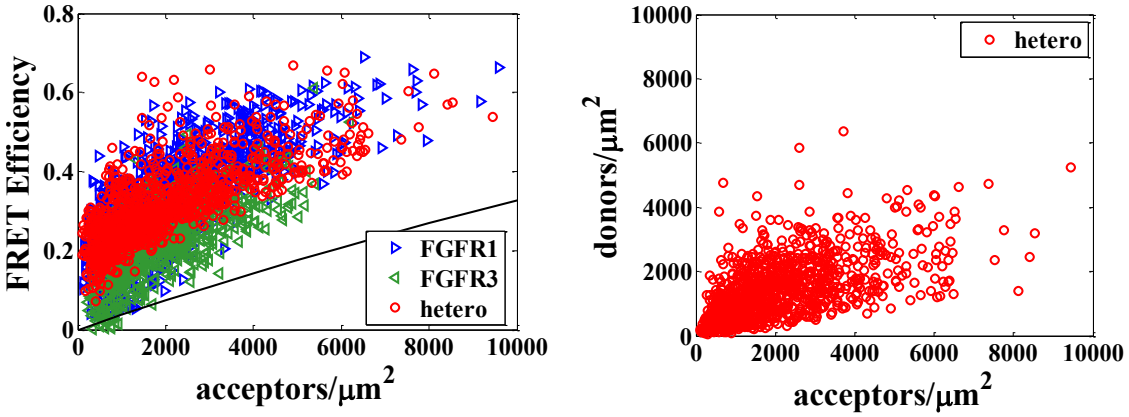
FRET Efficiency
acceptors/μm2
FGFR1
FGFR3
hetero
donors/μm2
acceptors/μm2
hetero

C

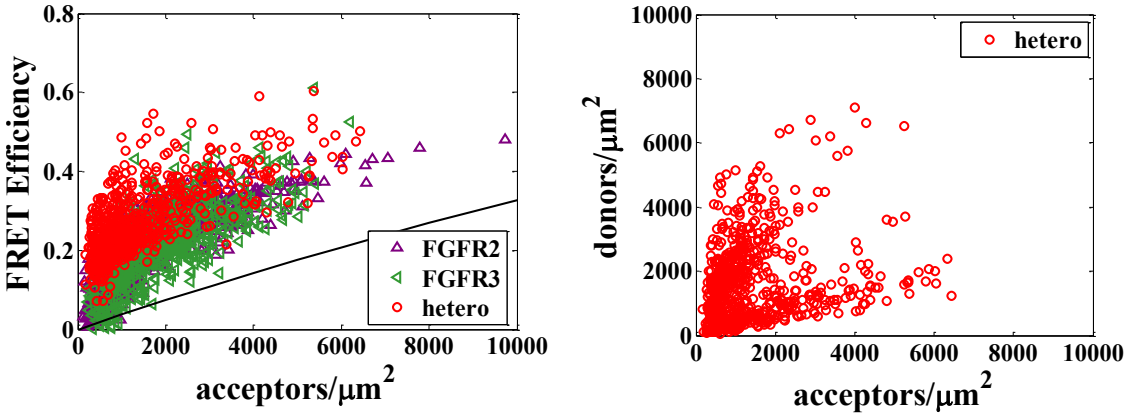
FRET Efficiency
acceptors/μm2
FGFR2
FGFR3
hetero
donors/μm2
acceptors/μm2
hetero

D

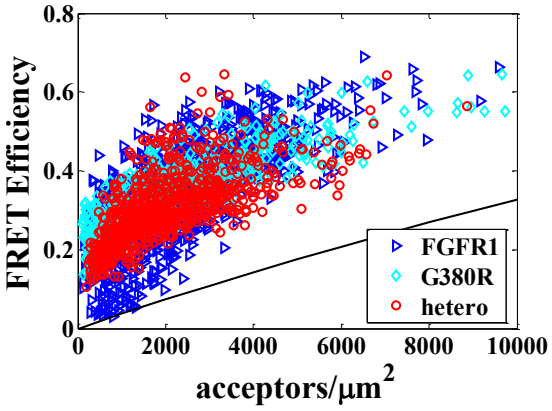
FRET Efficiency
acceptors/μm2
FGFR1
G380R
hetero

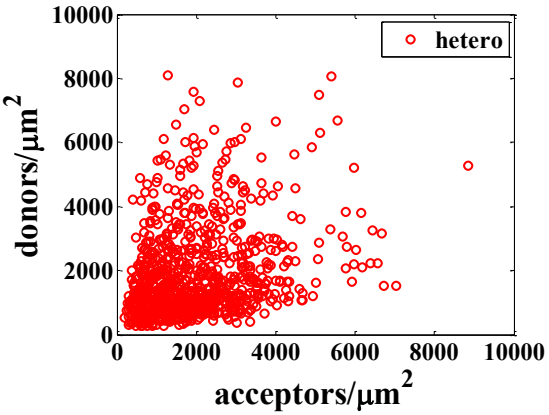
donors/μm2
acceptors/μm2
hetero

E

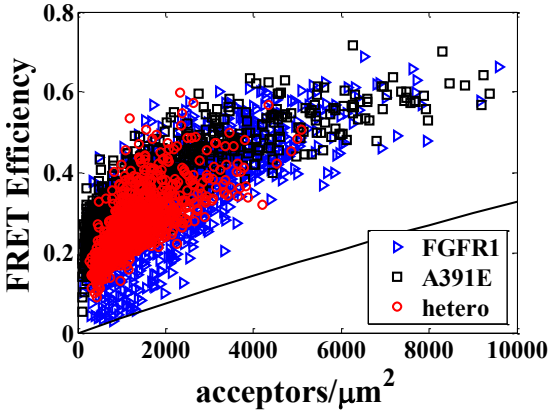
FRET Efficiency
acceptors/μm2
FGFR1
A391E
hetero

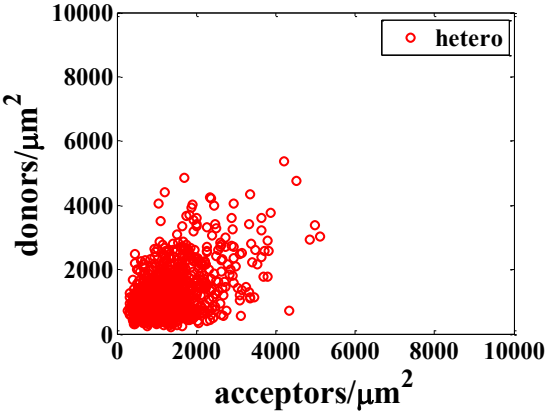
donors/μm2
acceptors/μm2
hetero

F

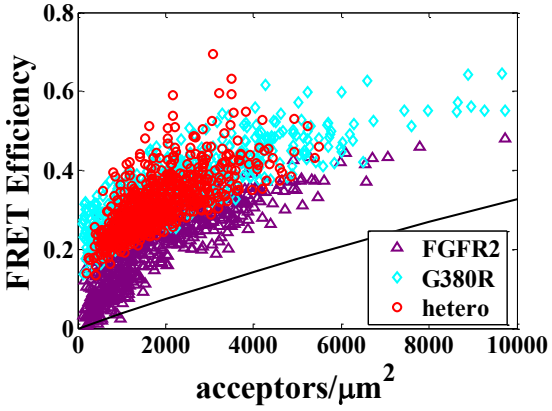
FRET Efficiency
acceptors/μm2
FGFR2
G380R
hetero

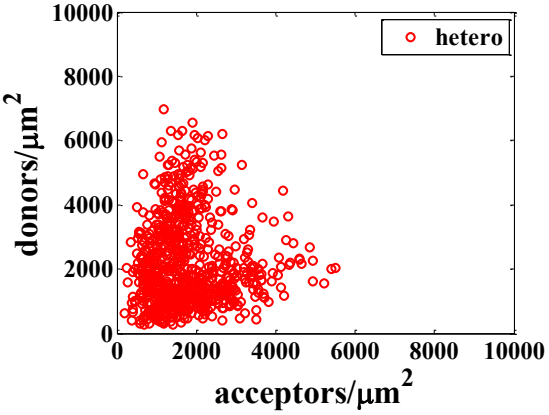
donors/μm2
acceptors/μm2
hetero

G

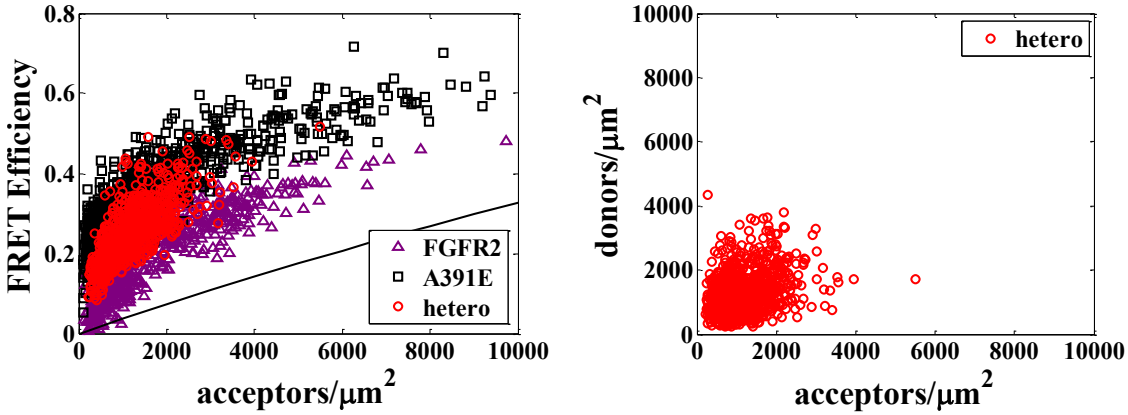
FRET Efficiency
0.8
0.6
0.4
0.2
0
0
2000
4000
6000
8000
10000
acceptors/μm2
FGFR2
A391E
hetero
donors/μm2
10000
8000
6000
4000
2000
0
hetero

H

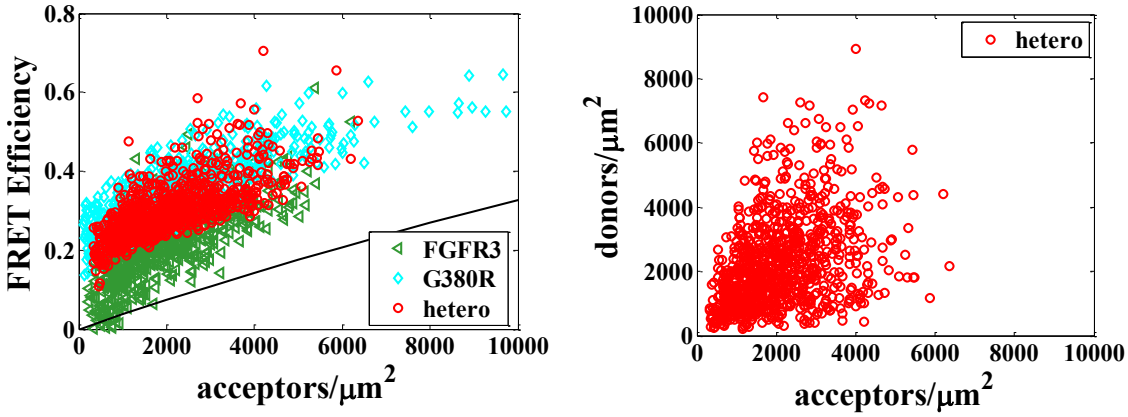
FRET Efficiency
0.8
0.6
0.4
0.2
0
0
2000
4000
6000
8000
10000
acceptors/μm2
FGFR3
G380R
hetero
donors/μm2
10000
8000
6000
4000
2000
0
hetero

I

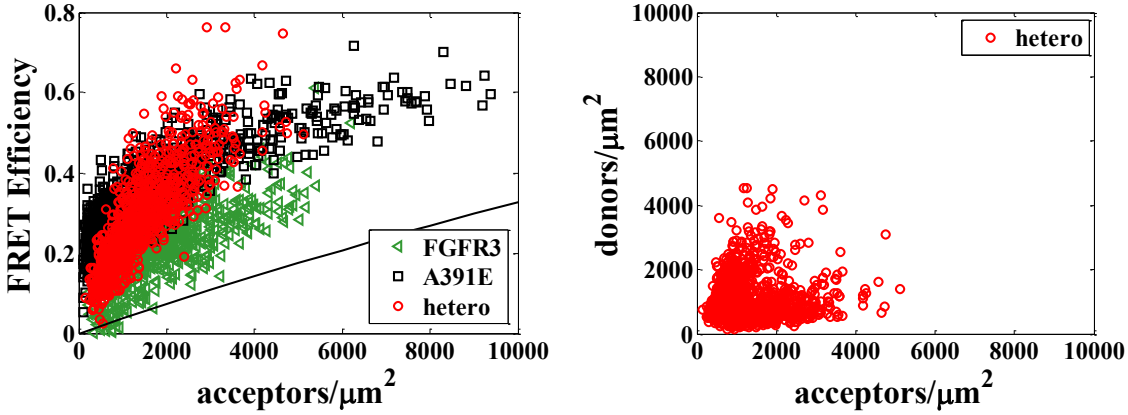
FRET Efficiency
0.8
0.6
0.4
0.2
0
0
2000
4000
6000
8000
10000
acceptors/μm2
FGFR3
A391E
hetero
donors/μm2
10000
8000
6000
4000
2000
0
hetero

Figure 5-3. Vesicle FRET data for the (A-C) wild-type and (D-I) mutant FGFR heterodimers.

The dark blue right-pointing triangles, purple up-pointing triangles, green left-pointing triangles, light blue diamonds, and black squares represent the FGFR1, FGFR2, FGFR3, FGFR3_G380R, and FGFR3_A391E homodimer FRET data (18,34,118,119). Data collected during heterodimer FRET experiments are always shown with red circles. For both homodimer and heterodimer data, each point represents a single vesicle. In the left-hand panels, the measured FRET efficiencies are plotted as a function of acceptor concentration. Proximity FRET, or the FRET due to non-specific close approach of two receptors, is shown as a black line (77,82). The measured FRET efficiencies exceed proximity FRET in every case, which suggests that specific heterodimeric interactions occur for all heterodimers investigated. In subsequent analysis, the measured FRET efficiency is corrected for proximity FRET to find the dimer-specific FRET efficiency. In the right-hand panels, donor concentrations are plotted against acceptor concentrations.

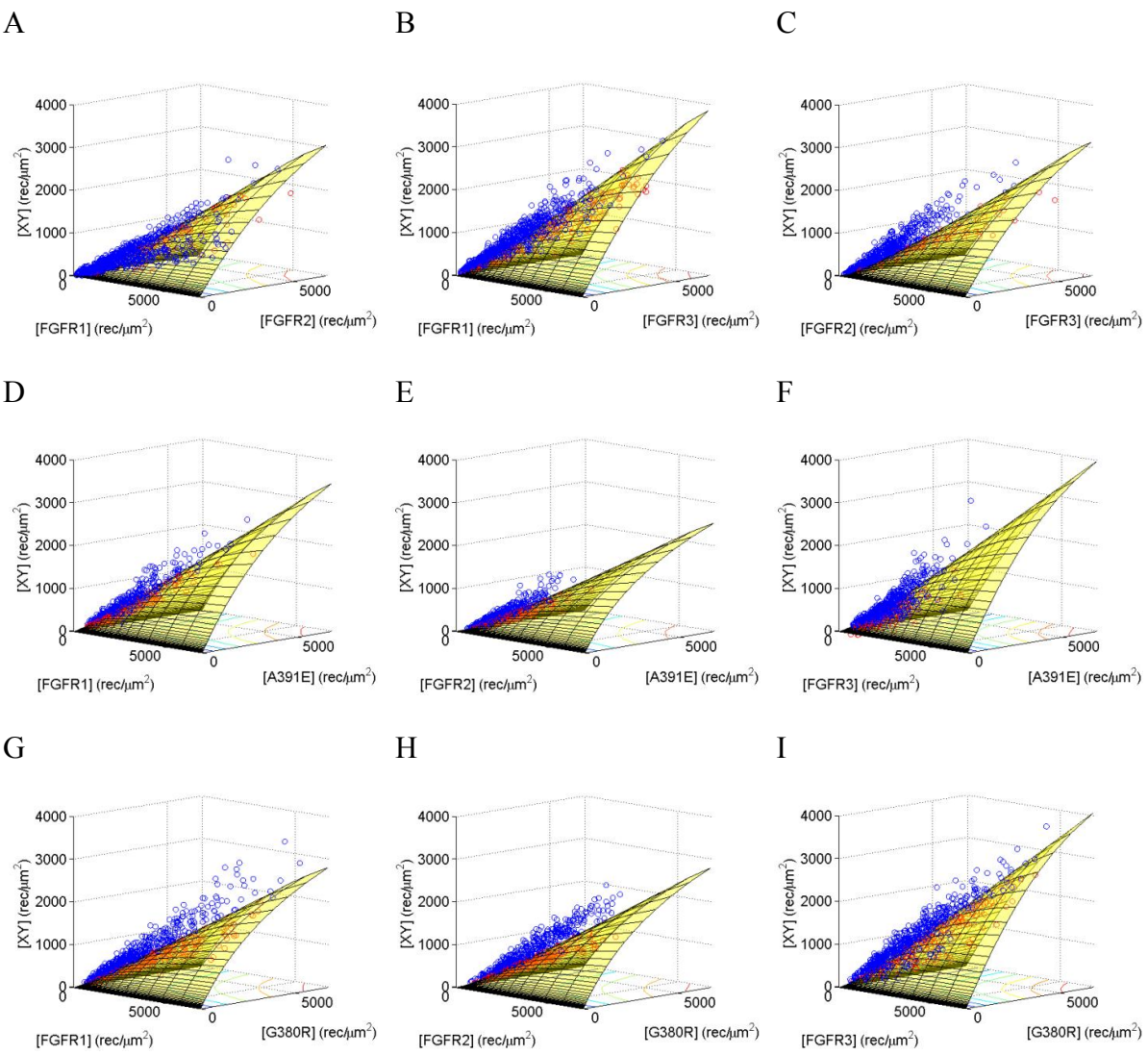

Figure 5-4. Experimentally determined and theoretically predicted heterodimer concentrations [XY], as a function of the two receptor concentrations.

The model is plotted as a yellow surface with contour lines and experimentally determined values are shown as blue (points above model surface) or red (points below) circles. Experimental heterodimer concentrations are calculated according to Equation 5-9 and theoretical predictions are made using Equation 5-5. The best fit values are plotted here for the (A-C) wild-type, (D-E) Achondroplasia, and (G-I) Crouzon syndrome FGFR heterodimer pairs.

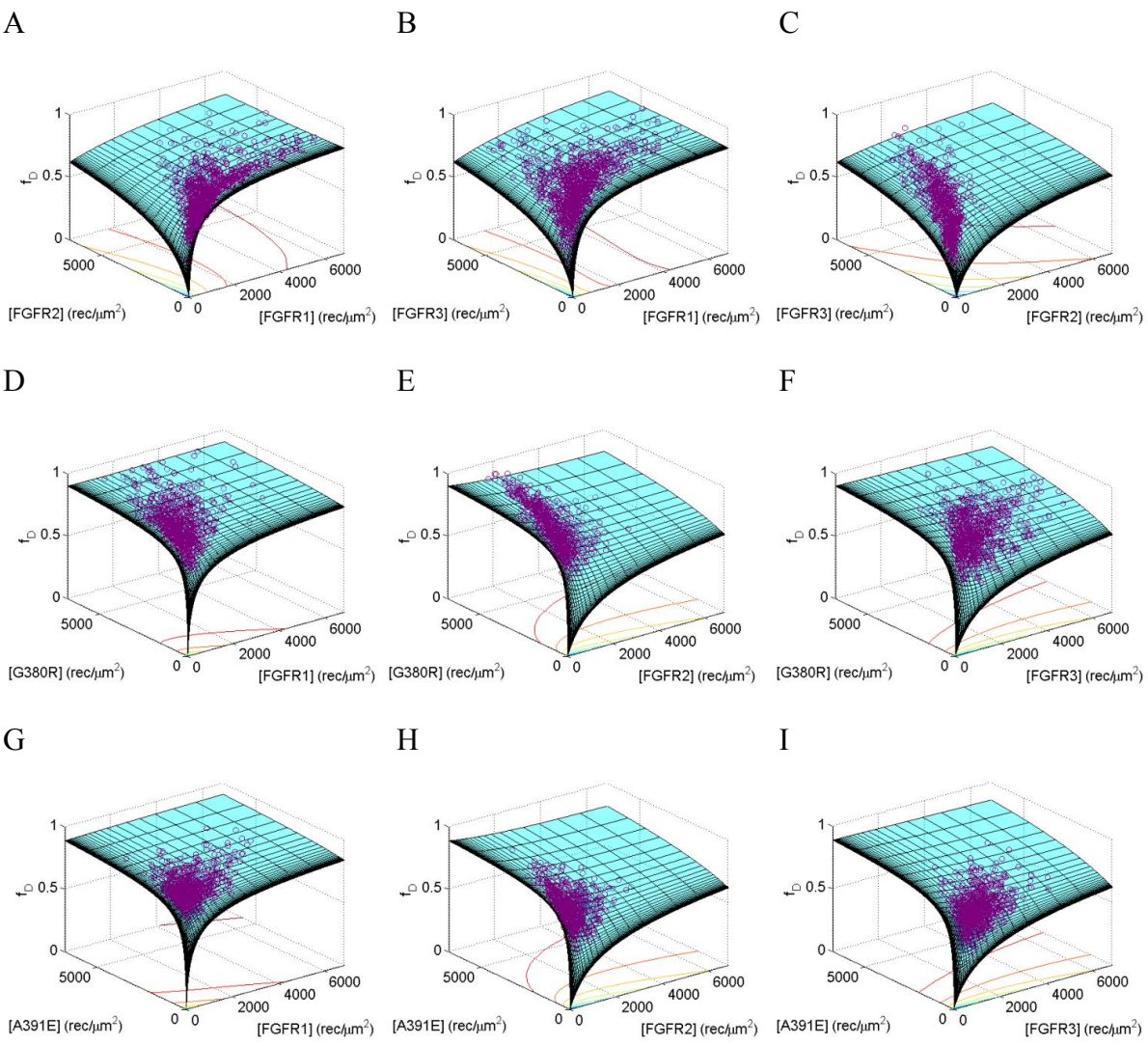

Figure 5-5. Total dimer fractions for wild-type and mutant FGFR heterodimers. Equation 5-6 is used to calculate the total dimeric fraction, f_D, as a function of the receptor concentrations. Experimental data (purple circles) is compared to the best fit heterodimerization model (cyan surface with contour lines). Shown are results for the (A-C) wild-type, (D-E) Achondroplasia, and (G-I) Crouzon syndrome FGFR heterodimer pairs.

A

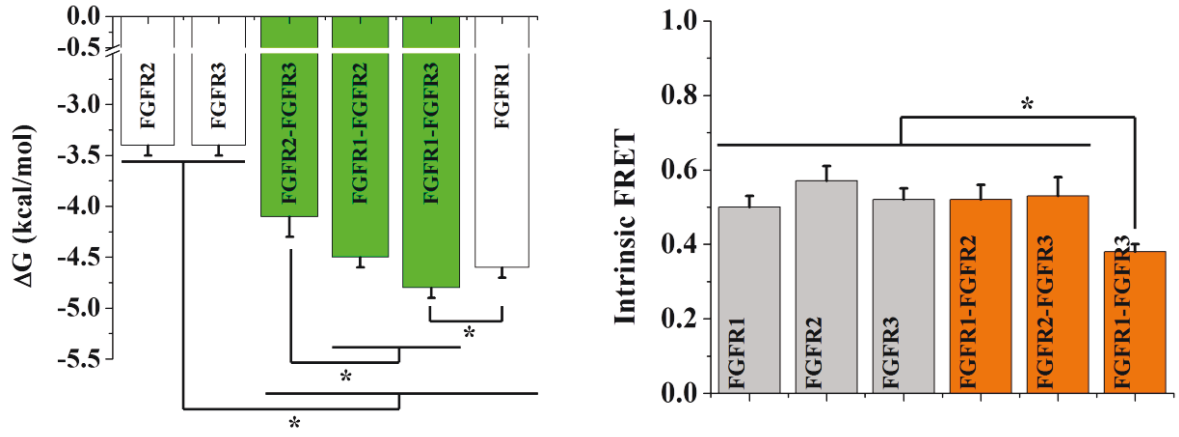
ΔG (kcal/mol)
0.0
-0.5
-3.0
-3.5
-4.0
-4.5
-5.0
-5.5
FGFR2
FGFR3
FGFR2-FGFR3
FGFR1-FGFR2
FGFR1-FGFR3
FGFR1
*
*
*
*
Intrinsic FRET
1.0
0.8
0.6
0.4
0.2
0.0
FGFR1
FGFR2
FGFR3
FGFR1-FGFR2
FGFR2-FGFR3
FGFR1-FGFR3
*

B

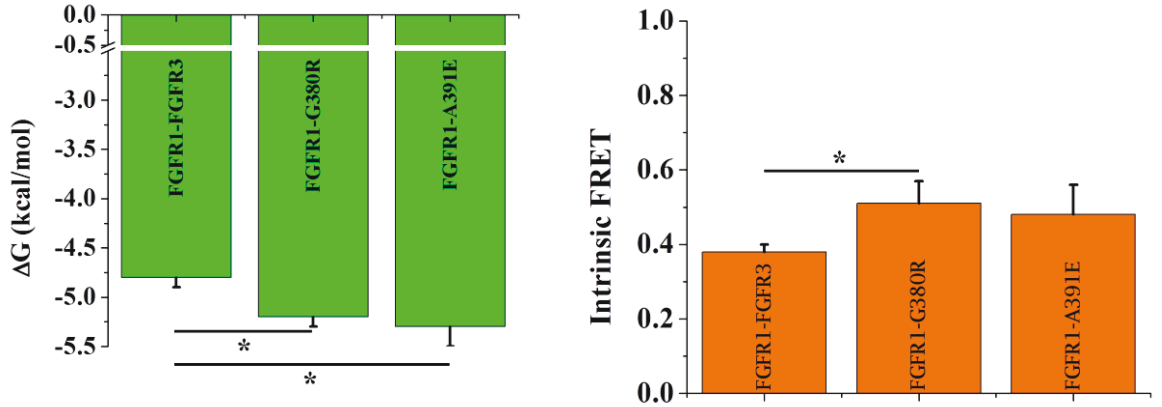
ΔG (kcal/mol)
0.0
-0.5
-3.0
-3.5
-4.0
-4.5
-5.0
-5.5
FGFR1-FGFR3
FGFR1-G380R
FGFR1-A391E
*
*
Intrinsic FRET
1.0
0.8
0.6
0.4
0.2
0.0
FGFR1-FGFR3
FGFR1-G380R
FGFR1-A391E
*

C

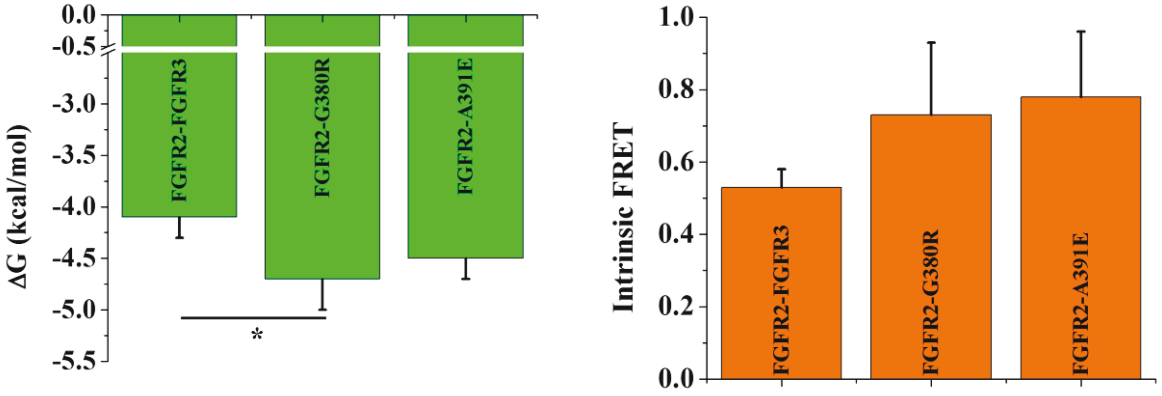
ΔG (kcal/mol)
0.0
-0.5
-3.0
-3.5
-4.0
-4.5
-5.0
-5.5
FGFR2-FGFR3
FGFR2-G380R
FGFR2-A391E
*
Intrinsic FRET
1.0
0.8
0.6
0.4
0.2
0.0
FGFR2-FGFR3
FGFR2-G380R
FGFR2-A391E

D

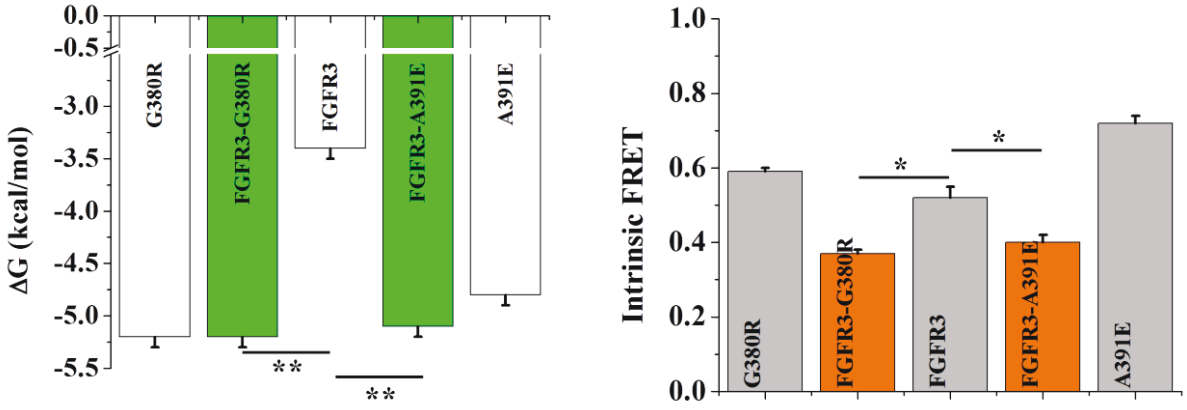

Figure 5-6. Optimal parameters from the fit of the heterodimerization model to experimental FGFR data.

Results are shown for the (A) wild-type FGFR heterodimers and homodimers, (B) wild-type and mutant FGFR1•FGFR3 heterodimers, (C) wild-type and mutant FGFR2•FGFR3 heterodimers, and (D) wild-type and mutant FGFR3 heterodimers and homodimers. The left-hand panel displays heterodimer stabilities (green bars) alongside homodimer values (18,34,118,119) (white bars) to facilitate comparison. Heterodimer stabilities are calculated from association constants using Equation 3-3. The right-hand panel shows the Intrinsic FRET values, with heterodimer results in orange and homodimer values in gray. ANOVA is employed to compare wild-type homodimers and heterodimers. Unpaired t-tests are performed to determine the significance of the differences between wild-type and mutant heterodimers: * indicates $p < 0.05$ and ** identifies $p < 0.005$.

		Dimer Stability		Dimer Conformation	
		Association Constant, K (μm^2/rec)	**ΔG (kcal/mol)**	**Intrinsic FRET**	**d (Å)**
Homodimers	**FGFR1**[a]	(2336 ± 484) * 10^{-6}	-4.6 ± 0.1	0.50 ± 0.03	53.1 ± 0.7
	FGFR2[a]	(309 ± 57) * 10^{-6}	-3.4 ± 0.1	0.57 ± 0.04	50.7 ± 1.0
	FGFR3[a,b]	(309 ± 65) * 10^{-6}	-3.4 ± 0.1	0.52 ± 0.03	52.4 ± 1.0
	FGFR3_G380R[c]	(6430 ± 1212) * 10^{-6}	-5.2 ± 0.1	0.59 ± 0.01	50.0 ± 0.4
	FGFR3_A391E[d]	(5000 ± 670) * 10^{-6}	-4.8 ± 0.1	0.72 ± 0.02	45.5 ± 0.6
Heterodimers	**FGFR1•FGFR2**	(2109 ± 379) * 10^{-6}	-4.5 ± 0.1	0.52 ± 0.04	52.3 ± 1.3
	FGFR1•FGFR3	(3540 ± 432) * 10^{-6}	-4.8 ± 0.1	0.38 ± 0.02	57.4 ± 0.6
	FGFR2•FGFR3	(988 ± 308) * 10^{-6}	-4.1 ± 0.2	0.53 ± 0.05	52.0 ± 1.9
	FGFR1•FGFR3_G380R	(6428 ± 1302) * 10^{-6}	-5.2 ± 0.1	0.51 ± 0.06	52.6 ± 2.0
	FGFR2•FGFR3_G380R	(2829 ± 1207) * 10^{-6}	-4.7 ± 0.3	0.73 ± 0.20	43.5 ± 9.7
	FGFR3•FGFR3_G380R	(6435 ± 180) * 10^{-6}	-5.2 ± 0.1	0.37 ± 0.01	57.9 ± 0.4
	FGFR1•FGFR3_A391E	(8463 ± 2715) * 10^{-6}	-5.3 ± 0.2	0.48 ± 0.08	53.7 ± 2.9
	FGFR2•FGFR3_A391E	(2106 ± 714) * 10^{-6}	-4.5 ± 0.2	0.78 ± 0.18	41.6 ± 8.6
	FGFR3•FGFR3_A391E	(5356 ± 551) * 10^{-6}	-5.1 ± 0.1	0.40 ± 0.02	56.7 ± 0.8

Table 5-1. Optimal parameters describing FGFR homodimerization and heterodimerization.

Previously published homodimer results (top of table) (18,118,119) are used to solve Equation 5-10, which describes heterodimer formation in FRET experiments. The heterodimer results (bottom of table) are listed as averages and standard deviations, as calculated using the bootstrap method (see the Heterodimerization Model section for details). Dimer stability, ΔG, is calculated from the association constant using Equation 3-3. Under the assumption of freely rotating fluorophores, the distance between fluorescent proteins in a dimer, d, is estimated using Equation 3-8.

[a]Data from (18)

[b]Data from (34)

[c]Data from (119)

[d]Data from (118)

	Dimer Stability		Dimer Conformation	
	ΔΔG (kcal/mol)	**p-value**	**Δ Ẽ**	**p-value**
FGFR1•FGFR3_G380R	-0.4 ± 0.1	0.024	↑ 0.13	0.021
FGFR1•FGFR3_A391E	-0.5 ± 0.1	0.016	ns	0.103
FGFR2•FGFR3_G380R	-0.6 ± 0.1	0.034	ns	0.173
FGFR2•FGFR3_A391E	ns	0.060	ns	0.0797
FGFR3•FGFR3_G380R	-1.8 ± 0.1	0.000107	↓ 0.15	0.0146
FGFR3•FGFR3_A391E	-1.7 ± 0.1	0.000202	↓ 0.12	0.0365

Table 5-2. Effects of the Achondroplasia and Crouzon syndrome mutations on FGFR heterodimerization.

Unpaired t-tests are performed for the null hypothesis that the wild-type and mutant heterodimers are the same, and the resulting p-values are shown. “ns” indicates that any measured difference is not significant. The largest stabilization effects are observed in wild-type\mutant FGFR3 dimers, and these ΔΔG values are accompanied by decreases in Intrinsic FRET. FGFR1•FGFR3 is slightly stabilized by each mutation and also experiences an increase in Intrinsic FRET for the Achondroplasia mutation only. The only statistically significant change in FGFR2•FGFR3 due to the presence of a mutation is a small increase in stability in the presence of the Achondroplasia mutation.

CHAPTER SIX Characterization of the Interaction Between EGFR and Grb2 in Live Cells

RTK-Adapter Protein Interactions and EGFR-Grb2

Despite having no inherent activity, adapter proteins play an essential role in cellular signaling networks. These small proteins are composed of highly specific, modular binding domains (ie, SH2 and PTB domains), and are responsible for mediating many protein-protein interactions. In the special case of RTKs, adapter proteins such as Grb2, Shc, and Nck bind to phosphorylated residues in the IC domain, initiating the recruitment and activation of other cytoplasmic proteins and triggering downstream signaling cascades, including the MAPK, PI3K, PKC, and STAT pathways (4,11,12,144,145).

Many RTKs are over-expressed and over-active in tumor tissue, and adapter proteins are the direct link between receptors and biological activity. Hence, a class of anti-cancer drugs, Tyrosine Kinase Inhibitors (TKIs), has been developed to specifically disrupt the interaction between RTKs and adapter proteins, and thereby eliminate aberrant RTK activity. TKIs like Gefitinib can improve patient outcomes, but their efficacy has fallen short of initial projections (15,28). Many TKIs are small molecules that were discovered through *in vitro* screenings conducted with short peptides representing the adapter protein and the phosphorylated RTK IC domain (146,147). An *in vivo* model system of RTK-adapter protein interactions would be a valuable experimental tool, allowing for screening of TKIs in a system consisting of full-length receptors and adapter proteins.

Here, we present an *in vivo* model system for the study of RTK-adapter protein interactions. In this system, live cells are placed under reversible osmotic stress using a hypotonic buffer. In these swollen cells, the membrane is stretched out, eliminating its complex topology, and the cytoplasm is retained. This combination of a model membrane in the presence of the cytoplasm allows for the study of interactions between membrane proteins and soluble proteins.

In the canonical model of RTK activation, ligand binding induces dimer formation, followed by cross-phosphorylation of the IC domains and recruitment of adapter proteins (4,11). Indeed, previous studies show that recruitment of adapter proteins to the IC domain of RTKs increases following ligand addition (139,147-150). However, emerging evidence suggests that, even in the absence of ligand, RTKs form dimers (18,19) and that some of these unliganded dimers are active (5,151). The phosphorylation level of these unliganded RTK dimers remains an open question, but can be assessed by monitoring the recruitment of adapter proteins to RTKs in the absence of ligand.

Here, we study the interaction between the RTK EGFR and the adapter protein Grb2. Following receptor activation, Grb2 is recruited to the tail of EGFR and mediates the receptor's connection to the MAPK signaling pathway. This interaction takes place through Grb2's SH2 domain, which binds to the phosphorylated Y1068 and Y1086 residues of EGFR (5,10,15,139,152). Of the many possible pairs of receptors and adapter proteins, EGFR and Grb2 were selected because i) the recruitment of Grb2 to EGFR following phosphorylation has been well-documented (147,148,150,152-157) and ii) the interaction can be observed via FRET (139,149,158). These two characteristics make the EGFR-Grb2 binding reaction a suitable model system in which to develop and implement

the new FRET microscopy method reported here. Experiments are performed in the absence and presence of the ligand EGF. We obtain parameters describing both the thermodynamics of the EGFR-Grb2 interaction and the level of unliganded EGFR dimer phosphorylation.

Model to Describe RTK-Adapter Protein Interactions

Thermodynamic cycles are an increasingly popular way to describe and model the RTK activation process (123,159). In this work, we present a thermodynamic cycle for RTK activation that includes dimer formation, ligand binding, phosphorylation, and adapter protein binding (see Figure 6-1). We depict unliganded receptors as open black squares, liganded receptors as filled black squares, phosphorylation as filled red circles, and adapter proteins as filled green arcs. Equilibrium reactions occur between two receptors (α_i), upon dimer phosphorylation (β_i), between receptors and adapter proteins (γ_i), and upon ligand binding (ε_i).

In Chapter Three, Chapter Four, and Chapter Five, we examined interactions between two receptors. In this chapter, we focus on receptor phosphorylation and the interaction between a receptor and a soluble protein. We continue to use a monomer-dimer equilibrium model to describe the interaction of two receptors, and we consider the binding reaction between monomeric ligands and receptors as an equilibrium process (159).

Receptor phosphorylation only occurs within dimers (5,123). When ligand binds to an RTK dimer, a conformational change occurs in the kinase domains of the receptors. Specifically, the kinase domains adopt an active asymmetric configuration, which allows for phosphorylation and subsequent interactions with adapter proteins and other soluble

proteins. Here, we model this process as a conformational change from an inactive dimer (D) to an active dimer (D*):

$$[D] \overset{\beta}{\leftrightarrow} [D^*] \tag{6-1}$$

The equilibrium constant describing this conformational change, β, can be written as:

$$\beta = \frac{[D^*]}{[D]} \tag{6-2}$$

where [D] and [D*] are in two-dimensional units of proteins/μm^2 and β has no units.

The interaction between a membrane protein and a soluble protein is an equilibrium reaction that has been previously described (160-163). In the special case of the adapter protein-RTK system, adapter proteins (A) only bind to phosphorylated dimers:

$$D^* + nA \overset{\gamma}{\leftrightarrow} D^*A_n \tag{6-3}$$

where D*A is the complex formed by a phosphorylated dimer and adapter proteins, and n is the number of adapter proteins bound to each dimer. The association constant γ can be written as:

$$\gamma = \frac{[D^*A_n]}{[D^*][A]^n} \tag{6-4}$$

where [D*] and [D*A$_n$] are in two-dimensional units of proteins/μm^2, [A] is in three-dimensional units of proteins/μm^3, and γ is in units of μm^3/protein.

Here, experiments are performed in swollen cells. In swollen cells, endocytosis is inhibited (50), so mass conservation of receptors can be employed:

$$[T] = [M] + 2[D] + 2[D^*] + 2[D^*A_n] \tag{6-5}$$

where T and M denote total receptors and monomers, respectively. In this model, the concentration of adapter proteins in the cytoplasm is high, so it is an unlimited pool of binding molecules and can be considered as a constant. Equation 6-5 can be used in

conjunction with the thermodynamic equilibrium equations to characterize the parameters of the RTK activation cycle.

Finally, we can calculate the fraction of receptors found in each species:

$$f_M = \frac{[M]}{[T]}$$

$$f_D = \frac{2[D]}{[T]}$$

$$f_{D^*} = \frac{2[D^*]}{[T]}$$

$$f_{D^*A_n} = \frac{2[D^*A_n]}{[T]} \quad (6\text{-}6).$$

where f_M, f_D, f_{D^*}, and f_{D^*An} denote the fraction of receptors that exist as monomers, in inactive dimers, in active dimers, and in dimer-adapter protein complexes, respectively.

Interpretation of FRET Data

The receptor is labeled with a FRET donor and the adapter protein is labeled with a FRET acceptor. If an adapter protein binds to a receptor, FRET will occur. The concentration of the donor (equivalently, the receptor), the acceptor (or, the adapter protein), and the FRET efficiency (E) can be measured using the FSI technique (46). FRET efficiency, which is defined in terms of change in donor fluorescence, can be directly related to the formation of the dimer-adapter protein complex (121,126,127) according to:

$$E = \frac{[D^*A_n]E_{complex}}{[donor]} \quad (6\text{-}7)$$

where $E_{complex}$ is a geometrical parameter that depends on the separation and orientation of the two fluorophores in the dimer-adapter protein complex. Specifically, $E_{complex}$ is the FRET efficiency in a dimer-adapter protein complex. This geometrical parameter must be determined and accounted for, in order to correctly interpret FRET data.

$E_{complex}$ depends on the oligomeric size and geometric configuration of the dimer-adapter protein complex. Here, we consider the pairwise FRET efficiency between a donor and an acceptor, E_p, and follow the approach of Raicu and Singh (164) to calculate $E_{complex}$ as a function of E_p for various oligomeric sizes and goemetric configurations of $[D^*A_n]$. Since the number of adapter proteins, n, in each dimer-adapter protein complex is still under debate, we consider $E_{complex}$ for n = 0, 1, 2, 3, and 4. The geometrical configurations we consider are depicted in Figure 6-2, and the $E_{complex}$ values as a function of E_p are listed next to each configuration.

Results

We use the thermodynamic cycle for RTK activation described above to characterize both the phosphorylation of EGFR dimers and the interaction between EGFR and Grb2. We engineer plasmids coding for full-length EGFR fused to a flexible GGS linker followed by mTurquoise (a FRET donor) and full-length Grb2 followed by GGS and YFP (a FRET acceptor). Earlier studies have verified that the interaction between EGFR and Grb2 is observable in this experimental design (139,158).

CHO cells are co-transfected with the EGFR and Grb2 plasmids. After 24 hours, the full cell culture media is removed and replaced with a limited cell culture media that lacks growth factors. Starving the CHO cells in this manner eliminates the presence of any natively-expressed EGFR ligands. Twelve hours later, the media is again replaced, this time with so-called "swelling media". This buffer causes CHO cells to swell (see Figure 2-1, Panel B) in a reversible process that stretches and unwrinkles the plasma membrane, enabling accurate measurements of donor concentration, acceptor concentration, and FRET efficiency in the membrane of live cells (46). For experiments

in the presence of ligand, swelling media is supplemented with 300 nM EGF and 1 mg/mL BSA.

CHO cells equilibrate with the hypotonic buffer for 20 minutes, and then are imaged using the FSI method (46). In the FSI method, the cross-section of each cell is imaged twice: once at the excitation of the donor (840 nm) and again at the excitation of the acceptor (960 nm). The microscope is calibrated using solutions of free fluorescent protein and CHO cells transfected with only the donor-labeled receptor or the acceptor-labeled adapter protein. This calibration empowers pixel-level deconvolution of measured fluorescence spectra to fluorophore concentrations and FRET efficiency. In these experiments, two regions were selected in each swollen cell: a membrane region and a cytoplasmic region. We measure three quantities per pair of regions. In the membrane region, we measure i) the concentration of the donor (equivalently, the receptor) and ii) the FRET efficiency. In the cytoplasmic region, we measure iii) the concentration of the acceptor (equivalently, the adapter protein). See Figure 2-3, Panel B for an example of a swollen cell analyzed using FSI.

Here, we use this FRET data to consider two special cases of this thermodynamic cycle: saturating ligand conditions and ligand-free conditions. In both cases, the model in Figure 6-1 reduces substantially, allowing us to determine some of the parameters characterizing the system.

In the presence of ligand, the thermodynamics of the binding reaction between Grb2 and EGFR be quantified in live cells

In the first special case of the thermodynamic cycle of RTK activation (circled in blue in Figure 6-1), we consider receptor-adapter protein interactions under saturating

ligand conditions. We assume that, in the presence of excess ligand, all receptors exist as double-liganded, phosphorylated dimers. Since all receptors are found as phosphorylated dimers, the mass conservation equation (Equation 6-5) can be reduced to:

$$[T] = 2[D^*] + [D^*A_n] \tag{6-8}.$$

The relationship between liganded, phosphorylated RTK dimers bound and unbound to the adapter protein is governed by the association constant γ_2 (Equation 6-4). If we substitute this equilibrium relationship into Equation 6-8, we arrive at a single equation that describes the interaction between receptors and adapter proteins:

$$\frac{[T]}{2} = \frac{[D^*A_n]}{\gamma_2[A]^n} + [D^*A_n] \tag{6-9}.$$

Note that the concentration of dimer-adapter protein complexes, $[D^*A_n]$, depends on the variables [T] and $[A_n]$ and the parameter γ_2.

To facilitate comparison of this model with FRET data, we rearrange Equation 6-7 to describe $[D^*A_n]$ as a function of FRET efficiency:

$$[D^*A_n] = \frac{E[donor]}{E_{complex}} \tag{6-10}$$

and substitute into Equation 6-9 to find:

$$\frac{[T]}{2} = \left(\frac{E[donor]}{E_{complex}}\right)\left(\frac{1}{K[A]^n} + 1\right) \tag{6-11}.$$

The quantities [donor], [A], and E are all measured in FSI experiments. Non-linear least squares (128,165) (MATLAB's "nlinfit") is used to fit Equation 6-11 to experimental data, yielding the association constant, γ_2, and the geometrical parameter, $E_{complex}$, and their 95% confidence intervals. This fitting process is repeated for the possible receptor-adapter protein complex stoichiometries and geometries described in Figure 6-2. For each number of adapter proteins, n, we calculate the mean square error (MSE) between the best fit model and the experimental data according to:

$$MSE = \frac{\sum_{i=1}^{k}(FRET_{ex,i} - FRET_{th,i})^2}{k} \quad (6\text{-}12)$$

where k is the number of pairs of regions, $FRET_{ex,i}$ is the experimentally measured FRET efficiency, and $FRET_{th,i}$ is theoretical FRET efficiency (predicted by Equation 6-7). The value of n that minimizes the MSE is taken as the number of adapter proteins per dimer-adapter protein complex.

In Figure 6-3, we show data for the EGFR-Grb2 binding reaction, collected under saturating ligand conditions. Panel A displays the experimentally measured receptor concentration, adapter protein concentration, and FRET efficiency. In the left-hand plot, FRET efficiency is plotted as a function of acceptor concentration. The steep dependence of FRET efficiency on acceptor concentration suggests the occurrence of specific interactions. In the right-hand plot, we graph donor concentration versus acceptor concentration. For both plots, each green diamond corresponds to data from one pair of membrane and cytoplasmic regions in a swollen cell. An average of two pairs of regions are selected per cell.

Next, we compare this data to the thermodynamic cycle for RTK activation, in the limiting case of saturating ligand conditions (circled in blue in Figure 6-1). We fit Equation 6-11 to the experimental data while varying the number of adapter proteins per complex, n. Each fit yields the association constant between active EGFR dimers and Grb proteins, γ_2, and the geometrical FRET parameter, $E_{complex}$. In Panel C, we show the MSE (calculated according to Equation 6-12) for each n. The minimum MSE corresponds to n = 1, which suggests that there is one Grb2 protein bound to each EGFR dimer. We use this result for all subsequent analyses.

Here, we report the parameters describing adapter protein binding to RTK dimers when n = 1. The association constant between phosphorylated EGFR dimers and Grb2 proteins is $\gamma_2 = (5.95 \pm 0.7)x10^{-3}$ μm^3/protein and the FRET efficiency in the dimer-adapter protein complex is $E_{complex} = 0.640 \pm 0.02$. The best fit receptor-adapter protein model (yellow surface) is plotted alongside experimental data (green diamonds) in Panel C. The model and data are plotted on a linear scale in the left-hand plot and on a semi-log scale in the right-hand plot.

To further illustrate how the thermodynamic cycle for RTK activation behaves under saturating ligand conditions, Panel D displays the fraction of receptors found in active dimers (red line) and in dimer-adapter protein complexes (yellow line) for the best fit parameters. In the left-hand plot, the adapter protein concentration, [A], is fixed at 500 proteins/μm^3 and the total receptor protein concentration, [T], is varied between 0 and 1000 receptors/μm^2. In the right-hand plot, [T] is fixed at 500 proteins/μm^3 and [A] is varied between 0 and 1000 receptors/μm^2. The fraction of receptors found in dimer-adapter protein complexes increases as the adapter protein increases but shows no dependence on total receptor concentration.

In the absence of ligand, some EGFR dimers are phosphorylated

In the second special case of the thermodynamic cycle of RTK activation (circled in yellow in Figure 6-1), we consider receptor-adapter protein interactions in the absence of ligand. We must consider monomers, inactive dimers, active dimers, and dimer-adapter protein complexes. For the analysis presented here, the monomer-dimer equilibrium constant, α_0, must have been previously measured (here, we use $\alpha_0 = 6.8x10^{-3}$ μm^2/rec, as measured by Daniel Leahy's lab in unpublished work). We assume that the

binding reaction between active dimers and adapter proteins is independent of ligand (that is, $\gamma_2 = \gamma_0$ and the geometrical parameter $E_{complex}$ is the same as that measured under saturating ligand conditions). Thus, the only remaining unknown is β_0, the conformational parameter describing the relationship between inactive and active dimers.

We can use the thermodynamic relationships in Equations 3-2, 6-2, and 6-4 to relate the concentrations of receptor species to each other:

$$[D] = \alpha_0[M]^2$$

$$[D^*] = \beta_0[D]$$

$$[D^*A_n] = \gamma_0[D^*][A]^n \quad (6\text{-}13).$$

Using the relationships in Equation 6-13, we can write the mass conservation equation in terms of monomer concentration only:

$$[T] = [M] + 2\alpha_0[M]^2 + 2\beta_0\alpha_0[M]^2 + 2\gamma_0\beta_0\alpha_0[M]^2[A]^n \quad (6\text{-}14)$$

where α_0, β_0, and γ_0, and n are all known. We can solve for [M] as a function of [A] and [T] using the quadratic formula (125). Then, we can substitute into the three statements in Equation 6-13 to find the concentrations of the other three receptor species.

We use Equation 6-10 to calculate the concentration of the receptor-adapter protein complex [D*A_n] from the FRET efficiency. Combining the relationships in Equation 6-13, [D*A_n] can also be written as

$$[D^*A_n] = \gamma_0\beta_0\alpha_0[M]^2[A]^n \quad (6\text{-}15)$$

and this equation can be set equal to [D*A_n] as calculated from the FRET efficiency. Hence, we are left with two equations, 6-14 and 6-15, and two unknowns, β_0 and [M]. Non-linear least squares (MATLAB's "nlinfit") is used to simultaneously solve for [M] and fit for β_0 and its 95% confidence interval.

Data collected for EGFR-Grb2 interactions in the absence of ligand are presented in Figure 6-4. Panel A displays the experimentally measured receptor concentration, adapter protein concentration, and FRET efficiency. The left-hand plot shows FRET efficiency as a function of acceptor concentration. FRET efficiency increases with increasing acceptor concentration, but the dependence is less pronounced than that observed in the presence of ligand. Donor concentration versus acceptor concentration is plotted in the left-hand panel. Each green diamond corresponds to a pair of membrane and cytoplasmic regions.

We compare this experimental data to the thermodynamic cycle for RTK activation, in the absence of ligand. Here, we find $\beta_0 = 1.05 \pm 0.3$. In Panel B, the best fit model for $[D^*A_n]$ (yellow surface) is plotted alongside experimental data (green diamonds) on a linear scale (left-hand plot) and a semi-log scale (right-hand plot).

Panel C demonstrates how the thermodynamic cycle for RTK activation behaves in the absence of ligand. The fraction of receptors found as monomers (green line), inactive dimers (blue line), active dimers (red line), and dimer-adapter protein complexes (yellow line) are plotted as functions of the two variables [T] and [A], using the parameters for the best fit model. In the left-hand panel, adapter protein concentration is fixed at 500 proteins/μm^2 while [T] varies, and in the right-hand panel, total receptor concentration is fixed at 500 receptors/μm^2 while [A] varies. The fraction of receptors found in each species depends on both adapter protein concentration and total receptor concentration.

Discussion

The interaction between RTKs and adapter proteins has been studied extensively. These experiments can generally be sorted into two broad categories: traditional biophysical methods (152,156,157,161) and emerging cell-based techniques (139,147,148,163). In the first category of experiments (162,166), fluorescence spectroscopy, FRET, surface plasmon resonance, and isothermal titration calorimetry have all been used to characterize RTK-adapter protein interactions, yielding quantitative measures of thermodynamic and/or kinetic binding parameters. However, these traditional biophysical techniques require reducing the system to short peptides representing the RTK and adapter protein. Furthermore, they use synthetic lipids or surface display of RTK peptides to model the membrane, and are sometimes conducted in solution. In the second category of experiments, live cells are an increasingly popular model system for the study of protein-protein interactions, and they capture the native complexities of both the plasma membrane and the cytoplasm. These experiments incorporate full-length RTKs and adapter proteins, but typically consist of qualitative observations of adapter protein recruitment to receptors. In this work, we combine the quantitative power of traditional biophysical techniques with the biological relevance of live cell model systems and measure the thermodynamic association constant between a receptor and an adapter protein. This new method can be used to quantify RTK-adapter protein interactions and as a screening platform for TKIs.

Here, we examine the interaction of EGFR and Grb2. The SH2 domain binds to the phosphorylated Y1068 and Y1086 residues of EGFR (156,157). The stoichiometry of this reaction is debated in the literature (148,149,155), with estimates ranging between

one and four Grb2 proteins per EGFR dimer. We fit models with one, two, three, or four Grb2 proteins per EGFR dimer to our experimental data, and find the best fit for the model with one Grb2 protein per EGFR dimer. The model of one adapter protein per dimer seems reasonable in the context of both geometrical considerations and the current literature (5,153,154).

We characterize the thermodynamics of EGFR-Grb2 binding interactions under saturating ligand conditions. The high ligand concentration ensures that all receptors exist as dimers (167), and we assume that all of these dimers are phosphorylated. The association constant is measured as $\gamma_2 = (5.95 \pm 0.7)\text{x}10^{-3}$ μm^3/protein, equivalent to 279 ± 34 nM. This value is of the same order of magnitude as was previously measured using traditional biophysical techniques (5). We also report $E_{complex}$, a geometrical parameter that depends on the separation of the fluorescent proteins in the EGFR-Grb2 complex. The fluorophores are attached to the C-terminus of each protein, and we measure $E_{complex} = 0.640 \pm 0.02$. This corresponds to a fluorophore separation of 49.5 ± 0.7 Å in the receptor-adapter protein complex. This distance was calculated using Equation 3-8 and the Förster radius for the mTurquoise-YFP FRET pair (54.5 Å), under the assumption of free fluorophore rotation.

We also examine the EGFR-Grb2 binding interaction in the absence of ligand, in order to estimate the equilibrium between inactive (D) and active (D*) EGFR dimers. There is a literature consensus that some unliganded EGFR dimers are phosphorylated (5,15,147), but very few quantitative estimates for the relationship between D and D*. This is most likely due to a scarcity of experimental techniques capable of specifically measuring phosphorylation. Here, we leverage our newly developed FRET microscopy

technique to observe EGFR phosphorylation in live cells, through the recruitment of the adapter protein Grb2. We employ the two parameters describing RTK-adapter protein interactions measured under saturating ligand conditions, and the full-length EGFR homodimer association constant, to determine that the conformational parameter describing the equilibrium between D and D* is $\beta_0 = 1.05$. This result indicates that, in the absence of ligand, approximately one-half of EGFR dimers are phosphorylated. Our estimate for unliganded EGFR phosphorylation can be used to predict EGFR activity in the absence of ligand and contributes to the growing mechanistic understanding of the EGFR activation process.

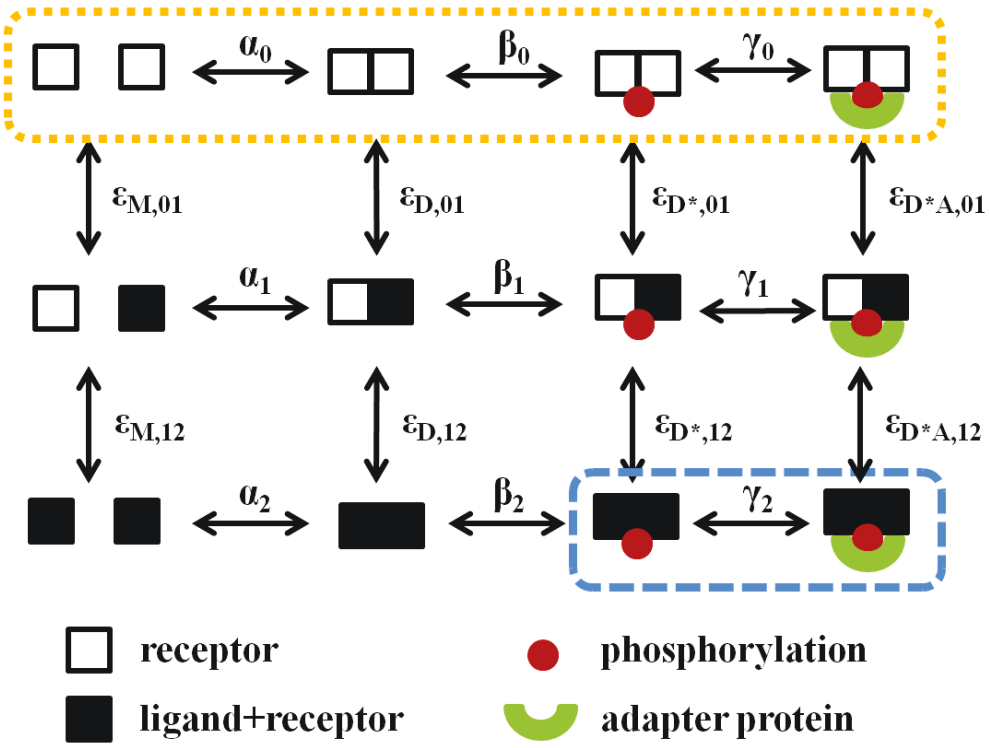

Figure 6-1. The thermodynamic cycle describing the RTK activation process. This model considers ligand binding, dimer formation, phosphorylation, and adapter protein binding. The model reduces under saturating ligand conditions (circled in blue) and in ligand-free conditions (circled in yellow).

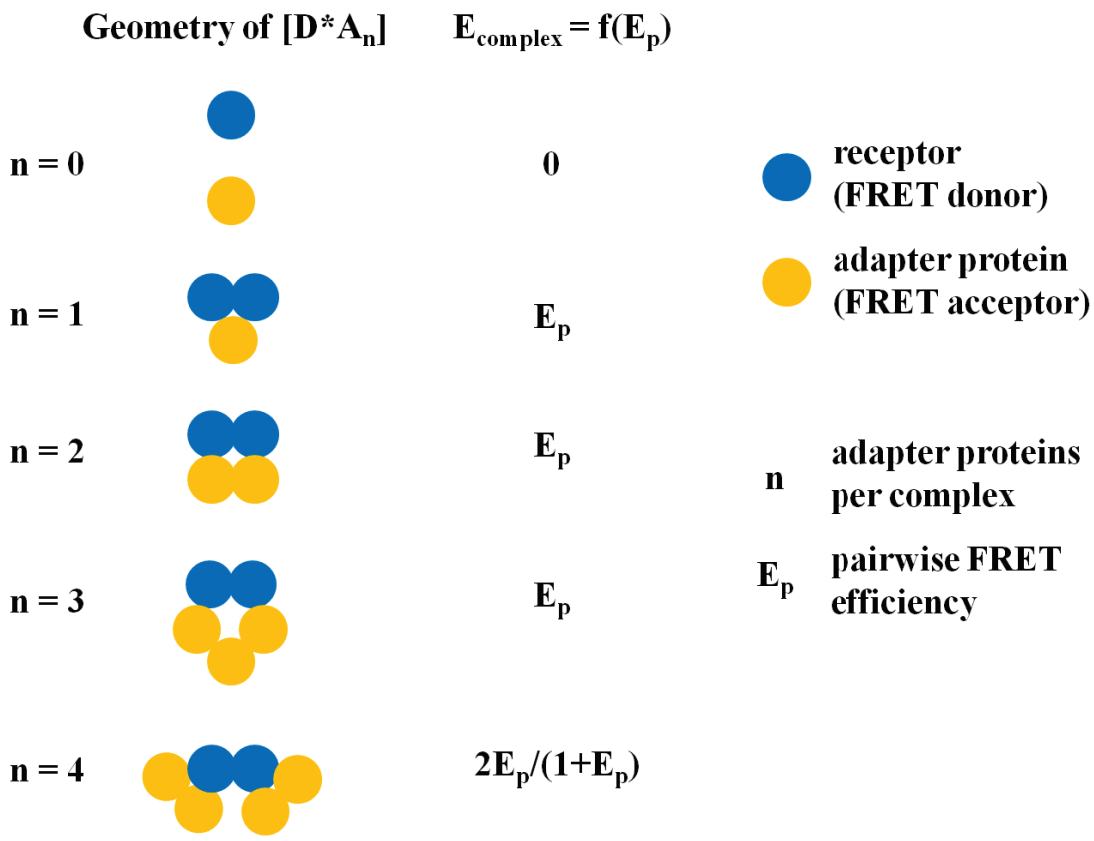

Figure 6-2. FRET efficiency for possible geometries of the dimer-adapter protein complex.

The number of adapter proteins, n, in the dimer-adapter protein complex remains a source of debate. Here, we consider the geometry of dimer-adapter protein complexes with zero, one, two, three, or four adapter proteins per complex. The FRET efficiency in each complex ($E_{complex}$) depends on the pairwise FRET efficiency (E_p) between one donor and one acceptor, as described by Raicu and Singh (164).

A

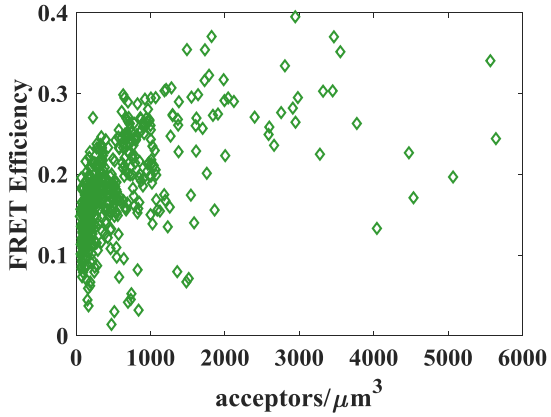
FRET Efficiency
0.4
0.3
0.2
0.1
0
0
1000
2000
3000
4000
5000
6000
acceptors/μm^3

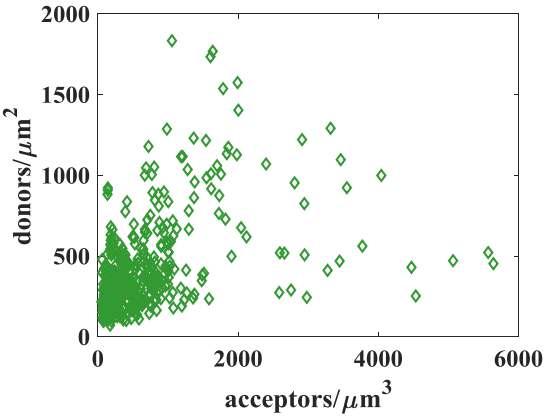
donors/μm^2
2000
1500
1000
500
0
0
2000
4000
6000
acceptors/μm^3

B

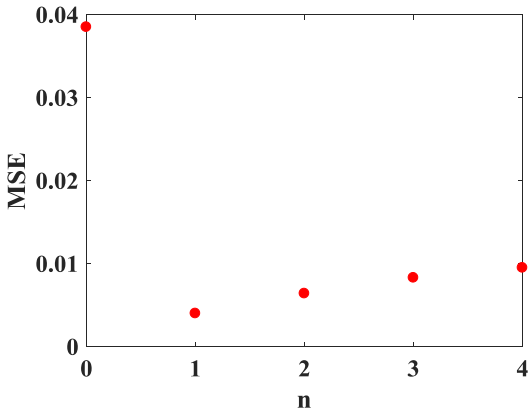
MSE
0.04
0.03
0.02
0.01
0
0
1
2
3
4
n

C

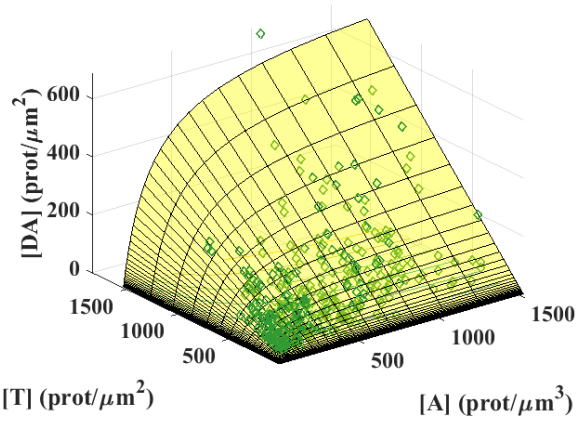
[DA] (prot/μm^2)
600
400
200
0
1500
1000
500
0
500
1000
1500
[T] (prot/μm^2)
[A] (prot/μm^3)

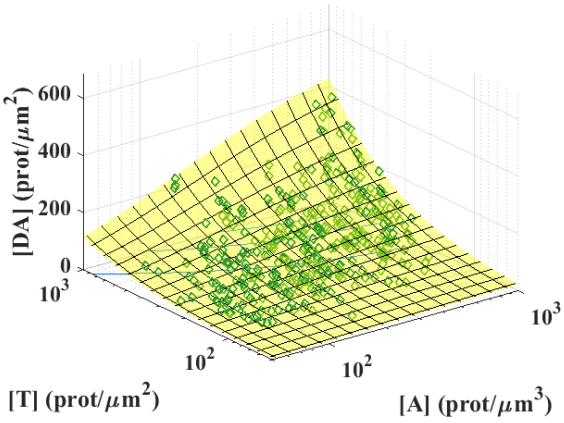
[DA] (prot/μm^2)
600
400
200
0
10^3
10^2
10^2
10^3
[T] (prot/μm^2)
[A] (prot/μm^3)

D

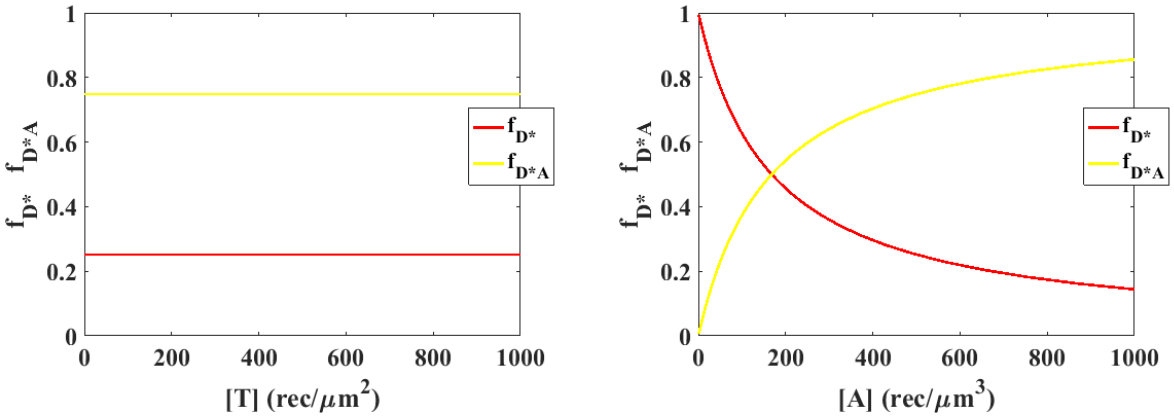

Figure 6-3. FRET data for the interaction between EGFR and Grb2, under saturating ligand conditions.

(A) In the left-hand plot, FRET efficiency is shown as a function of acceptor concentration. In the right-hand plot, we present the ratio between donor concentration and acceptor concentration. Each green diamond corresponds to one pair of membrane and cytoplasmic regions. (B) The MSE for fits to Equation 6-8 when the number of adapter proteins, n, is varied between zero and four. The model with one Grb2 per EGFR dimer gives the best fit. (C) The best fit model (yellow surface) and experimental data (green diamonds) on linear (left-hand plot) and semi-log (right-hand plot) scales. (D) The fraction of receptors found in phosphorylated dimers (red line) and in dimer-adapter protein complexes (yellow line) for the best fit model. In the left-hand panel, the adapter protein concentration is fixed at 500 proteins/μm^3 and the total receptor concentration is varied. In the right-hand plot, [T] is fixed at 500 receptors/μm^2 and [A] is varied.

A

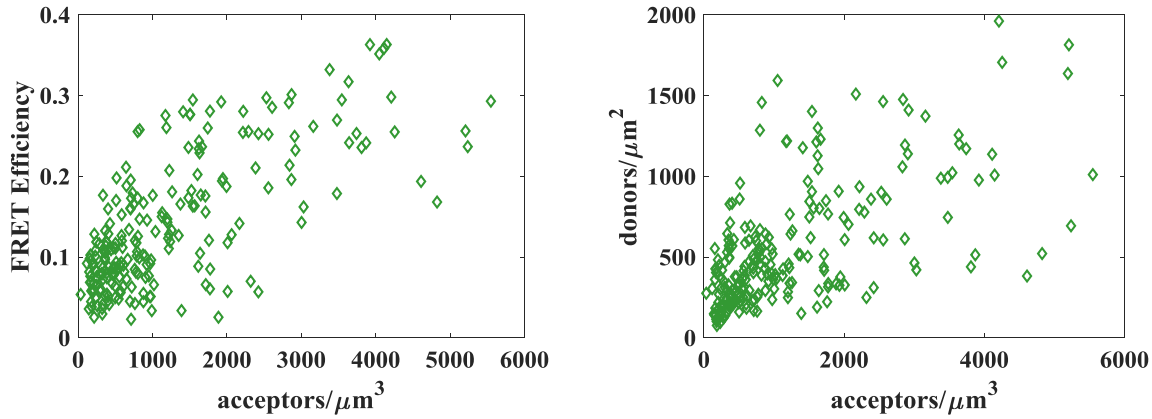
FRET Efficiency
acceptors/μm^3
donors/μm^2
acceptors/μm^3

B

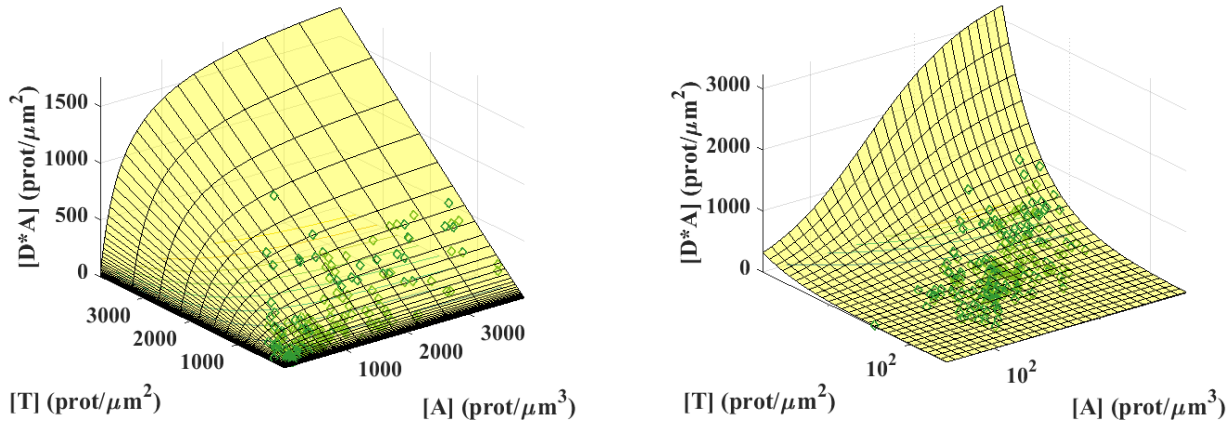
[D*A] (prot/μm^2)
[T] (prot/μm^2)
[A] (prot/μm^3)
[D*A] (prot/μm^2)
[T] (prot/μm^2)
[A] (prot/μm^3)

C

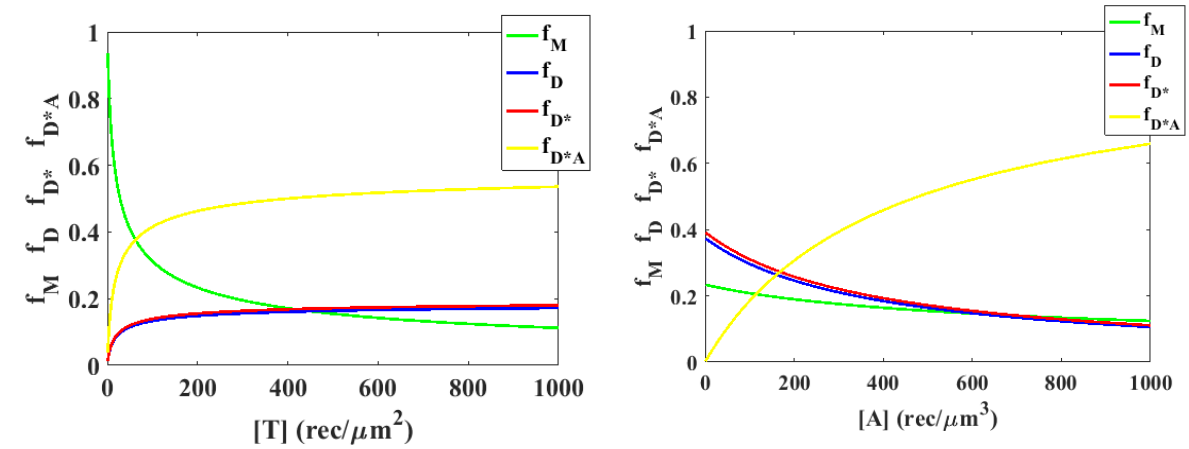
f_M f_D f_{D^*} f_{D^*A}
[T] (rec/μm^2)
[A] (rec/μm^3)

Figure 6-4. FRET data for the interaction between EGFR and Grb2, in the absence of ligand.

(A) In the left-hand plot, FRET efficiency is shown as a function of acceptor concentration and the right-hand plot depicts donor concentration versus acceptor concentration, for EGFR-Grb2 experiments in the absence of ligand. We fit Equation 6-14 to experimental data in order to determine the conformational parameter, β_0, describing the relationship between inactive and active dimers. (B) The best fit model (yellow surface) is plotted alongside experimental data (green diamonds) on both a linear (left-hand plot) and semi-log (right-hand plot) scale. (C) f_M, f_D, f_{D*}, and f_{D*A} are graphed as functions of [T] when [A] = 500 proteins/μm^3 (left-hand panel) and functions of [A] when [T] = 500 receptors/μm^2 (right-hand panel).

CHAPTER SEVEN Conclusions

Recent advances in microscopy have enabled the study of biological systems with unprecedented resolution in space and time. In the field of membrane protein research, improved microscopy techniques allow for the study of these complex proteins in their native environment. In this thesis, I leverage novel quantitative fluorescence microscopy techniques to examine RTKs in model membrane systems. I focus on the protein-protein interactions involved in the RTK activation process, through the implementation of existing protocols and the development of new techniques. My results both support and contribute to the emerging model for RTK activation (see Figure 1-1, Panel B).

In Chapter Three and Chapter Five, I study unliganded dimers. I contribute to the growing body of evidence that wild-type FGFRs can form unliganded homodimers and show, for the first time, that wild-type FGFRs can also form unliganded heterodimers. Since both FGFR homodimers and heterodimers form with similar propensities, both species must be considered in analyses of FGFR functions. This principle may also be applicable to other families of RTKs. Additionally, I show that, when FGFRs carry certain pathogenic point mutations, both homodimer and heterodimer thermodynamics and conformation can be altered. The observed changes in unliganded FGFR dimers might contribute to the progression of developmental disorders and should be considered during the development of therapeutics.

In Chapter Four, I study liganded homodimers. My results indicate that ligand addition can induce conformational changes in FGFR homodimers, which supports the proposed role of ligand in the emerging model for RTK activation. Additionally, my work suggests that homodimer conformation can depend on the identity of the ligand,

which may be one way that receptors differentiate between ligands and generate the biological outcomes unique to each ligand. Again, this is a principle of RTK activation that might be relevant to other receptors.

In Chapter Six, I study the recruitment of an adapter protein to a phosphorylated RTK dimer, an event that directly links activated receptors to intracellular signaling cascades. I develop a procedure for measuring the thermodynamics of this interaction in live cells, and apply it to the interaction between the adapter protein Grb2 and EGFR homodimers. Leveraging results obtained in the presence of ligand, I evaluate the phosphorylation of the unliganded EGFR dimer and find that approximately one-half of unliganded EGFR dimers are phosphorylated. This suggests that, in the emerging model for RTK activation, the unliganded dimer species can be an important signaling entity.

Overall, thesis work i) illustrates the usefulness of fluorescence microscopy for the study of protein-protein interactions and membrane proteins, ii) presents new techniques for the study of protein-protein interactions in the plasma membrane, and iii) advances the scientific community's understanding of the RTK activation process.

REFERENCES

1. Chene, P. (2012) Can biochemistry drive drug discovery beyond simple potency measurements? *Drug discovery today* **17**, 388-395
2. Oda, K., Matsuoka, Y., Funahashi, A., and Kitano, H. (2005) A comprehensive pathway map of epidermal growth factor receptor signaling. *Molecular systems biology* **1**, 2005 0010
3. Qutub, A. A., Mac Gabhann, F., Karagiannis, E. D., Vempati, P., and Popel, A. S. (2009) Multiscale models of angiogenesis. *IEEE engineering in medicine and biology magazine : the quarterly magazine of the Engineering in Medicine & Biology Society* **28**, 14-31
4. Lemmon, M. A., and Schlessinger, J. (2010) Cell signaling by receptor tyrosine kinases. *Cell* **141**, 1117-1134
5. Hsieh, M. Y., Yang, S., Raymond-Stinz, M. A., Edwards, J. S., and Wilson, B. S. (2010) Spatio-temporal modeling of signaling protein recruitment to EGFR. *BMC systems biology* **4**, 57
6. Overington, J. P., Al-Lazikani, B., and Hopkins, A. L. (2006) How many drug targets are there? *Nature reviews. Drug discovery* **5**, 993-996
7. von Heijne, G. (1999) A Day in the Life of Dr K. or How I Learned to Stop Worrying and Love Lysozyme: a tragedy in six acts. *Journal of molecular biology* **293**, 367-379
8. Hong, H., Joh, N. H., Bowie, J. U., and Tamm, L. K. (2009) Methods for measuring the thermodynamic stability of membrane proteins. *Methods in enzymology* **455**, 213-236
9. Mackenzie, K. R. (2006) Folding and stability of alpha-helical integral membrane proteins. *Chemical reviews* **106**, 1931-1977
10. Lemmon, M. A., Schlessinger, J., and Ferguson, K. M. (2014) The EGFR family: not so prototypical receptor tyrosine kinases. *Cold Spring Harbor perspectives in biology* **6**, a020768
11. Schlessinger, J. (2000) Cell signaling by receptor tyrosine kinases. *Cell* **103**, 211-225
12. Schlessinger, J. (2014) Receptor tyrosine kinases: legacy of the first two decades. *Cold Spring Harbor perspectives in biology* **6**
13. Eswarakumar, V. P., Lax, I., and Schlessinger, J. (2005) Cellular signaling by fibroblast growth factor receptors. *Cytokine & growth factor reviews* **16**, 139-149
14. Ornitz, D. M., and Itoh, N. (2015) The Fibroblast Growth Factor signaling pathway. *Wiley interdisciplinary reviews. Developmental biology* **4**, 215-266
15. Hynes, N. E., and Lane, H. A. (2005) ERBB receptors and cancer: the complexity of targeted inhibitors. *Nature reviews. Cancer* **5**, 341-354
16. Olayioye, M. A., Neve, R. M., Lane, H. A., and Hynes, N. E. (2000) The ErbB signaling network: receptor heterodimerization in development and cancer. *The EMBO journal* **19**, 3159-3167
17. Gschwind, A., Fischer, O. M., and Ullrich, A. (2004) The discovery of receptor tyrosine kinases: targets for cancer therapy. *Nature reviews. Cancer* **4**, 361-370
18. Sarabipour, S., and Hristova, K. (2016) Mechanism of FGF receptor dimerization and activation. *Nature communications* **7**, 10262

19. Sarabipour, S., Ballmer-Hofer, K., and Hristova, K. (2016) VEGFR-2 conformational switch in response to ligand binding. *eLife* **5**, e13876
20. He, L., Horton, W., and Hristova, K. (2010) Physical basis behind achondroplasia, the most common form of human dwarfism. *The Journal of biological chemistry* **285**, 30103-30114
21. He, L., Shobnam, N., Wimley, W. C., and Hristova, K. (2011) FGFR3 heterodimerization in achondroplasia, the most common form of human dwarfism. *The Journal of biological chemistry* **286**, 13272-13281
22. Wilkie, A. O., Morriss-Kay, G. M., Jones, E. Y., and Heath, J. K. (1995) Functions of fibroblast growth factors and their receptors. *Current biology : CB* **5**, 500-507
23. Foldynova-Trantirkova, S., Wilcox, W. R., and Krejci, P. (2012) Sixteen years and counting: the current understanding of fibroblast growth factor receptor 3 (FGFR3) signaling in skeletal dysplasias. *Human mutation* **33**, 29-41
24. Cunningham, M. L., Seto, M. L., Ratisoontorn, C., Heike, C. L., and Hing, A. V. (2007) Syndromic craniosynostosis: from history to hydrogen bonds. *Orthodontics & craniofacial research* **10**, 67-81
25. Schlessinger, J., Plotnikov, A. N., Ibrahimi, O. A., Eliseenkova, A. V., Yeh, B. K., Yayon, A., Linhardt, R. J., and Mohammadi, M. (2000) Crystal structure of a ternary FGF-FGFR-heparin complex reveals a dual role for heparin in FGFR binding and dimerization. *Molecular cell* **6**, 743-750
26. Chen, L., Placone, J., Novicky, L., and Hristova, K. (2010) The extracellular domain of fibroblast growth factor receptor 3 inhibits ligand-independent dimerization. *Science signaling* **3**, ra86
27. Bocharov, E. V., Lesovoy, D. M., Goncharuk, S. A., Goncharuk, M. V., Hristova, K., and Arseniev, A. S. (2013) Structure of FGFR3 transmembrane domain dimer: implications for signaling and human pathologies. *Structure* **21**, 2087-2093
28. Yewale, C., Baradia, D., Vhora, I., Patil, S., and Misra, A. (2013) Epidermal growth factor receptor targeting in cancer: a review of trends and strategies. *Biomaterials* **34**, 8690-8707
29. Huang, Y., Bharill, S., Karandur, D., Peterson, S. M., Marita, M., Shi, X., Kaliszewski, M. J., Smith, A. W., Isacoff, E. Y., and Kuriyan, J. (2016) Molecular basis for multimerization in the activation of the epidermal growth factor receptor. *eLife* **5**
30. Duneau, J. P., Vegh, A. P., and Sturgis, J. N. (2007) A dimerization hierarchy in the transmembrane domains of the HER receptor family. *Biochemistry* **46**, 2010-2019
31. Needham, S. R., Roberts, S. K., Arkhipov, A., Mysore, V. P., Tynan, C. J., Zanetti-Domingues, L. C., Kim, E. T., Losasso, V., Korovesis, D., Hirsch, M., Rolfe, D. J., Clarke, D. T., Winn, M. D., Lajevardipour, A., Clayton, A. H., Pike, L. J., Perani, M., Parker, P. J., Shan, Y., Shaw, D. E., and Martin-Fernandez, M. L. (2016) EGFR oligomerization organizes kinase-active dimers into competent signalling platforms. *Nature communications* **7**, 13307
32. Placone, J., and Hristova, K. (2012) Direct assessment of the effect of the Gly380Arg achondroplasia mutation on FGFR3 dimerization using quantitative imaging FRET. *PloS one* **7**, e46678

33. Sarabipour, S., and Hristova, K. (2013) FGFR3 transmembrane domain interactions persist in the presence of its extracellular domain. *Biophysical journal* **105**, 165-171
34. Del Piccolo, N., Placone, J., and Hristova, K. (2015) Effect of thanatophoric dysplasia type I mutations on FGFR3 dimerization. *Biophysical journal* **108**, 272-278
35. Liu, P., Cleveland, T. E. t., Bouyain, S., Byrne, P. O., Longo, P. A., and Leahy, D. J. (2012) A single ligand is sufficient to activate EGFR dimers. *Proceedings of the National Academy of Sciences of the United States of America* **109**, 10861-10866
36. Baycin-Hizal, D., Tabb, D. L., Chaerkady, R., Chen, L., Lewis, N. E., Nagarajan, H., Sarkaria, V., Kumar, A., Wolozny, D., Colao, J., Jacobson, E., Tian, Y., O'Meally, R. N., Krag, S. S., Cole, R. N., Palsson, B. O., Zhang, H., and Betenbaugh, M. (2012) Proteomic analysis of Chinese hamster ovary cells. *Journal of proteome research* **11**, 5265-5276
37. Li, F., Vijayasankaran, N., Shen, A. Y., Kiss, R., and Amanullah, A. (2010) Cell culture processes for monoclonal antibody production. *mAbs* **2**, 466-479
38. Mohan, C., Kim, Y. G., Koo, J., and Lee, G. M. (2008) Assessment of cell engineering strategies for improved therapeutic protein production in CHO cells. *Biotechnology journal* **3**, 624-630
39. Mueller, N. S., Wedlich-Soldner, R., and Spira, F. (2012) From mosaic to patchwork: matching lipids and proteins in membrane organization. *Molecular membrane biology* **29**, 186-196
40. Levental, K. R., and Levental, I. (2015) Giant plasma membrane vesicles: models for understanding membrane organization. *Current topics in membranes* **75**, 25-57
41. Sinha, B., Koster, D., Ruez, R., Gonnord, P., Bastiani, M., Abankwa, D., Stan, R. V., Butler-Browne, G., Vedie, B., Johannes, L., Morone, N., Parton, R. G., Raposo, G., Sens, P., Lamaze, C., and Nassoy, P. (2011) Cells respond to mechanical stress by rapid disassembly of caveolae. *Cell* **144**, 402-413
42. Adler, J., Shevchuk, A. I., Novak, P., Korchev, Y. E., and Parmryd, I. (2010) Plasma membrane topography and interpretation of single-particle tracks. *Nature methods* **7**, 170-171
43. Del Piccolo, N., Placone, J., He, L., Agudelo, S. C., and Hristova, K. (2012) Production of plasma membrane vesicles with chloride salts and their utility as a cell membrane mimetic for biophysical characterization of membrane protein interactions. *Analytical chemistry* **84**, 8650-8655
44. Sarabipour, S., Chan, R. B., Zhou, B., Di Paolo, G., and Hristova, K. (2015) Analytical characterization of plasma membrane-derived vesicles produced via osmotic and chemical vesiculation. *Biochimica et biophysica acta* **1848**, 1591-1598
45. Scott, R. E., Perkins, R. G., Zschunke, M. A., Hoerl, B. J., and Maercklein, P. B. (1979) Plasma membrane vesiculation in 3T3 and SV3T3 cells. I. Morphological and biochemical characterization. *Journal of cell science* **35**, 229-243

46. King, C., Stoneman, M., Raicu, V., and Hristova, K. (2016) Fully quantified spectral imaging reveals in vivo membrane protein interactions. *Integrative biology : quantitative biosciences from nano to macro* **8**, 216-229
47. Scott, R. E. (1976) Plasma membrane vesiculation: a new technique for isolation of plasma membranes. *Science* **194**, 743-745
48. Scott, R. E., and Maercklein, P. B. (1979) Plasma membrane vesiculation in 3T3 and SV3T3 cells. II. Factors affecting the process of vesiculation. *Journal of cell science* **35**, 245-252
49. Cohen, S., Ushiro, H., Stoscheck, C., and Chinkers, M. (1982) A native 170,000 epidermal growth factor receptor-kinase complex from shed plasma membrane vesicles. *The Journal of biological chemistry* **257**, 1523-1531
50. Rauch, C., and Farge, E. (2000) Endocytosis switch controlled by transmembrane osmotic pressure and phospholipid number asymmetry. *Biophysical journal* **78**, 3036-3047
51. Lichtman, J. W., and Conchello, J. A. (2005) Fluorescence microscopy. *Nature methods* **2**, 910-919
52. Raicu, V. (2007) Efficiency of resonance energy transfer in homo-oligomeric complexes of proteins. *Journal of biological physics* **33**, 109-127
53. Li, E., Placone, J., Merzlyakov, M., and Hristova, K. (2008) Quantitative measurements of protein interactions in a crowded cellular environment. *Analytical chemistry* **80**, 5976-5985
54. Chen, L., Novicky, L., Merzlyakov, M., Hristov, T., and Hristova, K. (2010) Measuring the energetics of membrane protein dimerization in mammalian membranes. *Journal of the American Chemical Society* **132**, 3628-3635
55. Sarabipour, S., Del Piccolo, N., and Hristova, K. (2015) Characterization of membrane protein interactions in plasma membrane derived vesicles with quantitative imaging Forster resonance energy transfer. *Accounts of chemical research* **48**, 2262-2269
56. Biener, G., Stoneman, M. R., Acbas, G., Holz, J. D., Orlova, M., Komarova, L., Kuchin, S., and Raicu, V. (2013) Development and experimental testing of an optical micro-spectroscopic technique incorporating true line-scan excitation. *International journal of molecular sciences* **15**, 261-276
57. So, P. T., Dong, C. Y., Masters, B. R., and Berland, K. M. (2000) Two-photon excitation fluorescence microscopy. *Annual review of biomedical engineering* **2**, 399-429
58. Cohen, M. M., Jr. (2006) The new bone biology: pathologic, molecular, and clinical correlates. *American journal of medical genetics. Part A* **140**, 2646-2706
59. Cohen, M. M., Jr. (2002) Some chondrodysplasias with short limbs: molecular perspectives. *American journal of medical genetics* **112**, 304-313
60. Passos-Bueno, M. R., Wilcox, W. R., Jabs, E. W., Sertie, A. L., Alonso, L. G., and Kitoh, H. (1999) Clinical spectrum of fibroblast growth factor receptor mutations. *Human mutation* **14**, 115-125
61. Rousseau, F., el Ghouzzi, V., Delezoide, A. L., Legeai-Mallet, L., Le Merrer, M., Munnich, A., and Bonaventure, J. (1996) Missense FGFR3 mutations create cysteine residues in thanatophoric dwarfism type I (TD1). *Human molecular genetics* **5**, 509-512

62. L'Hote, C. G., and Knowles, M. A. (2005) Cell responses to FGFR3 signalling: growth, differentiation and apoptosis. *Experimental cell research* **304**, 417-431
63. Tavormina, P. L., Shiang, R., Thompson, L. M., Zhu, Y. Z., Wilkin, D. J., Lachman, R. S., Wilcox, W. R., Rimoin, D. L., Cohn, D. H., and Wasmuth, J. J. (1995) Thanatophoric dysplasia (types I and II) caused by distinct mutations in fibroblast growth factor receptor 3. *Nature genetics* **9**, 321-328
64. Adar, R., Monsonego-Ornan, E., David, P., and Yayon, A. (2002) Differential activation of cysteine-substitution mutants of fibroblast growth factor receptor 3 is determined by cysteine localization. *Journal of bone and mineral research : the official journal of the American Society for Bone and Mineral Research* **17**, 860-868
65. d'Avis, P. Y., Robertson, S. C., Meyer, A. N., Bardwell, W. M., Webster, M. K., and Donoghue, D. J. (1998) Constitutive activation of fibroblast growth factor receptor 3 by mutations responsible for the lethal skeletal dysplasia thanatophoric dysplasia type I. *Cell growth & differentiation : the molecular biology journal of the American Association for Cancer Research* **9**, 71-78
66. Krejci, P., Salazar, L., Kashiwada, T. A., Chlebova, K., Salasova, A., Thompson, L. M., Bryja, V., Kozubik, A., and Wilcox, W. R. (2008) Analysis of STAT1 activation by six FGFR3 mutants associated with skeletal dysplasia undermines dominant role of STAT1 in FGFR3 signaling in cartilage. *PloS one* **3**, e3961
67. Naski, M. C., Wang, Q., Xu, J., and Ornitz, D. M. (1996) Graded activation of fibroblast growth factor receptor 3 by mutations causing achondroplasia and thanatophoric dysplasia. *Nature genetics* **13**, 233-237
68. Bonaventure, J., Horne, W. C., and Baron, R. (2007) The localization of FGFR3 mutations causing thanatophoric dysplasia type I differentially affects phosphorylation, processing and ubiquitylation of the receptor. *The FEBS journal* **274**, 3078-3093
69. Harada, D., Yamanaka, Y., Ueda, K., Tanaka, H., and Seino, Y. (2009) FGFR3-related dwarfism and cell signaling. *Journal of bone and mineral metabolism* **27**, 9-15
70. Deng, C., Wynshaw-Boris, A., Zhou, F., Kuo, A., and Leder, P. (1996) Fibroblast growth factor receptor 3 is a negative regulator of bone growth. *Cell* **84**, 911-921
71. Goetz, R., and Mohammadi, M. (2013) Exploring mechanisms of FGF signalling through the lens of structural biology. *Nature reviews. Molecular cell biology* **14**, 166-180
72. Ornitz, D. M. (2000) FGFs, heparan sulfate and FGFRs: complex interactions essential for development. *BioEssays : news and reviews in molecular, cellular and developmental biology* **22**, 108-112
73. Ornitz, D. M., and Itoh, N. (2001) Fibroblast growth factors. *Genome biology* **2**, REVIEWS3005
74. Greulich, H., Kaplan, B., Mertins, P., Chen, T. H., Tanaka, K. E., Yun, C. H., Zhang, X., Lee, S. H., Cho, J., Ambrogio, L., Liao, R., Imielinski, M., Banerji, S., Berger, A. H., Lawrence, M. S., Zhang, J., Pho, N. H., Walker, S. R., Winckler, W., Getz, G., Frank, D., Hahn, W. C., Eck, M. J., Mani, D. R., Jaffe, J. D., Carr, S. A., Wong, K. K., and Meyerson, M. (2012) Functional analysis of receptor tyrosine kinase mutations in lung cancer identifies oncogenic extracellular domain

mutations of ERBB2. *Proceedings of the National Academy of Sciences of the United States of America* **109**, 14476-14481
75. Phay, J. E., and Shah, M. H. (2010) Targeting RET receptor tyrosine kinase activation in cancer. *Clinical cancer research : an official journal of the American Association for Cancer Research* **16**, 5936-5941
76. Iyer, G., and Milowsky, M. I. (2013) Fibroblast growth factor receptor-3 in urothelial tumorigenesis. *Urologic oncology* **31**, 303-311
77. King, C., Sarabipour, S., Byrne, P., Leahy, D. J., and Hristova, K. (2014) The FRET signatures of noninteracting proteins in membranes: simulations and experiments. *Biophysical journal* **106**, 1309-1317
78. Evers, T. H., van Dongen, E. M., Faesen, A. C., Meijer, E. W., and Merkx, M. (2006) Quantitative understanding of the energy transfer between fluorescent proteins connected via flexible peptide linkers. *Biochemistry* **45**, 13183-13192
79. Bevington, P. R., Robinson, D. Keith. (2003) *Data Reduction and Error Analysis for the Physical Sciences*, 3 ed., McGraw-Hill, New York, NY
80. Placone, J., He, L., Del Piccolo, N., and Hristova, K. (2014) Strong dimerization of wild-type ErbB2/Neu transmembrane domain and the oncogenic Val664Glu mutant in mammalian plasma membranes. *Biochimica et biophysica acta* **1838**, 2326-2330
81. Sarabipour, S., and Hristova, K. (2013) Glycophorin A transmembrane domain dimerization in plasma membrane vesicles derived from CHO, HEK 293T, and A431 cells. *Biochimica et biophysica acta* **1828**, 1829-1833
82. Wolber, P. K., and Hudson, B. S. (1979) An analytic solution to the Forster energy transfer problem in two dimensions. *Biophysical journal* **28**, 197-210
83. Freire, E., and Snyder, B. (1982) Quantitative characterization of the lateral distribution of membrane proteins within the lipid bilayer. *Biophysical journal* **37**, 617-624
84. Betz, S. F. (1993) Disulfide bonds and the stability of globular proteins. *Protein science : a publication of the Protein Society* **2**, 1551-1558
85. McAuley, A., Jacob, J., Kolvenbach, C. G., Westland, K., Lee, H. J., Brych, S. R., Rehder, D., Kleemann, G. R., Brems, D. N., and Matsumura, M. (2008) Contributions of a disulfide bond to the structure, stability, and dimerization of human IgG1 antibody CH3 domain. *Protein science : a publication of the Protein Society* **17**, 95-106
86. Fathi, S., Nayak, C. R., Feld, J. J., and Zilman, A. G. (2016) Absolute Ligand Discrimination by Dimeric Signaling Receptors. *Biophysical journal* **111**, 917-920
87. Olsson, A. K., Dimberg, A., Kreuger, J., and Claesson-Welsh, L. (2006) VEGF receptor signalling - in control of vascular function. *Nature reviews. Molecular cell biology* **7**, 359-371
88. Peters, K. G., Werner, S., Chen, G., and Williams, L. T. (1992) Two FGF receptor genes are differentially expressed in epithelial and mesenchymal tissues during limb formation and organogenesis in the mouse. *Development* **114**, 233-243
89. Xu, X., Weinstein, M., Li, C., and Deng, C. (1999) Fibroblast growth factor receptors (FGFRs) and their roles in limb development. *Cell and tissue research* **296**, 33-43

90. Martin, G. R. (1998) The roles of FGFs in the early development of vertebrate limbs. *Genes & development* **12**, 1571-1586
91. Su, N., Jin, M., and Chen, L. (2014) Role of FGF/FGFR signaling in skeletal development and homeostasis: learning from mouse models. *Bone research* **2**, 14003
92. Mariani, F. V., Ahn, C. P., and Martin, G. R. (2008) Genetic evidence that FGFs have an instructive role in limb proximal-distal patterning. *Nature* **453**, 401-405
93. Yu, K., and Ornitz, D. M. (2008) FGF signaling regulates mesenchymal differentiation and skeletal patterning along the limb bud proximodistal axis. *Development* **135**, 483-491
94. Delezoide, A. L., Benoist-Lasselin, C., Legeai-Mallet, L., Le Merrer, M., Munnich, A., Vekemans, M., and Bonaventure, J. (1998) Spatio-temporal expression of FGFR 1, 2 and 3 genes during human embryo-fetal ossification. *Mechanisms of development* **77**, 19-30
95. Bell, G. W., Yatskievych, T. A., and Antin, P. B. (2004) GEISHA, a whole-mount in situ hybridization gene expression screen in chicken embryos. *Developmental dynamics : an official publication of the American Association of Anatomists* **229**, 677-687
96. Darnell, D. K., Kaur, S., Stanislaw, S., Davey, S., Konieczka, J. H., Yatskievych, T. A., and Antin, P. B. (2007) GEISHA: an in situ hybridization gene expression resource for the chicken embryo. *Cytogenetic and genome research* **117**, 30-35
97. Olsen, S. K., Li, J. Y., Bromleigh, C., Eliseenkova, A. V., Ibrahimi, O. A., Lao, Z., Zhang, F., Linhardt, R. J., Joyner, A. L., and Mohammadi, M. (2006) Structural basis by which alternative splicing modulates the organizer activity of FGF8 in the brain. *Genes & development* **20**, 185-198
98. Chen, F., and Hristova, K. (2011) The physical basis of FGFR3 response to fgf1 and fgf2. *Biochemistry* **50**, 8576-8582
99. Mohammadi, M., Olsen, S. K., and Ibrahimi, O. A. (2005) Structural basis for fibroblast growth factor receptor activation. *Cytokine & growth factor reviews* **16**, 107-137
100. Ornitz, D. M., Xu, J., Colvin, J. S., McEwen, D. G., MacArthur, C. A., Coulier, F., Gao, G., and Goldfarb, M. (1996) Receptor specificity of the fibroblast growth factor family. *The Journal of biological chemistry* **271**, 15292-15297
101. Ibrahimi, O. A., Zhang, F., Eliseenkova, A. V., Itoh, N., Linhardt, R. J., and Mohammadi, M. (2004) Biochemical analysis of pathogenic ligand-dependent FGFR2 mutations suggests distinct pathophysiological mechanisms for craniofacial and limb abnormalities. *Human molecular genetics* **13**, 2313-2324
102. Bell, C. A., Tynan, J. A., Hart, K. C., Meyer, A. N., Robertson, S. C., and Donoghue, D. J. (2000) Rotational coupling of the transmembrane and kinase domains of the Neu receptor tyrosine kinase. *Molecular biology of the cell* **11**, 3589-3599
103. Tamagaki, H., Furukawa, Y., Yamaguchi, R., Hojo, H., Aimoto, S., Smith, S. O., and Sato, T. (2014) Coupling of transmembrane helix orientation to membrane release of the juxtamembrane region in FGFR3. *Biochemistry* **53**, 5000-5007
104. Reddy, T., Manrique, S., Buyan, A., Hall, B. A., Chetwynd, A., and Sansom, M. S. (2014) Primary and secondary dimer interfaces of the fibroblast growth factor

receptor 3 transmembrane domain: characterization via multiscale molecular dynamics simulations. *Biochemistry* **53**, 323-332
105. Low-Nam, S. T., Lidke, K. A., Cutler, P. J., Roovers, R. C., van Bergen en Henegouwen, P. M., Wilson, B. S., and Lidke, D. S. (2011) ErbB1 dimerization is promoted by domain co-confinement and stabilized by ligand binding. *Nature structural & molecular biology* **18**, 1244-1249
106. Chung, I., Akita, R., Vandlen, R., Toomre, D., Schlessinger, J., and Mellman, I. (2010) Spatial control of EGF receptor activation by reversible dimerization on living cells. *Nature* **464**, 783-787
107. Lin, C. C., Melo, F. A., Ghosh, R., Suen, K. M., Stagg, L. J., Kirkpatrick, J., Arold, S. T., Ahmed, Z., and Ladbury, J. E. (2012) Inhibition of basal FGF receptor signaling by dimeric Grb2. *Cell* **149**, 1514-1524
108. Dietz, M. S., Hasse, D., Ferraris, D. M., Gohler, A., Niemann, H. H., and Heilemann, M. (2013) Single-molecule photobleaching reveals increased MET receptor dimerization upon ligand binding in intact cells. *BMC biophysics* **6**, 6
109. Krejci, P. (2014) The paradox of FGFR3 signaling in skeletal dysplasia: why chondrocytes growth arrest while other cells over proliferate. *Mutation research. Reviews in mutation research* **759**, 40-48
110. He, L., and Hristova, K. (2008) Pathogenic activation of receptor tyrosine kinases in mammalian membranes. *Journal of molecular biology* **384**, 1130-1142
111. Drevs, J., Medinger, M., Schmidt-Gersbach, C., Weber, R., and Unger, C. (2003) Receptor tyrosine kinases: the main targets for new anticancer therapy. *Current drug targets* **4**, 113-121
112. Pantaleo, M. A., Nannini, M., Lopci, E., Castellucci, P., Maleddu, A., Lodi, F., Nanni, C., Allegri, V., Astorino, M., Brandi, G., Di Battista, M., Boschi, S., Fanti, S., and Biasco, G. (2008) Molecular imaging and targeted therapies in oncology: new concepts in treatment response assessment. a collection of cases. *International journal of oncology* **33**, 443-452
113. Tzahar, E., Waterman, H., Chen, X., Levkowitz, G., Karunagaran, D., Lavi, S., Ratzkin, B. J., and Yarden, Y. (1996) A hierarchical network of interreceptor interactions determines signal transduction by Neu differentiation factor/neuregulin and epidermal growth factor. *Molecular and cellular biology* **16**, 5276-5287
114. Gerber, D., Sal-Man, N., and Shai, Y. (2004) Two motifs within a transmembrane domain, one for homodimerization and the other for heterodimerization. *The Journal of biological chemistry* **279**, 21177-21182
115. Vajo, Z., Francomano, C. A., and Wilkin, D. J. (2000) The molecular and genetic basis of fibroblast growth factor receptor 3 disorders: the achondroplasia family of skeletal dysplasias, Muenke craniosynostosis, and Crouzon syndrome with acanthosis nigricans. *Endocrine reviews* **21**, 23-39
116. Webster, M. K., and Donoghue, D. J. (1997) FGFR activation in skeletal disorders: too much of a good thing. *Trends in genetics : TIG* **13**, 178-182
117. Bellot, F., Crumley, G., Kaplow, J. M., Schlessinger, J., Jaye, M., and Dionne, C. A. (1991) Ligand-induced transphosphorylation between different FGF receptors. *The EMBO journal* **10**, 2849-2854

118. Sarabipour, S., and Hristova, K. (2015) FGFR3 unliganded dimer stabilization by the juxtamembrane domain. *Journal of molecular biology* **427**, 1705-1714
119. Sarabipour, S., and Hristova, K. (2016) Effect of the achondroplasia mutation on FGFR3 dimerization and FGFR3 structural response to fgf1 and fgf2: A quantitative FRET study in osmotically derived plasma membrane vesicles. *Biochimica et biophysica acta* **1858**, 1436-1442
120. Ahmad, I., Iwata, T., and Leung, H. Y. (2012) Mechanisms of FGFR-mediated carcinogenesis. *Biochimica et biophysica acta* **1823**, 850-860
121. Merzlyakov, M., You, M., Li, E., and Hristova, K. (2006) Transmembrane helix heterodimerization in lipid bilayers: probing the energetics behind autosomal dominant growth disorders. *Journal of molecular biology* **358**, 1-7
122. Chen, F., Sarabipour, S., and Hristova, K. (2013) Multiple consequences of a single amino acid pathogenic RTK mutation: the A391E mutation in FGFR3. *PloS one* **8**, e56521
123. He, L., and Hristova, K. (2012) Physical-chemical principles underlying RTK activation, and their implications for human disease. *Biochimica et biophysica acta* **1818**, 995-1005
124. Merzlyakov, M., Chen, L., and Hristova, K. (2007) Studies of receptor tyrosine kinase transmembrane domain interactions: the EmEx-FRET method. *The Journal of membrane biology* **215**, 93-103
125. Press, W. H., Teukolsky, S. A., Vetterling, W. T., and Flannery, B. P. (2007) *Numerical Recipes 3rd Edition: The Art of Scientific Computing*, Cambridge University Press
126. You, M., Li, E., Wimley, W. C., and Hristova, K. (2005) Forster resonance energy transfer in liposomes: measurements of transmembrane helix dimerization in the native bilayer environment. *Analytical biochemistry* **340**, 154-164
127. Li, E., You, M., and Hristova, K. (2005) Sodium dodecyl sulfate-polyacrylamide gel electrophoresis and forster resonance energy transfer suggest weak interactions between fibroblast growth factor receptor 3 (FGFR3) transmembrane domains in the absence of extracellular domains and ligands. *Biochemistry* **44**, 352-360
128. Johnson, M. L., and Faunt, L. M. (1992) Parameter estimation by least-squares methods. *Methods in enzymology* **210**, 1-37
129. Shankaran, H., Wiley, H. S., and Resat, H. (2006) Modeling the effects of HER/ErbB1-3 coexpression on receptor dimerization and biological response. *Biophysical journal* **90**, 3993-4009
130. Samna Soumana, O., Garnier, N., and Genest, M. (2008) Insight into the recognition patterns of the ErbB receptor family transmembrane domains: heterodimerization models through molecular dynamics search. *European biophysics journal : EBJ* **37**, 851-864
131. Li, E., Wimley, W. C., and Hristova, K. (2012) Transmembrane helix dimerization: beyond the search for sequence motifs. *Biochimica et biophysica acta* **1818**, 183-193
132. Cymer, F., Veerappan, A., and Schneider, D. (2012) Transmembrane helix-helix interactions are modulated by the sequence context and by lipid bilayer properties. *Biochimica et biophysica acta* **1818**, 963-973

133. Fink, A., Sal-Man, N., Gerber, D., and Shai, Y. (2012) Transmembrane domains interactions within the membrane milieu: principles, advances and challenges. *Biochimica et biophysica acta* **1818**, 974-983
134. Kenworthy, A. K., Petranova, N., and Edidin, M. (2000) High-resolution FRET microscopy of cholera toxin B-subunit and GPI-anchored proteins in cell plasma membranes. *Molecular biology of the cell* **11**, 1645-1655
135. Lazar, J., Bondar, A., Timr, S., and Firestein, S. J. (2011) Two-photon polarization microscopy reveals protein structure and function. *Nature methods* **8**, 684-690
136. Khadria, A. S., and Senes, A. (2013) The transmembrane domains of the bacterial cell division proteins FtsB and FtsL form a stable high-order oligomer. *Biochemistry* **52**, 7542-7550
137. Chen, Y., Li, X., Eswarakumar, V. P., Seger, R., and Lonai, P. (2000) Fibroblast growth factor (FGF) signaling through PI 3-kinase and Akt/PKB is required for embryoid body differentiation. *Oncogene* **19**, 3750-3756
138. Ueno, H., Gunn, M., Dell, K., Tseng, A., Jr., and Williams, L. (1992) A truncated form of fibroblast growth factor receptor 1 inhibits signal transduction by multiple types of fibroblast growth factor receptor. *The Journal of biological chemistry* **267**, 1470-1476
139. Sorkin, A., McClure, M., Huang, F., and Carter, R. (2000) Interaction of EGF receptor and grb2 in living cells visualized by fluorescence resonance energy transfer (FRET) microscopy. *Current biology : CB* **10**, 1395-1398
140. Jura, N., Endres, N. F., Engel, K., Deindl, S., Das, R., Lamers, M. H., Wemmer, D. E., Zhang, X., and Kuriyan, J. (2009) Mechanism for activation of the EGF receptor catalytic domain by the juxtamembrane segment. *Cell* **137**, 1293-1307
141. Red Brewer, M., Choi, S. H., Alvarado, D., Moravcevic, K., Pozzi, A., Lemmon, M. A., and Carpenter, G. (2009) The juxtamembrane region of the EGF receptor functions as an activation domain. *Molecular cell* **34**, 641-651
142. Thiel, K. W., and Carpenter, G. (2007) Epidermal growth factor receptor juxtamembrane region regulates allosteric tyrosine kinase activation. *Proceedings of the National Academy of Sciences of the United States of America* **104**, 19238-19243
143. Endres, N. F., Das, R., Smith, A. W., Arkhipov, A., Kovacs, E., Huang, Y., Pelton, J. G., Shan, Y., Shaw, D. E., Wemmer, D. E., Groves, J. T., and Kuriyan, J. (2013) Conformational coupling across the plasma membrane in activation of the EGF receptor. *Cell* **152**, 543-556
144. Schlessinger, J., and Lemmon, M. A. (2003) SH2 and PTB domains in tyrosine kinase signaling. *Science's STKE : signal transduction knowledge environment* **2003**, RE12
145. Kuriyan, J., and Cowburn, D. (1997) Modular peptide recognition domains in eukaryotic signaling. *Annual review of biophysics and biomolecular structure* **26**, 259-288
146. Kraskouskaya, D., Duodu, E., Arpin, C. C., and Gunning, P. T. (2013) Progress towards the development of SH2 domain inhibitors. *Chemical Society reviews* **42**, 3337-3370

147. Lanzerstorfer, P., Borgmann, D., Schutz, G., Winkler, S. M., Hoglinger, O., and Weghuber, J. (2014) Quantification and kinetic analysis of Grb2-EGFR interaction on micro-patterned surfaces for the characterization of EGFR-modulating substances. *PloS one* **9**, e92151
148. Fortian, A., and Sorkin, A. (2014) Live-cell fluorescence imaging reveals high stoichiometry of Grb2 binding to the EGF receptor sustained during endocytosis. *Journal of cell science* **127**, 432-444
149. Kozer, N., Barua, D., Henderson, C., Nice, E. C., Burgess, A. W., Hlavacek, W. S., and Clayton, A. H. (2014) Recruitment of the adaptor protein Grb2 to EGFR tetramers. *Biochemistry* **53**, 2594-2604
150. Morimatsu, M., Takagi, H., Ota, K. G., Iwamoto, R., Yanagida, T., and Sako, Y. (2007) Multiple-state reactions between the epidermal growth factor receptor and Grb2 as observed by using single-molecule analysis. *Proceedings of the National Academy of Sciences of the United States of America* **104**, 18013-18018
151. Li, E., and Hristova, K. (2010) Receptor tyrosine kinase transmembrane domains: Function, dimer structure and dimerization energetics. *Cell adhesion & migration* **4**, 249-254
152. Batzer, A. G., Rotin, D., Urena, J. M., Skolnik, E. Y., and Schlessinger, J. (1994) Hierarchy of binding sites for Grb2 and Shc on the epidermal growth factor receptor. *Molecular and cellular biology* **14**, 5192-5201
153. Maignan, S., Guilloteau, J. P., Fromage, N., Arnoux, B., Becquart, J., and Ducruix, A. (1995) Crystal structure of the mammalian Grb2 adaptor. *Science* **268**, 291-293
154. Rahuel, J., Gay, B., Erdmann, D., Strauss, A., Garcia-Echeverria, C., Furet, P., Caravatti, G., Fretz, H., Schoepfer, J., and Grutter, M. G. (1996) Structural basis for specificity of Grb2-SH2 revealed by a novel ligand binding mode. *Nature structural biology* **3**, 586-589
155. Oh, D., Ogiue-Ikeda, M., Jadwin, J. A., Machida, K., Mayer, B. J., and Yu, J. (2012) Fast rebinding increases dwell time of Src homology 2 (SH2)-containing proteins near the plasma membrane. *Proceedings of the National Academy of Sciences of the United States of America* **109**, 14024-14029
156. Chook, Y. M., Gish, G. D., Kay, C. M., Pai, E. F., and Pawson, T. (1996) The Grb2-mSos1 complex binds phosphopeptides with higher affinity than Grb2. *The Journal of biological chemistry* **271**, 30472-30478
157. Lemmon, M. A., Ladbury, J. E., Mandiyan, V., Zhou, M., and Schlessinger, J. (1994) Independent binding of peptide ligands to the SH2 and SH3 domains of Grb2. *The Journal of biological chemistry* **269**, 31653-31658
158. Poland, S. P., Krstajic, N., Monypenny, J., Coelho, S., Tyndall, D., Walker, R. J., Devauges, V., Richardson, J., Dutton, N., Barber, P., Li, D. D., Suhling, K., Ng, T., Henderson, R. K., and Ameer-Beg, S. M. (2015) A high speed multifocal multiphoton fluorescence lifetime imaging microscope for live-cell FRET imaging. *Biomedical optics express* **6**, 277-296
159. Macdonald, J. L., and Pike, L. J. (2008) Heterogeneity in EGF-binding affinities arises from negative cooperativity in an aggregating system. *Proceedings of the National Academy of Sciences of the United States of America* **105**, 112-117

160. Devaux, P. F., and Seigneuret, M. (1985) Specificity of lipid-protein interactions as determined by spectroscopic techniques. *Biochimica et biophysica acta* **822**, 63-125
161. Gilbert, G. E., Furie, B. C., and Furie, B. (1990) Binding of human factor VIII to phospholipid vesicles. *The Journal of biological chemistry* **265**, 815-822
162. Cho, W., Bittova, L., and Stahelin, R. V. (2001) Membrane binding assays for peripheral proteins. *Analytical biochemistry* **296**, 153-161
163. Smith, E. M., Hennen, J., Chen, Y., and Mueller, J. D. (2015) In situ quantification of protein binding to the plasma membrane. *Biophysical journal* **108**, 2648-2657
164. Raicu, V., and Singh, D. R. (2013) FRET spectrometry: a new tool for the determination of protein quaternary structure in living cells. *Biophysical journal* **105**, 1937-1945
165. Motulsky, H. J., and Ransnas, L. A. (1987) Fitting curves to data using nonlinear regression: a practical and nonmathematical review. *FASEB journal : official publication of the Federation of American Societies for Experimental Biology* **1**, 365-374
166. Day, Y. S., Baird, C. L., Rich, R. L., and Myszka, D. G. (2002) Direct comparison of binding equilibrium, thermodynamic, and rate constants determined by surface- and solution-based biophysical methods. *Protein science : a publication of the Protein Society* **11**, 1017-1025
167. Macdonald-Obermann, J. L., and Pike, L. J. (2014) Different epidermal growth factor (EGF) receptor ligands show distinct kinetics and biased or partial agonism for homodimer and heterodimer formation. *The Journal of biological chemistry* **289**, 26178-26188

CURRICULUM VITAE

NUALA DEL PICCOLO
970-379-5636 – nualadp@jhu.edu
https://www.linkedin.com/in/nuala-del-piccolo

EDUCATION

Johns Hopkins University **Baltimore, Maryland**
Doctor of Philosophy in Materials Science & Engineering **Dec 2016**
Thesis: Measuring the Thermodynamics of Receptor Tyrosine Kinase Interactions: A Study of Homodimers, Heterodimers, and Receptor-Adapter Protein Complexes
Master of Science in Materials Science & Engineering **May 2013**
Thesis: "Production of Plasma Membrane Vesicles with Chloride Salts and Their Utility as a Cell Membrane Mimetic for Biophysical Characterization of Membrane Protein Interactions" (Published in *Analytical Chemistry*)
GPA: 3.63
Bachelor of Science in Biomedical Engineering, Mathematics Minor **May 2012**
Honors in Biomedical Engineering
GPA: 3.81

RESEARCH EXPERIENCE

JHU Materials Science & Engineering (PI: Kalina Hristova) **Jan 2010-Dec 2016**
Graduate student research assistant; Undergraduate student
- Characterize the thermodynamics of receptor tyrosine kinase (RTK) interactions using quantitative Förster Resonance Energy Transfer (FRET) confocal microscopy
- Expand models describing the thermodynamics of protein-protein interactions in the cell membrane and apply updated models to experimental results in complex systems
- Develop and characterize methods of deriving vesicles from the plasma membrane of live cells, to be used as model membrane systems

Johns Hopkins School of Medicine, Pharmacology (PI: Jin Zhang) **Apr-Dec 2013**
Collaborative graduate student researcher
- Designed genetically encoded FRET biosensors to probe RTK activation in live cells using time-lapse wide field fluorescence microscopy

Vredenburg Scholarship **May-Aug 2011**
- Proposed project, awarded funds to support independent research project at Politecnico di Milano in Milan, Italy (PI: Maria Cristina Tanzi)
- Synthesized and mechanically characterized shape memory polymer scaffolds for bone tissue engineering

JHU-Tsinghua University BME Undergraduate Research Fellowship **June-July 2010**
- Conducted research project at Tsinghua University in Beijing, China (PI: Jing Liu)
- Studied the effects of nanoparticles on the freezing dynamics of liquids

PUBLICATIONS

N Del Piccolo, S Sarabipour, K Hristova. A New Method to Study Heterodimerization of Membrane Proteins and its Application to Fibroblast Growth Factor Receptors. **Papers in Press**. *J Biol Chem.*

S Sarabipour, **N Del Piccolo**, K Hristova. Characterization of Membrane Protein Interactions in Plasma Membrane Derived Vesicles with Quantitative Imaging Förster Resonance Energy Transfer. **2015**. *Acc Chem Res*, 48 (8): 2262-2269.

N Del Piccolo, J Placone, K Hristova. Effect of Thanatophoric Dysplasia Type I Mutations on FGFR3 Dimerization. **2015**. *Biophys J*, 108 (2): 272-278.

J Placone, L He, **N Del Piccolo**, K Hristova. Strong Dimerization of Wild-Type ErbB2/Neu Transmembrane Domain and the Oncogenic Val664Glu Mutant in Mammalian Plasma Membranes. **2014**. *Biochim Biophys Acta*, 1838 (9): 2326-2230.

N Del Piccolo, J Placone, L He, SC Agudelo, K Hristova. Production of Plasma Membrane Vesicles with Chloride Salts and Their Utility as a Cell Membrane Mimetic for Biophysical Characterization of Membrane Protein Interactions. **2012**. *Anal Chem*, 84 (20): 8650-8655.

PRESENTATIONS

N Del Piccolo, S Sarabipour, K Hristova. Heterodimerization of Wild-type and Mutant Fibroblast Growth Factor Receptors in Cell-derived Vesicles. Presented at the **Biophysical Society 60th Annual Meeting**. Los Angeles, California, February 29, 2016.

N Del Piccolo, K Hristova. Effect of Thanatophoric Dysplasia Type I Mutations on Fibroblast Growth Factor Receptor 3 Dimerization. Presented at the **Biophysical Society 59th Annual Meeting**. Baltimore, Maryland, February 9, 2015.

J Placone; **N Del Piccolo**, K Hristova. Measuring the Effect of Disulfide Bonds on the Stability of Membrane Protein Dimers in the Plasma Membrane. Presented at **FASEB's "Molecular Biophysics of Membranes" Science Research Conference**. Snowmass Village, Colorado, June 20, 2012.

N Del Piccolo, J Placone, L He, K Hristova. Development of Cell-derived Vesicles as a Plasma Membrane Mimetic System. Presented at FASEB's "Molecular Biophysics of Membranes" Science Research Conference. Snowmass Village, Colorado, June 18, 2012.

N Del Piccolo, J Liu. Effects of Nano-particles on Phase Change Curves in Liquids. Presented at the **2nd Annual JHU Biomedical Engineering Undergraduate Research Day**. Baltimore, Maryland, December 2, 2010.

TEACHING EXPERIENCE

Bard College Citizen Science Program Faculty **Jan 2017**

- Intensive science literacy program held during the January academic session
- Used problem-based learning, laboratory, and computing activities to teach students about infectious disease from a holistic perspective

Johns Hopkins University Instructor **Sept 2014-Dec 2015**

- Designed, proposed, and taught a semester-long seminar as part of a school-wide initiative to introduce freshman to engineering research
- My class, "Visualizing Biomolecules," focused on current microscopy techniques and applications in bioengineering research; registration reached capacity both semesters

Johns Hopkins University Graduate Teaching Assistant **Sept 2013-Dec 2015**

- **Biomaterials Lab**, Dr. Kalina Hristova: designed and taught two labs to introduce upperclassmen to mammalian cell culture and related standard assays
- **Molecules and Cells**, Dr. Eileen Haase: first course in biomedical engineering core; taught weekly section, created homework/exam rubrics, managed homework graders, corrected exams, held office hours
- **Modern Alchemy**, Dr. James Spicer: STEM course for non-science majors; updated course materials, graded papers
- **Biomaterials I**, Dr. Hai-Quan Mao: upper level engineering course; graded problem sets and exams, held office hours

Preparing Future Faculty Teaching Academy Certificate **Sept 2013-Dec 2014**

- Trained in both pedagogical theory and best educational practices

LEADERSHIP EXPERIENCE

Society of Women Engineers **Sept 2008-present**

- Baltimore-Washington Section Educational Outreach Volunteer (Sept 2011-present)
- JHU Collegiate Section President (Sept 2011-May 2012): supervised and organized all club activities, including a monthly speaker series, volunteer activities, and a keynote address
- JHU Collegiate Section Treasurer (Sept 2010-May 2011): managed budget of ~$2K

Mentor to Undergraduate Student Researcher **Jan-Dec 2016**

- Instruct student about lab protocols, literature reviews, and data analysis

JHU Women's Ultimate Frisbee Club Team **Sept 2008-Dec 2011**

- Secretary (Sept 2009-Dec 2011): managed team roster, coordinated player registration with national association

Lab Manager for Biomedical Engineering Modeling & Design Course Sept-Dec 2010

- Guided students through series of labs designed to introduce them to BME
- Advised freshman about academics and research

HONORS

SWE Collegiate Technical Poster Competition, Third Place **Oct 2016**
John W. and Mary Lou Ross, Paul V. Renoff Fellowships **Sept 2012-May 2013**
Tau Beta Pi (The Engineering Honor Society) **Inducted Nov 2011**
Robert C. Byrd, L.S. Woods, and Trashmasters Scholar **Sept 2008-May 2012**

PROFESSIONAL SKILLS & MEMBERSHIPS

Memberships: Biophysical Society, Society of Women Engineers, Tau Beta Pi
Computer: MATLAB; Origin; Microsoft Word, Excel, PowerPoint, and Outlook
Lab: Fluorescence Microscopy, Confocal Microscopy, Förster Resonance Energy Transfer (FRET), Mammalian Cell Culture, Western Blotting, Molecular Cloning, Protein Purification, Bacterial Culture
Language: English (native), Spanish (conversational), Italian (conversational)